

**Molecular biological and spectroscopic characterisation of  
the [NiFe]-hydrogenase from *Desulfovibrio vulgaris***

INAUGURAL-DISSERTATION

**zur**

Erlangung des Doktorgrades der Mathematisch-Naturwissenschaftlichen  
Fakultät der Heinrich-Heine-Universität Düsseldorf

**angefertigt am**

**Max-Planck-Institute für Bioanorganische Chemie  
Mülheim an der Ruhr, Germany**

vorgelegt von

**Aruna Goenka Agrawal**

**aus Indien**

**Düsseldorf 2005**

Gedruckt mit der Genehmigung der Mathematisch-Naturwissenschaftlichen Fakultät  
der Heinrich-Heine-Universität Düsseldorf

Referent: Prof. Dr. Wolfgang Gärtner

Korreferent: Prof. Dr. Peter Westhoff

Korreferent: Prof. Dr. Alfred R. Holzwarth

Tag(e) der mündlichen Prüfung: 11.07.2005

## Abstract

Goenka Agrawal, Aruna

Molecular hydrogen is a potential energy carrier for the future. [NiFe] hydrogenases are metalloenzymes, which catalyse the reversible conversion of molecular hydrogen. The hetero-bimetallic catalytic centre with a nickel and an iron atom is the essential structural element in this reaction. Crystallographic studies have revealed the atomic details of the active site, however, the exact reaction mechanism is not yet known, though different redox states are involved. The iron atom is diamagnetic, and thus EPR silent. However, it possesses inorganic ligands, CO and CN, that allow to follow the conversion of the various states by FTIR spectroscopy. In some of the redox states nickel is paramagnetic, which permits the use of EPR techniques. Besides the nature of the active site, its biological assembly is also not completely understood. The synthesis and installation of this NiFe(CN)<sub>2</sub>CO catalytic centre is a complex process in which a whole set of auxiliary proteins are involved. These so-called maturation proteins are very specific in their action on the target complex, and a knowledge of their function is essential for the generation of recombinant hydrogenases.

In this thesis, genes involved in the maturation of the [NiFe] hydrogenase of the closely related sulfur reducing bacteria, *Desulfovibrio vulgaris* Miyazaki F (DvMF) and *Desulfovibrio vulgaris* Hildenborough (DvH) were examined, and the possibility of employing genetically modified hydrogenase for hydrogen production has been investigated. Together with the maturation of the hydrogenase, the structure of the active site was investigated using the isotopically labeled protein. Protocols for the preparation of different redox states of the [NiFe] hydrogenase from DvMF were optimised and the states thus prepared were subjected to advanced spectroscopy techniques.

The operon sequence of the DvMF [NiFe] hydrogenase was characterised, and was found to be a long operon with a  $\sigma_{54}$ -type promoter present upstream and maturation genes present downstream of the structural genes. The endopeptidase (C-subunit) was further investigated for its possible secondary and tertiary structure. Also, the complete set of maturation genes for DvH [NiFe] hydrogenase was analysed for its function as compared to known maturation genes from other organisms.

The potential for producing a genetically modified hydrogenase was investigated by generating and studying a mutant strain of DvH, lacking the [NiFe] hydrogenase. The effect of deletion of the hydrogenase gene on its growth behavior in standard medium was found to be almost insignificant. The difficulties in generating the deletion for DvMF were traced by looking for other, if any, hydrogenases present in the strain by comparing the gel activity assays and electrochemical behaviour of all the species studied in this thesis. These assays give evidence that DvMF probably has only one hydrogenase which would cause its deletion a lethal process for the organism.

A synthetic medium was designed for the growth of DvMF, to achieve the isotope labeling in hydrogenase. Chelex cleaning was used to remove any natural abundant nickel and allowed to add the optimum concentration of <sup>61</sup>Ni to the medium. Determination of the <sup>61</sup>Ni hyperfine coupling constants by ELDOR detected NMR allowed us to investigate the direct environment of Ni in both the oxidized Ni-A and Ni-B states, and it was found that Ni-A and Ni-B have a bridging ligand of similar nature. Similarly, the natural abundance of <sup>14</sup>N in His residues was replaced by using <sup>15</sup>N-His in the growth medium in a separate culture growth experiment. This allowed the determination of the H-bond strength between His-88 and Cys-549 of the active [NiFe] centre. It could be demonstrated that this H-bond contributes to finetune the electronic structure of the active site.

This thesis advances the knowledge about the structure of the active site of DvMF [NiFe] hydrogenase on a molecular-biological and a spectroscopic level and opens possibilities for further development of the genetically modified hydrogenases.



## Acknowledgement

Much of this work is a result of teamwork. It involves the encouragement, support, suggestions and guidance of many people and I wish to express my sincere thanks to all of them for their help.

I would like to thank Prof. Dr. Wolfgang Lubitz for providing me the opportunity to work in his group and through the collaborations with different groups, besides his constant support and interest in the interdisciplinary approach.

My sincere thanks to Prof. Dr. Wolfgang Gärtner for his mentoring, trust, patience and tolerance through all the haps and mishaps during the course of my work. I am very grateful to him for inspiring me and for letting me try out my ideas. Also, he helped me to correct the complete thesis for technical and language errors.

The collaboration with Prof. Dr. Gerrit Voordouw from the University of Calgary, Canada contributed a lot to the molecular biology results. Joanna and Gerrit provided me with excellent lab support and supervision, respectively, to learn basic handling of *Desulfovibrio species* and the molecular biology techniques, besides a very nice working atmosphere in the group, during my four months of stay there.

Special thanks to Dr. Maurice van Gastel for generously sharing his expertise and labor in conducting the spectroscopy experiments and theoretical calculations on the labeled samples. He helped me a lot in learning the details of theoretical and practical aspects of EPR spectroscopy, besides editing parts of this thesis on a short notice.

I wish to convey my thanks to Prof. Dr. Bärbel Friedrich, Dr. Oliver Lenz and their group at the Humboldt-Universität Berlin, for motivating discussions, for allowing me to conduct the native gel activity assay in their labs and for providing the pJRD 215 plasmid and *E. coli* S17-1 strain.

Also, I extend my appreciation to PD Dr. Reiner Hedderich, from the MPI für terrestrische Mikrobiologie, Marburg, for providing me the opportunity to visit his lab and to understand the anaerobic working techniques.

My thanks to Dr. Eberhard Bothe, from our institute, for his guidance to conduct the electrochemistry experiments.

I thank Dr. John Berry, from our institute, for his advice on the practical chemistry of converting nickel to nickel chloride for labeling experiments.

Very special thanks to Ullrich Krauss for his timely assistance with the use of programmes to model the protein structure from the newly sequenced gene in this work.

I thank all my colleagues for their help and support. It was great to have the vivid and vivacious working group for their advice and discussions all through the conduction of this thesis: Dr. Edward Reijerse, Dr. Maurice van Gastel, Dr. Bettina Katterle, Dr. Hideaki Ogata, Dr. Marco Flores, Caroline Fichtner, Amrit Pal Kaur, Petra Kellers, Alexey Sikalov from the hydrogenase group and Dr. Helena JMM Jorissen, Julieta Mateos and Shivani Sharda from the biology group, and Christoph Breitenstein for his trouble shooting for computer related problems.

It was a great help to have Helena Steffen, Tanja Berndsen, Norbert Dickmann, Gudrun Klihm, Christoph Laurich and Michael Reus and I wish to thank them all for their technical assistance.

A warm heartfelt thanks to all my friends for their encouragement, emotional support and timely discussions about anything and everything to keep me going.

I am very grateful to my family for allowing me to choose my path, to let me pursue my dreams and constantly showering me with unconditional love and life long support that makes me feel so blessed and secure.

Last, but not the least, I wish to express my gratitude to my husband, Hemant, for his love, care and understanding. For always being there for me in all ups and downs with his smile and making everything look so beautiful with his contagious positive attitude.

### **List of Publications:**

1. Goenka A, Voordouw JK, Lubitz W, Gärtner W, Voordouw G  
Construction of a [NiFe]-hydrogenase deletion mutant of *Desulfovibrio vulgaris* Hildenborough. *Biochem Soc Trans.* 2005. *33(1)*, 59-60.
2. Aruna Goenka, Maurice van Gastel, Wolfgang Gärtner, Wolfgang Lubitz  
H-bonding in the [NiFe] Active Site of *Desulfovibrio vulgaris* Miyazaki F Hydrogenase. A study by <sup>14</sup>N/<sup>15</sup>N Hyperfine Sublevel Correlation Spectroscopy and Density Functional Theory. (To be submitted)
3. Aruna Goenka, Maurice van Gastel, Wolfgang Gärtner, Wolfgang Lubitz  
ELDOR detected NMR as a powerful tool to study metal hyperfine interactions: the oxidised states of the [NiFe] hydrogenase of *D. vulgaris* Miyazaki F. (To be submitted)

### **List of Posters presented:**

1. A. Goenka, C. Fichtner, M. van Gastel, W. Gärtner, W. Lubitz  
Spectroscopic and biochemical characterization of [NiFe] hydrogenase from *D. vulgaris* (Miyazaki F).  
COST 841, Biosynthesis and Regulation of Hydrogenases, Working Group 3 Workshop, October 5-8, 2002, Cercedilla, Madrid, Spain.
2. Aruna Goenka, Maurice van Gastel, Wolfgang Gärtner, Wolfgang Lubitz  
EPR of <sup>61</sup>Ni-enriched [NiFe] hydrogenase of *Desulfovibrio vulgaris* Miyazaki F.  
7th International Hydrogenase Conference, August 24-29, 2004, University of Reading, Reading, UK.
3. Aruna Goenka, Gerrit Voordouw, Wolfgang Gärtner, Wolfgang Lubitz  
Sequencing of *Desulfovibrio vulgaris* Miyazaki F [NiFe] hydrogenase operon and hydrogenase knock out mutant generation.  
7th International Hydrogenase Conference, August 24-29, 2004, University of Reading, Reading, UK.

## Abbreviations:

μM	micromolar
A	absorbance
AA	amino acid (s)
Amp	ampicillin
APS	adenosine-5'-phosphosulfate
BCIP	5-bromo-4-chloro-3-indolyl-β-D-phosphopyranoside
BV	Benzyl viologen
cm	centimeter
Cm	Chloramphenicol
cw	continuous wave
Cys	cysteine
DFT	Density Functional Theory
DH	Denhardts solution
DMF	N,N-dimethyl formamide
DMSO	Dimethyl sulfoxide
DTT	Sodium dithionite/ Sodium hydrosulfite
DvH	<i>Desulfovibrio vulgaris</i> Hildenborough
DvMF	<i>Desulfovibrio vulgaris</i> Miyazaki F
<i>E. coli</i>	<i>Escherichia coli</i>
EDTA	ethylene diamine tetra acetic acid
ENDOR	Electron Nuclear Double Resonance
EP	hepes+ glycerol
EPR	Electron Paramagnetic Resonance
ESEEM	Electron Spin Echo Envelope Modulation
EXAFS	Extended X-ray Absorption Fine Structure
FM	full medium
FT	Fourier transform
FTIR	Fourier Transform Infra Red (spectroscopy)
<i>h</i>	Planck constant, 66260755 _ 10 <sup>-34</sup> Js
HEPES	2-[4-(2-hydroxyethyl)-piperazinyl]-ethane-sulfonic acid
hf(c)	hyperfine coupling
His	histidine
Hmc	hexadecaheme high molecular weight cytochrome c complex
HYSCORE	Hyperfine Sublevel Correlation (spectroscopy)
IR	infrared
Km	kanamycin
LB	Luria Bertani medium
MALDI-TOF	matrix assisted laser desorption/ ionisation-time of flight
ml	milli litre
mM	milli molar
MM	Minimal medium
MS	mass spectrometry
mW	milli watt
NBT	nitroblue tetrazolium
NHE	normal hydrogen electrode
NQR	nuclear quadrupole resonance
O/N	overnight

OD	optical density
P.T.F.E	polytetrafluoroethylene
PAGE	polyacrylamide gel electrophoresis
PB	posgate medium B
PC	posgate medium C
PCR	polymerase chain reaction
PE	posgate medium E
PMS	Phenazine methosulfate
PVDF	membrane for western blot
rf	radio frequency
rpm	rotations per minute
SDS	sodium dodecyl sulfate
Sm	streptomycin
SRB	sulfate reducing bacteria
SSC buffer	sodium citrate+ sodium chloride buffer
Suc	Sucrose
tat	twin arginine transport
TBE	tris borate EDTA buffer
Tris	tris-(hydroxymethyl)-aminomethane
TTC	Triphenyl tetrazolium chloride
UV-VIS	Ultra violet and visible range, used for spectroscopy
WT	wild type



# Index

<b>1. INTRODUCTION.....</b>	<b>1</b>
<b>2. HYDROGENASE .....</b>	<b>5</b>
2.1 CLASSIFICATION OF HYDROGENASES.....	5
2.2 MOLECULAR STRUCTURE OF THE HYDROGENASE .....	7
2.3 MATURATION PATHWAY.....	10
2.4 HYDROGEN CYCLING .....	15
2.5 REDOX STATES .....	18
2.6 MOTIVATION OF THE WORK .....	20
<b>3. MATERIALS AND METHODS .....</b>	<b>23</b>
3.1 BACTERIAL STRAINS AND PLASMIDS AND VECTORS .....	23
3.2 CHEMICALS AND ENZYMES.....	25
3.2.1 CHEMICALS .....	25
3.2.2 ENZYMES .....	25
3.2.3 ANTIBODIES.....	26
3.2.4 ISOTOPES .....	26
3.2.4.1 RADIOACTIVE ISOTOPE.....	26
3.2.4.2 NON-RADIOACTIVE ISOTOPE .....	26
3.2.5 KITS .....	26
3.3 MEDIA AND SOLUTIONS.....	27
3.4 MICROBIOLOGY AND MOLECULAR BIOLOGY TECHNIQUES.....	30
3.4.1 CELL CULTURE .....	30
3.6.1.1 <i>E. COLI</i> CELL CULTURE .....	30
3.6.1.2 <i>DESULFOVIBRIO</i> CELL CULTURE.....	30
3.4.2 CHROMOSOMAL DNA ISOLATION.....	32
3.6.2.1 DNEASY <sup>®</sup> TISSUE KIT .....	32
3.6.2.2 CHROMOSOMAL DNA ISOLATION PROTOCOL .....	32
3.4.3 PLASMID DNA ISOLATION .....	33
3.4.4 POLYMERASE CHAIN REACTION .....	33
3.4.5 AGAROSE GEL ELECTROPHORESIS .....	34
3.4.6 ISOLATION OF DNA FROM AGAROSE.....	34
3.4.7 DETERMINATION OF DNA CONCENTRATIONS IN AQUEOUS SOLUTION.....	34
3.4.8 RESTRICTION DIGESTION.....	34
3.4.9 DEPHOSPHORYLATION .....	35
3.4.10 DESALTING OF DNA SOLUTIONS .....	35
3.4.11 LIGATION REACTIONS .....	35
3.4.12 PREPARATION OF <i>E. COLI</i> COMPETENT CELLS & DNA TRANSFORMATION.....	35
3.4.12.1 PREPARATION OF $CaCl_2$ COMPETENT <i>E. COLI</i> CELLS .....	36
3.4.12.2 TRANSFORMATION OF $CaCl_2$ COMPETENT <i>E. COLI</i> CELLS .....	36
3.4.12.3 PREPARATION OF ELECTROCOMPETENT <i>E. COLI</i> CELLS .....	36
3.4.12.4 TRANSFORMATION OF ELECTROCOMPETENT <i>E. COLI</i> CELLS .....	37
3.4.13 SUCROSE SENSITIVITY ASSAY .....	37
3.4.14 CONJUGATION .....	37
3.4.15 SOUTHERN HYBRIDIZATION.....	38
3.5 PROTEIN CHEMICAL METHODS .....	39
3.5.1 EXTRACTION OF HYDROGENASE PROTEIN FROM DVMF CELLS .....	39

3.5.2	PROTEIN PURIFICATION .....	40
3.5.3	DETERMINATION OF PROTEIN CONCENTRATION.....	41
3.5.4	METHY VILOGEN ACTIVITY ASSAY .....	41
3.5.5	MODIFIED CLARK ELECTRODE ASSAY .....	41
3.5.6	SDS-PAGE COMMASIE STAINING.....	42
3.5.7	WESTERN BLOT .....	42
3.5.8	NATIVE PAGE AND IN-GEL ACTIVITY ASSAY .....	43
3.5.9	PREPARATION OF DIFFERENT EPR ACTIVE REDOX STATES .....	44
3.5.10	MALDI-TOF MOLECULAR WEIGHT ANALYSIS .....	47
3.6	SPECTROSCOPIC METHODS.....	47
3.6.1	UV/VIS SPECTROSCOPY.....	47
3.6.2	EPR.....	48
3.7	DFT CALCULATIONS .....	49
3.8	ELECTROCHEMISTRY.....	49
3.9	SOFTWARES.....	51
<b>4.</b>	<b>DVMF [NIFE] HYDROGENASE: COMPLETE OPERON SEQUENCE.....</b>	<b>53</b>
4.1	RATIONAL FOR SEQUENCING THE OPERON.....	55
4.2	SEQUENCING STRATEGY I.....	56
4.3	SEQUENCING STRATEGY II.....	62
4.4	EXPRESSION OF THE PARTIAL AND THE COMPLETE DVMF [NIFE] HYDROGENASE OPERON IN <i>E. COLI</i> .....	65
4.5	CLONING OF HYNC IN PET28 AND EXPRESSION IN <i>E. COLI</i> BL21. ....	67
4.6	SECONDARY STRUCTURE PREDICTION .....	67
4.7	DISCUSSION.....	69
<b>5.</b>	<b>CONSTRUCTION OF A DVH [NIFE] HYDROGENASE DELETION MUTANT.....</b>	<b>77</b>
5.1	PLASMID CONSTRUCT .....	79
5.2	FIRST CROSS OVER MUTANT.....	81
5.3	SECOND CROSS OVER MUTANT .....	83
5.4	EXPRESSION STUDIES.....	86
5.5	ELECTROCHEMICAL STUDIES.....	87
5.6	NATIVE PAGE IN-GEL ACTIVITY ASSAY .....	92
5.7	DISCUSSION.....	94
<b>6.</b>	<b>ISOTOPE LABELING OF DVMF [NIFE] HYDROGENASE BY <sup>61</sup>Ni AND <sup>15</sup>N HISTIDINE.....</b>	<b>97</b>
6.1	SPECTROSCOPY THEORY .....	98
6.1.1	EPR.....	98
6.1.2	ENDOR .....	100
6.1.3	ELDOR-DETECTED NMR.....	100
6.1.4	ESEEM.....	101
6.1.5	HYSORE .....	102
6.2	OPTIMISATION OF REQUIRED Ni CONCENTRATION .....	102
6.3	PROTEIN PURITY DETERMINATION BY SDS-PAGE AND MALDI-TOF .....	104
6.4	EPR-SPECTROSCOPY ON <sup>61</sup> Ni LABELLED [NIFE] HYDROGENASE FROM DVMF.....	105
6.5	EPR INVESTIGATION OF <sup>15</sup> N HIS LABELED [NIFE] HYDROGENASE FROM DVMF.....	110
6.5.1	EPR.....	112
6.5.2	ESEEM, HYSORE AND SIMULATION.....	113
6.5.3	DFT CALCULATIONS .....	118

6.6 DISCUSSION.....	122
<b>7. SUMMARY AND OUTLOOK.....</b>	<b>125</b>
<b>8. BIBLIOGRAPHY .....</b>	<b>129</b>
<b>9. APPENDIX.....</b>	<b>141</b>
9.1 DVMF [NiFe] HYDROGENASE OPERON.....	141
9.2 DVH [NiFe] HYDROGENASE OPERON.....	143
9.3 LIST OF FIGURES .....	145
9.4 LIST OF TABLES .....	148
9.4 TABLE OF [NiFe] HYDROGENASE OPERONS COMPARED .....	149

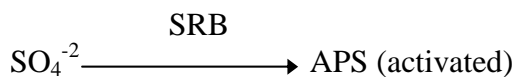
## **CURRICULUM VITAE**

# Chapter 1

## Introduction

Sulfate reducing bacteria (SRB) constitute a diverse group of anaerobic bacteria, found ubiquitously in nature and possessing the ability to use sulfate as terminal electron acceptor. All sulfate reducers convert sulfate to adenosine-5'-phosphosulfate (APS), which is the first step in activation of the sulfate anion before it can be utilized (Hansen TA, 1994).

Activation step:



This process can physiologically be linked to hydrogen oxidation (and the reverse process, hydrogen formation). Great progress has been made in the knowledge on the pathways and the enzymes used in the degradation of the substrates by sulfate reducers. This particularly applies to hydrogen oxidation and the enzyme performing this reaction, the hydrogenase.

The hydrogenase (EC 1.18.99.1) was first described by Stephenson and Stickland in 1931. Hydrogenases are the enzymes, which catalyse the hydrogen conversion reaction



They catalyse the reaction in one direction either way in most cases *in vivo*, but under special conditions like in presence of an unfavourable electron donor or acceptor, they can also catalyse the reverse reaction. The physiological function of the most prokaryotic hydrogenases is the oxidation of the hydrogen molecule and the reduction of electron acceptors coupled to the energy conservation process. Another physiological function of hydrogenases is the production of hydrogen, for the maintenance of intracellular pH and redox potential (Adams MW, *et al.*, 1981) that is not necessarily related to the energy conservation function.

Out of all sulfur reducing bacteria known, *Desulfovibrio* species are the most studied ones. *Desulfovibrio* strains have been shown to possess multiple hydrogenases (Voordouw G, 1992). These hydrogenases work either in the hydrogen production or in its consumption, forming a complete metabolism hydrogen cycle, in combination with other metabolic pathways of the species (Odom JM and Peck HD Jr, 1981).

The growing interest in hydrogenases has many facets. One of the major aspects is their role as a stable and cheap catalyst for the production of hydrogen, preferably at room temperature (RT) and at “normal” pH conditions. Hydrogenases have the potential to be a comparable catalyst to platinum, which is currently being used for fuel cells, although it is expensive and limited in availability. Hydrogen is considered as a clean energy source in comparison to other fossil fuels, as it reacts with oxygen forming only water and does not add to green house effect. Also, hydrogen provides the facility to be stored as energy source and transported when needed, unlike some of the other natural resources.

Recently, the chemical assembly of the iron-sulphur framework of the active site of iron-only hydrogenase (the H-cluster) has been reported (Tard C, *et al.*, 2005; Darensbourg MY, 2005), that can function as an electrocatalyst for proton reduction. Following, this study opens the path for using a freestanding analogue of the H-cluster to develop useful electrocatalytic materials for the application in reversible hydrogen fuel cells replacing platinum in future. Extrapolating the catalysing capacity of [Fe]-hydrogenases, it has been suggested that 1 mole of hydrogenase can produce enough hydrogen which could fill the airship *Graf Zeppelin* in ten minutes (Cammack R, 1999).

Besides having the high activity, [Fe] hydrogenase has some limitations too. It is much more sensitive to oxygen than [NiFe] hydrogenase. Other than this, they have their different  $K_m$  values and function in different hydrogen concentrations present in the atmosphere (Voordouw G, 1993). And finally, to construct and maintain these enzymes, all the resources present in the living cell are required. This is due to the complex mechanism involved in their maturation (chapter 2, 4), assembly and maintenance. So, in the above context, the use of bacterial cells as cell factories could be a possible approach.

In the effort to understand the scientific basis of hydrogen production, studies on the operons coding structural and maturational genes for [NiFe] hydrogenase, mutant construction and advanced spectroscopy techniques like ELDOR-detected NMR and HYSCORE (to study the effect of isotope labeled protein), have been attempted in this thesis.



## Chapter 2

# Hydrogenase

The [NiFe] hydrogenases are a group of enzymes with a fascinating hetero-bimetallic active site, which has a distorted symmetry and unusual inorganic ligands bound to the iron atom (one CO and two CNs). They catalyze the simple reaction involving heterolytical cleavage of the covalent bond of a hydrogen molecule. For only *Desulfovibrio gigas* and *Desulfovibrio vulgaris* Miyazaki F (DvMF), a detailed three-dimensional structure combined with functional information of the catalytic cycle has been presented. One of these enzymes, the [NiFe] hydrogenase from DvMF in its native form, has been the topic of fundamental research during recent years in our group. In the present experimental approach, for the first time a study of modified forms of the same enzyme was performed, using:

- mutagenesis and
- isotope labeling.

In view of this, a brief general introduction with emphasis on the biological and biochemical properties of the [NiFe] hydrogenase from DvMF, and hydrogenases in general is given in this chapter.

### 2.1 Classification of Hydrogenases

Based on phylogeny, hydrogenases can best be classified into two classes: - [NiFe] hydrogenases, and [Fe] only hydrogenases. This classification is based on the metal



content of the active site, where [NiFeSe] hydrogenases form a sub-class of the [NiFe] hydrogenases, in which a cysteine is replaced by a seleno-cysteine coordinated to the nickel (Garcin E *et al.*, 1999; He SH *et al.*, 1989; Sorgenfrei O *et al.*, 1993).

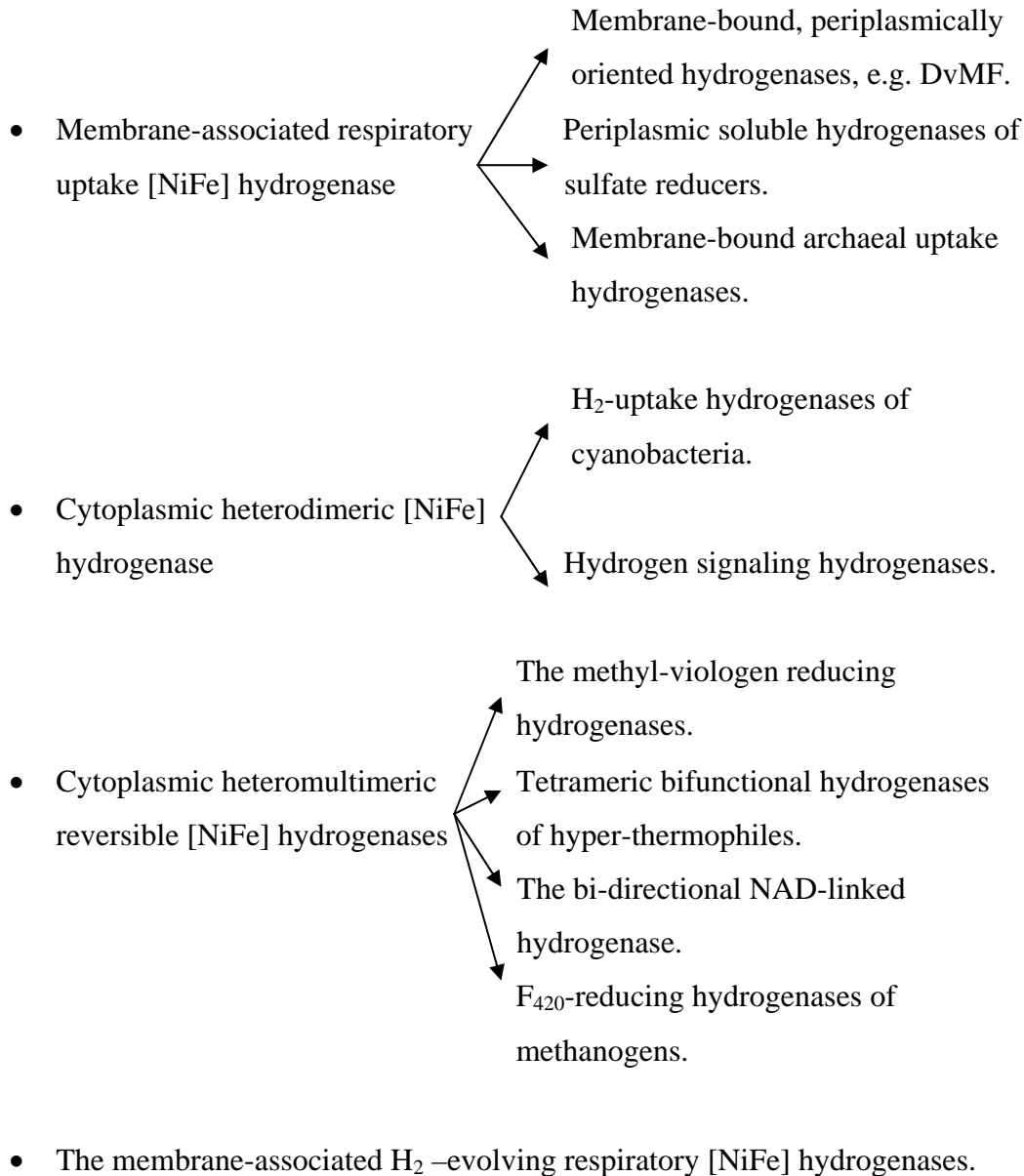


Fig. 2.1 Classification of [NiFe] hydrogenases, as adapted from Vignais PM *et al.*, 2001.

Hydrogenases may function as a catalyst to split or produce molecular hydrogen (DvMF), or as hydrogen sensor (*Ralstonia eutropha*), and they can be found at different cellular location. They all share a similar genetic arrangement (discussed in detail later). Comparing the conserved sequence elements in the nickel-binding regions, Voordouw has studied 16 [NiFe] hydrogenases (Voordouw G, 1992), and classified them in five

subgroups. Wu and Mandrand have compared sequence analysis, metal content and physiological function, for 30 different hydrogenases and proposed six classes of microbial hydrogenases (Wu LF and Mandrand MA, 1993). Since then the total number of hydrogenases sequenced has increased well beyond 100.

In the most recent classification (Vignais PM *et al.*, 2001), hydrogenases have been arranged into three classes where a so-called “metal-free” hydrogenase was also described that however, have recently been proven to contain Fe in the active site (Lyon EJ *et al.*, 2004). Besides classifying the newly discovered sequences and reclassifying few others, the four sub-classes of [NiFe] hydrogenases as described by Wu and Mandrand have been roughly kept the same by Vignais *et al.*, as described here in fig. 2.1.

Thus comparing the work presented in different reviews for [NiFe] hydrogenases, it can be stated that the classes defined by sequence similarity of the structural subunits and those by functional behavior are consistent. For [Fe] only hydrogenases more work at the gene level needs to be done before a similar classification for these enzymes can be made.

## 2.2 Molecular structure of the hydrogenase

Single crystals of several hydrogenases have been studied by X-ray crystallography. As a result of these studies, a three dimensional map of the electron density of the molecule is available, providing structural and biochemical data. Starting from the studies on the [NiFe] hydrogenase of *D. gigas* (Volbeda A *et al.*, 1995) at 2.85 Å resolution, followed by the [NiFe] hydrogenase of DvMF at 1.8 Å resolution (Higuchi Y *et al.*, 1997), the crystal structure analysis has also helped to understand the mechanism of action of hydrogenases better, besides giving information about the structure itself. The comparison of the structures of DvMF and *D. gigas* indicates that the folding patterns of the proteins and structural features of the metal centers are very similar.

The X-ray structure reveals that the [NiFe] hydrogenase from DvMF is a heterodimer of ca. 3 nm radius, consisting of a large and a small subunit. The large sub-unit contains the Ni-Fe active site, while the small subunit has the three [FeS] clusters. The [FeS]

clusters are arranged in a straight line from the active site to the periphery of the protein spaced at a distance of  $\sim 1.2$  nm from each other in the following order: - proximal [4Fe4S] cluster, [3Fe4S] cluster and distal [4Fe4S] cluster. For *D. gigas* the midpoint redox potentials of the [4Fe4S] clusters at pH 7.0 are known to be, -290 mV and -340 mV, respectively, while for the [3Fe4S] cluster it is much more positive at -30 mV upto -80 mV. Interestingly, the conversion of the [3Fe4S] cluster to the [4Fe4S] cluster in *D. gigas* by site directed mutagenesis (P238C), leading to a reduction of the cluster potential, had little effect on the activity of the enzyme (Rousset M *et al.*, 1998).

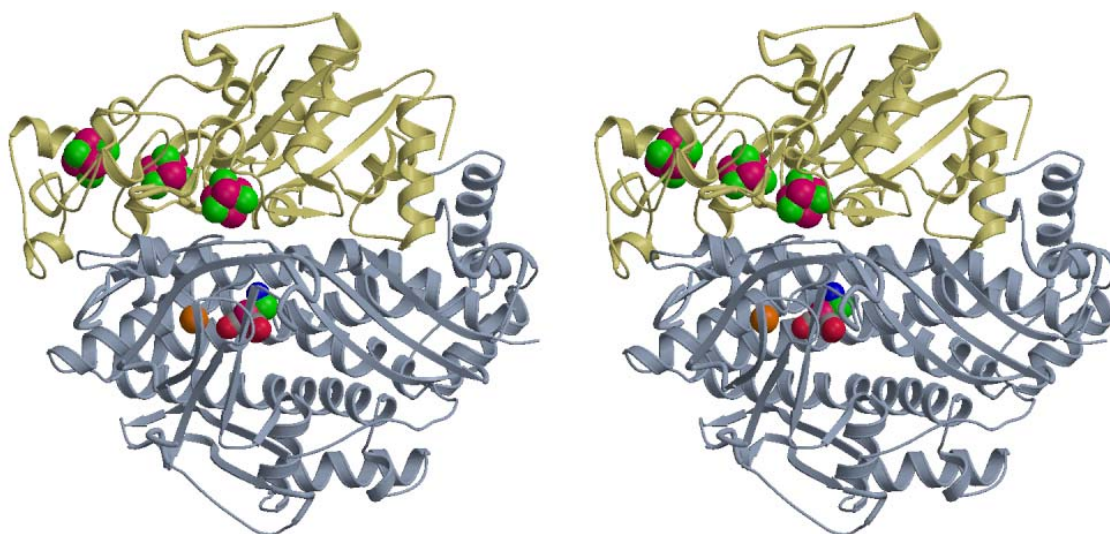


Fig. 2.2 Stereoview of the molecular structure of the [NiFe] hydrogenase from DvMF, showing the large subunit in blue containing the active site and the small subunit in green with three [FeS] clusters. Figure kindly provided by Dr. Hideaki Ogata.

The catalytic site is bimetallic, with a Ni and an Fe atom, coordinated by two cysteine residues. Other than these bridging ligands, the active site has another bridging ligand, when the enzyme is in the oxidized state; however, its exact nature is still a matter of debate. In a recent publication (Volbeda A *et al.*, 2005) a  $\mu$ -hydroxo ligand for Ni-B and a hydro-peroxide ligand for Ni-A has been proposed. Beside the bridging cysteines, Ni is ligated with two more cysteines, thus in total has four cysteine ligands (80, 84, 546 and 549, amino acid residues in case of DvMF). Two of these cysteines, Cys 84 and Cys 549 serve as bridging ligands to the iron atom. The Iron atom is further ligated with three inorganic diatomic ligands, known to be one CO and two CN for *D. gigas* (Volbeda A *et al.*, 1996). In case of DvMF, the presence of one SO as Fe ligand was initially proposed (Higuchi Y, 1997), but later SO/CN/CO, CO and CN have been

proposed (Higuchi Y, 1999; Higuchi Y, 2000). FTIR experiments in our group have shown that the ligands are identical to those of *D. gigas*, excluding the possibility of SO (C. Fichtner, PhD thesis).

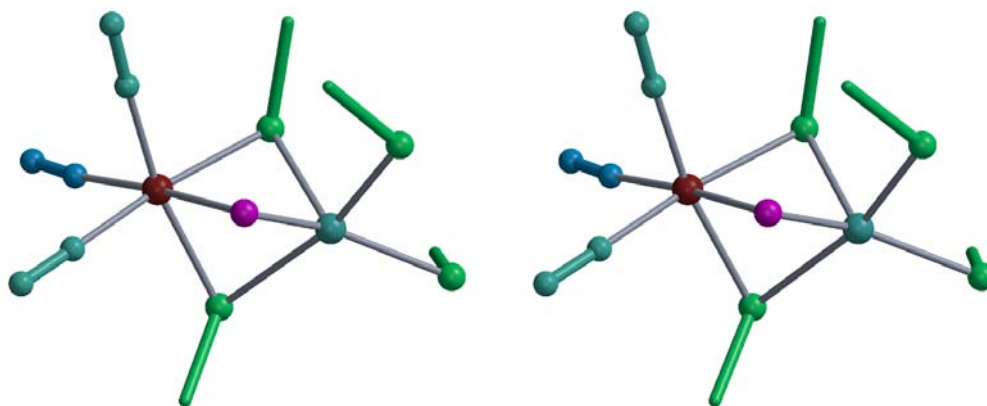


Fig. 2.3 Stereoview of the active site of the [NiFe] hydrogenase from DvMF in the oxidized state. One CO and two CN ligands of the iron atom are shown in blue and aqua respectively. Ni is shown in turquoise and the cysteine ligands in green. The bridging ligand of unknown nature is shown in purple. Figure kindly provided by Dr. Hideaki Ogata.

As the Ni-Fe active site is located at the center of the hydrogenase, electrons, protons, and molecular hydrogen need to move in channels through the protein structure for ~3 nm to reach the active site. For the electron transport, the chain of [FeS] clusters most probably serves as the pathway from the catalytic site to the electron acceptor.

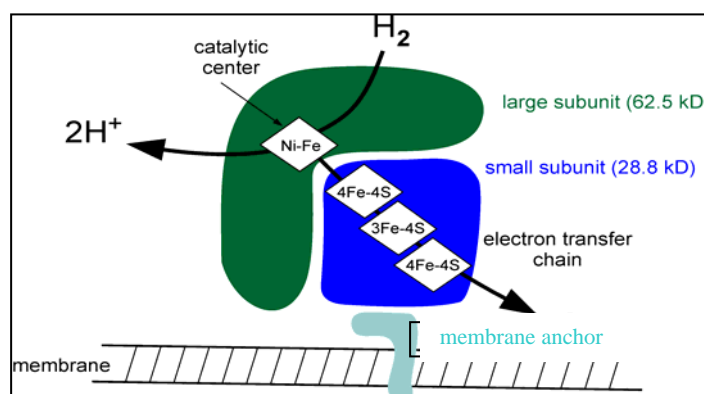
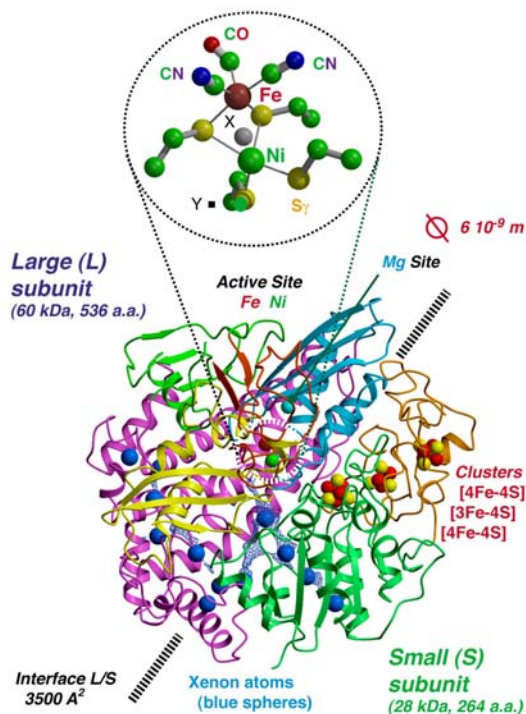


Fig 2.4 Electron transport chain from the [NiFe] active site to [FeS] clusters. Figure adapted from 'Hydrogen as a Fuel: Learning from nature'.

For the proton transfer pathway nothing concrete is known, but alternate, possible pathways have been proposed (Frey M., 2002). Probably, a chain of water molecules

and other groups serve as proton pathway, though a precise definition of any of such proposed pathway needs to be confirmed by mutagenesis studies.



The gas diffusion in hydrogenases was investigated by applying Xe-gas to hydrogenase crystals at elevated gas pressure (Montet *et al.*, 1997), leading to the conclusion that the hydrogen molecule does not simply diffuse through the protein randomly, but travel through specific hydrophobic channels. Since Xe has about the similar size as that of H<sub>2</sub>, an exposition of hydrogenase crystals to a high Xe pressure revealed Xe-binding sites in the enzyme interior from difference Fourier electron density maps. Ten Xe sites had been located in correlation with the calculated gas channels for *D. gigas* enzyme.

Fig. 2.5 [NiFe] hydrogenase from *D. gigas* showing the Xe sites marked with solid blue balls. Picture taken from Montet *et al.*, 1997.

### 2.3 Maturation pathway

The knowledge of the maturation pathway of hydrogenases is essential for attempts aiming at heterologous expression of the protein in larger amounts and in mutated form. However, the maturation turned out to be remarkably complex. The small subunit and the large subunit of [NiFe] hydrogenase are coded by *hynA* and *hynB* (commonly used nomenclature for *Desulfovibrio sp.*) respectively, present at the 5'-end of the operon coding for the enzyme. The presence of many genes coding for maturation and regulatory proteins downstream of the structural genes is known for a number of organisms, also from ~40 completed sequenced genome projects, and from ca. 100 hydrogenases sequenced. The accessory genes are organized in several transcription units. Some selected ones are compiled in table 9.1 in appendix. For few organisms, the role of these genes in maturation has been directly or indirectly identified by

constructing and characterizing specific mutants, especially for *Escherichia coli* and *Ralstonia eutropha*. The presence of such genes in *Desulfovibrio vulgaris* Hildenborough (DvH) has been recently reported from the genome sequence project (Heidelberg JF *et al.*, 2004), using sequence homology. For a detailed comparison of the genes present in DvH with those present in other organisms see chapter 4, table 4.1. From such comparisons, it appears clear that in the case of heterologous expression the maturation genes for the [NiFe] hydrogenase of the *Desulfovibrio* species are not provided by the host strain and would all need to be incorporated in the expression system.

The only exception from the functional selectivity appears to be hypG of *E. coli*, which belongs to hydrogenase 2, and is known to supplement the maturation of hydrogenase 1 also (Menon NK *et al.*, 1994). Also, the expression of *D. gigas* hydrogenase in *D. fructosovorans* has been reported, albeit with reduction to one sixth of the original expression (Rousset M *et al.*, 1998).

Beside the heterologous expression of [NiFe] hydrogenases, it is appropriate to mention here the recent report of the first heterologous expression of the [Fe] hydrogenase from *Chlamydomonas reinhardtii* in *E. coli* (Posewitz MC *et al.*, 2004) by cloning all the genes coding for the structural and maturational proteins in an expression vector and introducing it into the *E. coli* strain.

Though a function has been ascribed to most of the accessory proteins, the details of the maturation events in a cascade are still under extensive investigations and need further explanations. A brief account of the roles of the various genes as they are known now is introduced here, following the nomenclature as shown for DvH/ *E. coli* 3 in table 4.1 (since the nomenclature is not consistent between various organisms studied, a system DvH/ *E. coli* is used here). For a review on hydrogenase maturation, see Casalot and Rousset, 2001

The hynC/ hycI: endopeptidase

The hydrogenase large subunit has a 15 amino acid C-terminal sequence that is cleaved off as the last step of maturation, by an endopeptidase. It recognizes the conserved sequence His/Arg/Gln and cleaves following that. The crystal structure of hybD from

hydrogenase 2 of *E. coli* has been determined (Fritsche E *et al.*, 1999) at 2.2 Å resolution. It consists of a five-stranded β-sheet surrounded by three and four helices on each side, respectively. An aspartate at position 62, binding a cadmium (Cd) ion, has been considered important for catalysis (Theodoratou E *et al.*, 2005).

### The hypD/ hypC: chaperone/maturation

As the first step of the maturation, hypC forms a complex with the “pre” - large subunit, assisted by conserved cysteines (241, 244, 531, 534 for *E. coli* 3), to hold it in a proper conformation, which makes it accessible for metal insertion. The formation of a complex between hypC and hypD has been proved by a series of experiments on *E. coli* hydrogenase 3 (Blokesh M and Bock A, 2004).

### The hypA: Ni incorporation/maturation

This is a cysteine rich protein with four conserved cysteines, arranged in two CxxC motifs. They are suggested to be redox proteins carrying a [FeS] cluster. HypA cooperates with HypB in the insertion of nickel into the precursor of the large hydrogenase subunit (Olson JW *et al.*, 2001). The deletion of these genes blocks the protein maturation, which is partially restored by addition of nickel in high concentration (Hube M *et al.*, 2002).

### The hypB: Ni insertion

HypB protein has a conserved gene sequence, and specially the presence of His residues, pointing to a divalent metal binding function. These proteins were found to bind and store nickel (Rey *et al.*, 1994). HypB has a conserved GTP-binding motif at the carboxyl terminus, shown to be essential for nickel insertion (Maier, 1995; Olson JW, 1997; Olson JW and Maier RJ 2000).

### The hypD: CN/CO delivery

HypD is a monomeric protein possessing about four iron atoms per mol of protein. The iron atoms are present in a diamagnetic [4Fe-4S]<sup>(2+)</sup> cluster (Blokesh M *et al.*, 2004). A complex of hypD- hypC is formed in the maturation cycle.

### The hypE: Purine derivative binding, and CN/CO delivery

HypE together with hypF catalyzes the synthesis of the CN ligands of the active site iron of the NiFe-hydrogenases using carbamoylphosphate as a substrate (Blokesch M *et al.*, 2004). It consists of three domains, named 1, 2 and 3. Domain 1 and 2 show identity to a domain found in thiamine phosphate kinase, while domain 3 appears to be unique to the hypE proteins.

#### The hypF: CN/CO delivery

The active site assembly starts with the insertion of the three diatomic ligands of Fe. HypF plays a crucial role in this process together with hypE, though also hypD might be involved (Roseboom W *et al.*, 2005). It has a conserved domain with four CxxC motifs, resembling that of Zinc finger proteins and [FeS] cluster. The acylphosphatase domain is thought to support the conversion of carbamoylphosphate into CO. The 1.27 Å resolution HypF acylphosphatase domain crystal structure (Rosano C *et al.*, 2002) shows a domain fold of  $\beta\alpha\beta\beta\alpha\beta$  topology, as observed in mammalian acylphosphatases that specifically catalyze the hydrolysis of the carboxyl-phosphate bonds in acylphosphates.

### **Maturation of the large subunit**

The hypC protein forms a complex with pre-hycE, and keeps the precursor of the large subunit in the proper conformation throughout the entire processing. HypC, D, E, F interact with each other and with the pre-hycE and insert the diatomic CN and CO ligands, of iron in place. The synthesis of CN is mediated by carbamoyl phosphate (CP) (Blokesch M and Bock A, 2002). Acetyl-CoA synthase using acetate, most probably in the form of acetyl-CoA, catalyzes the incorporation of the CO ligand to iron in the appropriate place (Roseboom W *et al.*, 2005).

Whereas the insertion of Fe is not well understood, it is known that a complex of hypA and hypB delivers the Ni atom in a GTP hydrolysis-dependent reaction. The last identified step is the cleavage of 15 amino acid peptide sequence at the C-terminal of the large subunit, following a conserved histidine and insertion of Ni at the active side.



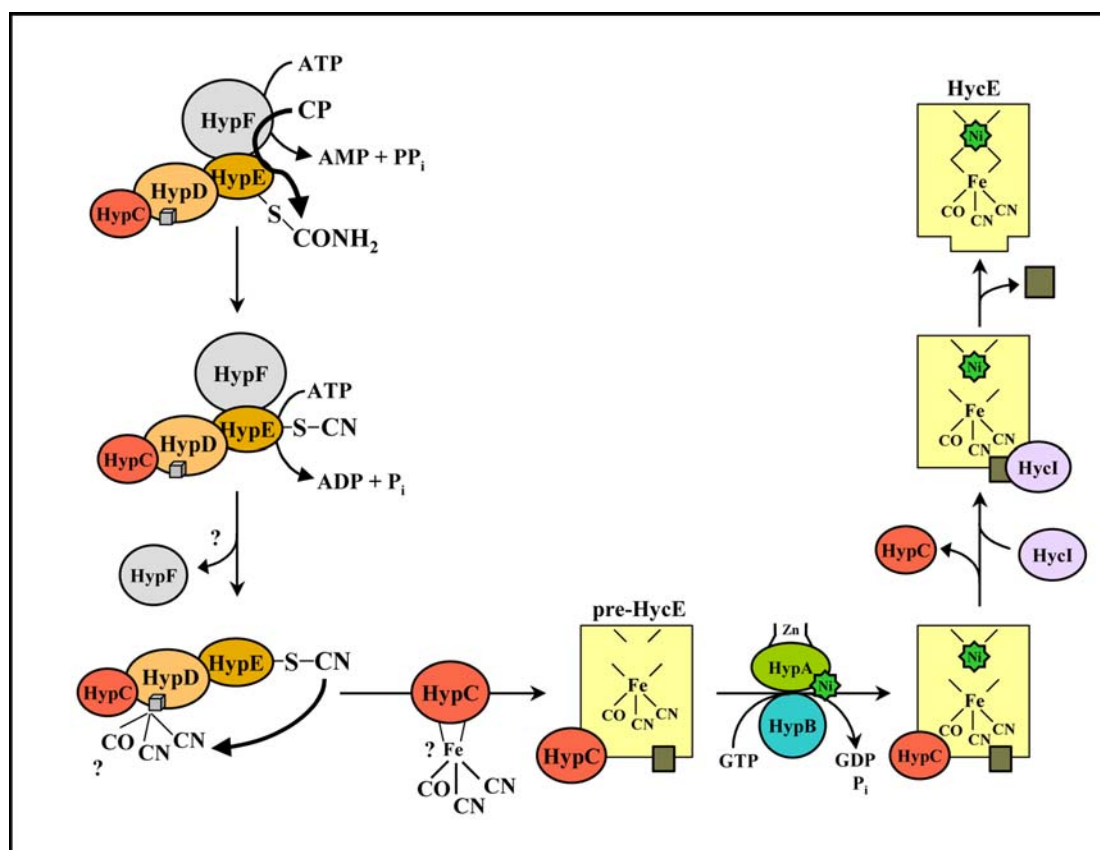


Fig. 2.6 The maturation pathway of the large subunit from *E. coli*. Modified from PhD thesis of Melanie Blokesch .

### Assembly of [NiFe] hydrogenase and transport across the membrane

The maturation of the large subunit takes place in the cytoplasm and the large subunit is then co-translocated with the small subunit, in a folded conformation, across the cytoplasmic membrane. None of the two subunits could be transported on its own (van Dongen *et al.*, 1988; Rodrigue A *et al.*, 1999). The N-terminus of the small subunit contains the conserved signal motif (S/T)-R-R-x-F-L-K (Voordouw G, 2000), which directs the export of the large and small subunit complex to the periplasm.

The small subunit is required both for the membrane targeting of the large subunit and for nickel acquisition (Rodrigue *et al.*, 1999). The interaction of the two subunits triggers the C-terminal cleavage of the large subunit and a conformational change of the complex, thus making the signal peptide accessible for proteolysis.

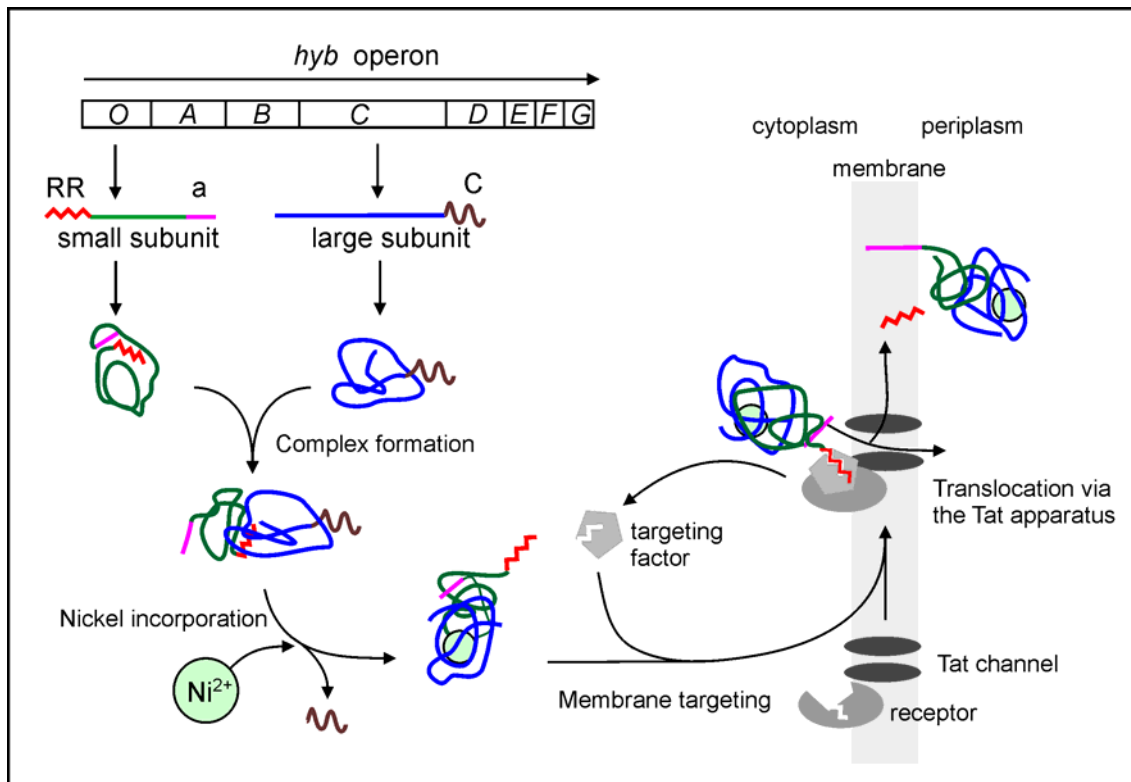


Fig. 2.7 The so-called “Hitchhiker” co-translocation of the large and the small subunit of [NiFe] hydrogenase. The twin-arginine signal peptide is indicated by *RR*, the C-terminal anchor sequence of the small subunit of hydrogenase 2 by *a*, the C-terminal extension sequence of the large subunit by *C*. Figure taken from Wu LF, *et. al.*, 2000.

The enzyme complex is recognized by a cytoplasmic targeting factor and translocated across the cytoplasmic membrane. Following the transport, the signal peptide is cleaved off and the complex is attached to the membrane with the C-terminal anchor of the small subunit.

## 2.4 Hydrogen cycling

A model for hydrogen cycling was first proposed by Odom and Peck in 1981 stating that, during growth on organic acids, molecular hydrogen is produced in the cytoplasm by a cytoplasmic hydrogenase from the oxidation of lactate or pyruvate, which then diffuses across the cytoplasmic membrane into the periplasm, where hydrogen splitting takes place. The generated electrons are then again imported across the membrane for cytoplasmic reduction of sulfate, whereas the generated protons are imported through ATP synthase for ATP synthesis.

The presence of cytoplasmic hydrogenases has been established for at least some species of *Desulfovibrio*: for *Desulfovibrio fructosovorans* (Casalot L *et. al.*, 2002) and for *Desulfovibrio vulgaris* Hildenborough (Heidelberg JF *et al.*, 2004), thus emphasizing the possibility of the proposed mechanism by Odom and Peck, as explained in more detail with the genome sequencing of DvH.

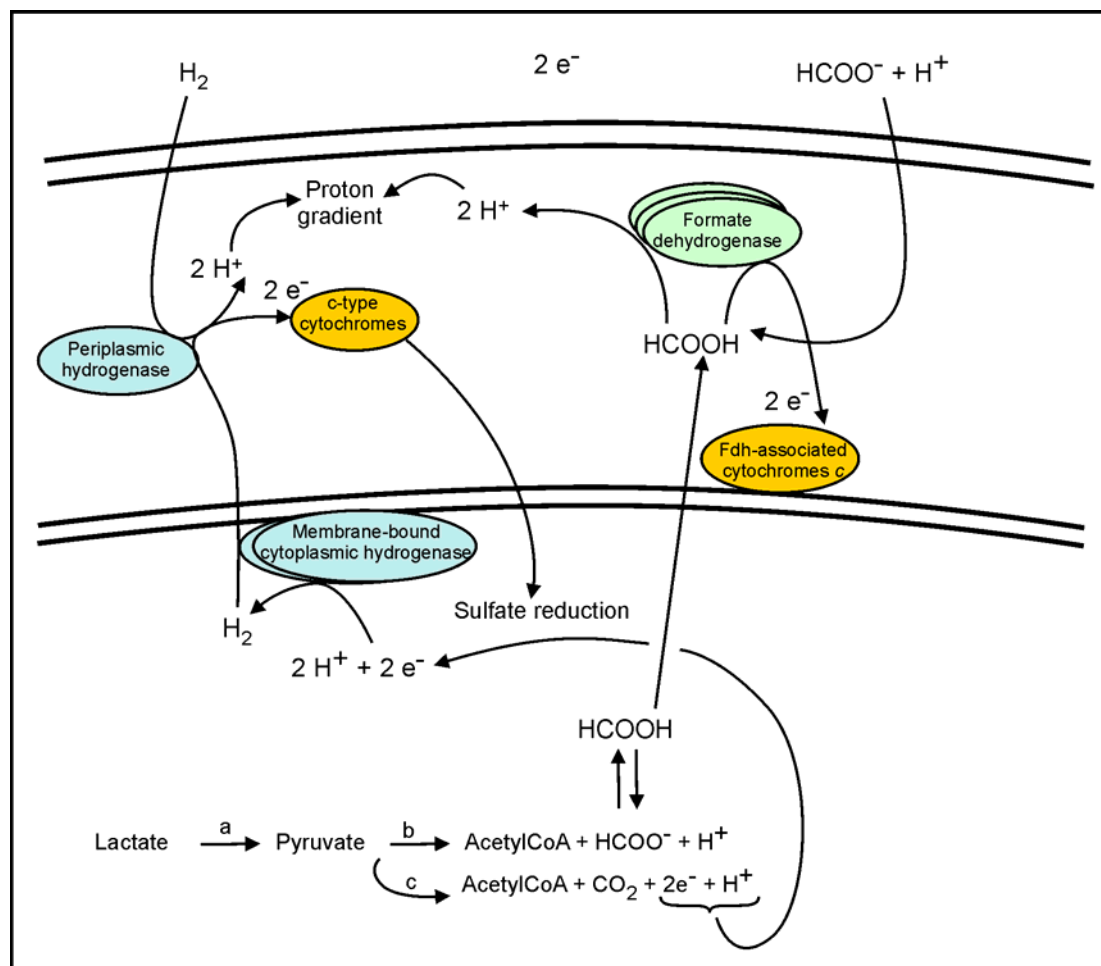


Fig. 2.8 Hydrogen and formate cycling in DvH. (fig adapted from Heidelberg JF *et. al.*, 2004). For hydrogen cycling, reducing equivalents ( $2\text{H}^+ + 2\text{e}^-$ ), generated from lactate or pyruvate oxidation, are suggested to be a substrate for one of the two membrane-bound hydrogenases that have a cytoplasmic orientation. The gaseous hydrogen diffuses to the periplasm where any of several candidate hydrogenases would oxidize the hydrogen while the released electrons are captured by the *c*-type cytochrome network. The electrons could then be channeled through the cytoplasmic membrane by one of several putative trans-membrane protein conduits.

The presence of multiple hydrogenases is best explained by taking their kinetic constants into account; enzymes with different  $K_m$  values and turnover number clearly can serve a role in environment with fluctuating H<sub>2</sub> concentrations (Voorodouw 1993). This helps bacteria to grow under different growth conditions, by switching between

several metabolic cycles. For example, the deletion of [NiFe] hydrogenase of *D. fructosovorans* and the deletion of [Fe] hydrogenase of DvH does not affect the bacterial growth in the presence of lactate and H<sub>2</sub> (Rousset M *et. al.*, 1991, Pohorelic BK *et. al.*, 2002), though the deletion mutant of [Fe] hydrogenase of DvH grew less well than the wild-type strain in media with sulfate as the electron acceptor and H<sub>2</sub> as the sole electron donor (Pohorelic BK *et. al.*, 2002). Also the deletion mutant of [NiFe] hydrogenase of DvH (generated in this thesis) shows similar growth behavior, as will be demonstrated later in this thesis (chapter 5).

The studies of deletion mutants have also provided insight into the complex metabolic pathways by looking at the specific role played by each enzyme. The physiological role of the periplasmic Fe-only hydrogenase and a hexadecaheme high molecular weight cytochrome c (Hmc)-complex from DvH in hydrogen uptake was similarly proposed (Pohorelic BK *et. al.*, 2002; Dolla A *et. al.*, 2000).

Very recently a model for electron transport in DvH species has been proposed (Guiral M *et. al.*, 2005) including the cytochrome c3 functioning as a central electron reservoir and shuttling electrons from [Fe] hydrogenase to HmC.

The hydrogen cycle can be very well explained for bacteria having multiple hydrogenases, but not much is known for the species containing single hydrogenases, for example the well characterized *D. vulgaris* Groningen (Hatchikian EC *et. al.*, 1995) and most probably DvMF and *D. gigas*. In these bacteria, the [NiFe] hydrogenase may be the only hydrogenase present, which is catalyzing the reaction in one or the other direction depending on the cellular requirements. Alternatively, there might be other metabolic pathways available. Preliminary growth studies experiments on *D. vulgaris* Miyazaki, performed by Tsuji and Yagi in 1980 lead to the observation that a net hydrogen evolution during early stages of growth is followed by its rapid uptake. Commencement of hydrogen uptake is followed by accumulation of hydrogen sulfide and hydrogen removal from the culture by argon sparging causes poor growth indicating that hydrogen is important to the growth of the cell. Still, a more detailed understanding of the growth metabolism of bacteria that contain single hydrogenase is needed.

## 2.5 Redox states

Since hydrogenases catalyse oxidation-reduction reactions, there are various different redox states of the active site and the [FeS] clusters. With each electron accepted or donated during the course of the reaction, a new redox state is formed. All these states are characterized as active-inactive, depending on whether the enzyme is ready to catalyze the reaction or dormant, and as “EPR active-silent” depending on the presence of an unpaired electron. There are several intermediates involved in the reaction cycle pathway.

The EPR active states have an unpaired electron, which is mainly localized on the Ni atom ( $S=1/2$ ) (Albracht SP *et al.*, 1982; Kojima N *et al.*, 1983). EPR experiments performed with a  $^{61}\text{Ni}$ -enriched protein sample from different bacteria (Lancaster JR Jr 1980; Graf EG and Thauer RK, 1981), showed the presence of hyperfine splittings ( $S=3/2$ ), indicating that the EPR signals originate from the Ni atom (details in chapter 6). The Fe atom is known to be diamagnetic ( $S=0$ ), and thus EPR silent (Huyett JE *et al.*, 1997) in all redox states of the active enzyme.

The aerobic purification of the enzymes yields a mixture of oxidized states, Ni-A and Ni-B (Fernandez VM *et al.*, 1985). The reduction of oxidized enzyme leads to activation, which can be achieved either by electrons under controlled conditions or in case of Ni-B by reduction in presence of hydrogen. It has been stated that electrons alone are sufficient to activate Ni-A, but more recent reports state that  $\text{H}_2$  is required in this process, thus the mechanism of activation of the unready (Ni-A) state is very different from that of the ready (Ni-B) state (Lamle SE *et al.*, 2004). Further reduction of the enzyme leads to the EPR detectable, active Ni-C state. Ni-C has been shown to carry two electrons more than Ni-A and Ni-B (Roberts LM and Lindahl PA 1994; Roberts LM and Lindahl PA. 1995; David P. *et al.*, 1994). Interestingly, the Ni-C state is light sensitive and can be converted at temperatures below 120 K upon illumination with strong light into Ni-L (Albracht S.P.J. 1994), which is a non-physiologically active state. The Ni-L state reverts back into Ni-C in the dark above 120 K. Further reduction of Ni-C leads to the EPR silent,  $\text{H}_2$  saturated Ni-R form. This cycle is shown schematically in fig. 2.9.

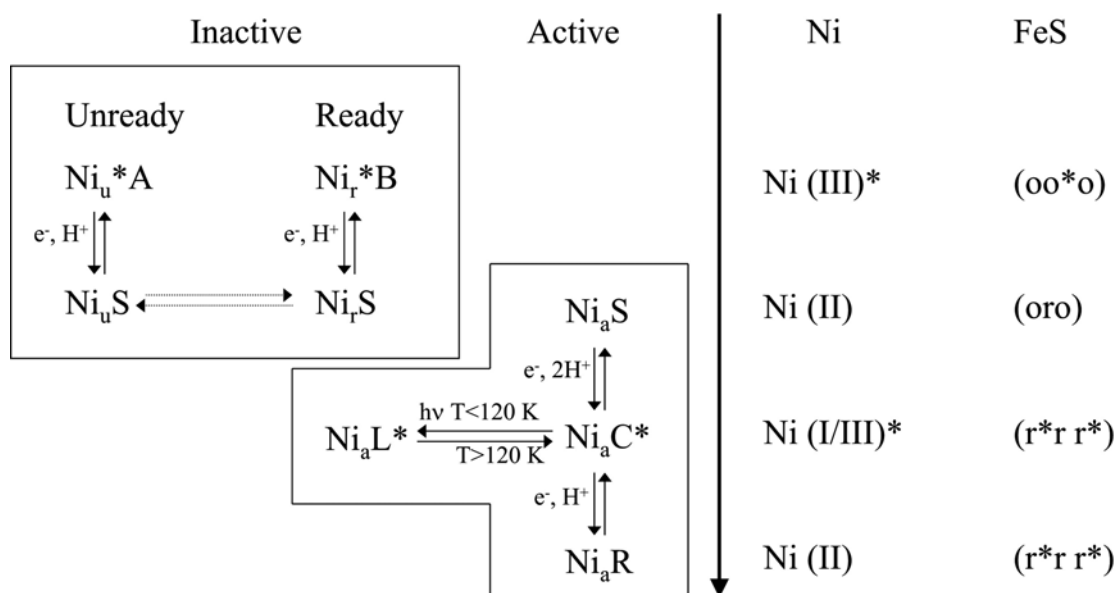


Fig 2.9 A simplified overview of the redox states for the Ni-Fe active site of the [NiFe] hydrogenase. States marked with \* are EPR active. The indices u, r, a (on the left hand side) stands for unready, ready and active respectively. The oxidation state of nickel and the [FeS] clusters are shown with o and r for oxidized and reduced (on the right hand side) respectively. The nomenclature for the [FeS] cluster is such that, the one closest to Ni stands for proximal, then middle and distal [FeS] cluster. The interconversion of Ni-A and Ni-B is not defined and probably goes through one of the reduced states (Lamle SE, *et al.*, 2004). The direction of arrow indicates the reducing potential.

The reduction of the [FeS] clusters, along with the Ni-Fe active site is also summarized in fig. 2.9. The interaction of proximal [4Fe4S] cluster in the reduced state leads to splitting of the Ni-C EPR signals and is detectable below 10-15 K (Teixeira M *et al.*, 1989; Cammack R, *et al.*, 1985). Also the reduced [3Fe4S] cluster shows a broad signal under at  $g=2.01$  under oxidising conditions.

While only the EPR active states can be studied using EPR spectroscopy, all states can be studied by FTIR spectroscopy, by monitoring the stretching frequencies of the diatomic ligands of the iron. The C=O stretching frequency around  $1930-1940 \text{ cm}^{-1}$  and the C $\equiv$ N stretching frequency above  $2040 \text{ cm}^{-1}$  have been used to characterize the redox states (Bagley KA *et al.*, 1985; de Lacey AL *et al.*, 1997; Davidson G, *et al.*, 2000). The best characterized FTIR-data for *D. gigas* and *A. vinosum* are presented in table 2.1.

Redox State	Infra-red bands $\text{cm}^{-1}$					
	<i>Allochromatium vinosum</i>			<i>Desulfovibrio gigas</i>		
	CO	CN		CO	CN	
Ni-A	1945	2083	2093	1947	2083	2093
Ni-B	1944	2079	2090	1946	2079	2090
Ni-C	1950	2074	2087	1952	2073	2086
Ni-L	1898	2043	2058			
Ni-R	1936	2059	2073	1940	2060	2073
Ni-SU	1950	2089	2099	1950	2089	2099
Ni-SI <sub>I</sub>	1910	2051	2067	1914	2055	2069
Ni-SI <sub>II</sub>	1932	2074	2086	1934	2075	2086

Table 2.1 Different redox states of the [NiFe] hydrogenase from *A. vinosum* (Davidson G, *et. al.*, 2000) and *D. gigas* (Volbeda, A, *et. al.*, 1996) characterized by the IR bands of the ligands of Fe at the active site.

As seen from the table, the shift in the IR bands is rather small between the different redox states of the hydrogenases, and may not be sufficient to characterize precisely the particular state. Thus a parallel approach using EPR and FTIR is required for an exact description of a particular state, which compensates for the shortcomings and combines the strength of each method.

## 2.6 Motivation of the work

With the increasing advance in scientific knowledge, and with the availability of more and more advanced techniques to study finer details of every facet using interdisciplinary approaches, it becomes possible to unfold the mysteries of nature turn by turn.

Following the detailed introduction on various aspects of hydrogenase research, as presented in this chapter, it is clear that by using these techniques, still a lot of work needs to be done to understand the hydrogen metabolism and the mechanism of action of hydrogenases.

DvMF [hydrogenase] has been studied much in detail. Its highly resolved crystal structure is available already. The study of the recombinant protein could give important information on the importance of individual amino acids for the mechanism of action of the enzyme. Since the heterologous expression is not yet known for *Desulfovibrio* species, homologous expression in the mutant lacking the structural genes could be a possibility. The function can be restored by reintroducing the genes on a compatible plasmid, following the study on mutants.

Also further knowledge about the various genes involved in the maturation pathway can lead to the expression in other hosts.

Besides the genetic modification of the enzyme, it can also be modified at the biochemical level.

Nickel is the “business end” of the enzyme, it carries the H<sub>2</sub> and helps to convert it. Fortunately the electron spin is at the Ni, but it has no magnetic isotopes. Therefore labeling it with <sup>61</sup>Ni is a possibility. The <sup>61</sup>Ni hyperfine interaction with the unpaired electron is the most sensitive probe for the electronic structure changes in the catalytic cycle and in the activation, inhibition and photo-conversion process. Together with DFT calculation it will yield the final proof for the structure of the intermediates.

The <sup>15</sup>N labeling identifies amino acids (having <sup>14</sup>N) that interacts with the spin center, e.g. via “ligation” or “H-bonding” and might reveal the electron transfer pathway.

Experiments related to bacterial growth under different conditions to achieve better efficiency of labeling needs to be attempted to improve the protocols.

Since in this thesis a variety of methods - biological and spectroscopic - have been applied to elucidate the function of the [NiFe]-hydrogenase from DvMF, a short theoretical introduction is given where-ever applicable or at the beginning of the various chapters that deal with particular techniques.





## Chapter 3

# Materials and Methods

### 3.1 Bacterial strains, plasmids and vectors (see table 3-1)

**Table 3-1 Bacterial strains, plasmids and vectors**

#### *Desulfovibrio vulgaris* subsp. *vulgaris*

Miyazaki F	IAM 12604.
Hildenborough	NCIMB 8303; isolated from clay soil near Hildenborough, United Kingdom, source of the [NiFe] hydrogenase gene used here; Cm <sup>S</sup> , Suc <sup>R</sup> (Postgate, 1984).
<i>D. vulgaris</i> hyn 1	a derivative of Hildenborough with pNotΔNiFeCm Mob integrated into its chromosome; Km <sup>R</sup> , Cm <sup>R</sup> , Suc <sup>S</sup> (this study).
Hyn 100	A [NiFe] hydrogenase gene deletion derivative of Hildenborough. The hydrogenase gene was interrupted by inserting a cat gene cassette from pUC19Cm; Km <sup>R</sup> , Cm <sup>R</sup> , Suc <sup>R</sup> (this study).

#### *Escherichia coli*

<i>E. coli</i> TG2	<i>supE hsdΔ5 thi Δ(lac-proAB) Δ(srl-recA) 306::Tn10 (Tet<sup>r</sup>) F' [traD36 proAB<sup>+</sup> lacI<sup>q</sup> lacZΔM15]</i> (Sambrook <i>et al.</i> , 1989).
--------------------	---

- E. coli* S17-1      *thi pro hsdR hsdM<sup>+</sup> recA* RP4-2 (Tc::Mu Km::Tn7) (Simon *et al.*, 1983)
- E. coli* Dh5 $\alpha$       *supE44 dlacU169 (p80 lacZdM15) hsdR17 recA1 endA1 gyrA96 thi-1 relA1* (Hanahan, 1985).
- E.coli*(BL21DE3RIL)B F<sup>-</sup> *ompT hsdS (r<sub>B</sub><sup>-</sup>m<sub>B</sub><sup>-</sup>) dcm<sup>+</sup> Tet<sup>r</sup> gal endA Hte [argU, ileY, leuW, Cam<sup>r</sup>]*.

### Plasmids

- pUC19Cm      plasmid pUC19 carrying the *cat* gene (1.4 kb Sac II-Tth111I fragment from pSUP104) inserted at its BamHI site, a 1.4 kb SacII- Tth111I fragment from pSUP104 (Fu *et al.*, 1997).
- pNOT19      modified pUC19 cloning vector; NdeI site replaced by a NotI site (Schweizer, 1992).
- pMOB2      Contains *oriT* of plasmid RP4 and *Bacillus subtilis sacBR* genes on a 4.5-kb NotI fragment; Km<sup>R</sup> Cm<sup>R</sup> (Schweizer, 1992).
- pNotNiFe      pNot19 containing the [NiFe] hydrogenase gene of DvH on a 4.0 kb HindIII-KpnI fragment; Ap<sup>R</sup> (this study).
- pNot $\Delta$ NiFe      A reverse PCR product of pNotNiFe with the 2.5 kb gene fragment deleted, but still containing 750bp flanking sequence of [NiFe] hydrogenase gene on both sides of pNot19, with BamHI sites at the free ends of PCR product; Ap<sup>R</sup> (this study).
- pNot $\Delta$ NiFeCm      pNot $\Delta$ NiFe with *cat* gene insertion at BamHI site; Cm<sup>R</sup>, Ap<sup>R</sup> (this study).
- pNot $\Delta$ NiFeCmMob      A mobilizable derivative of pNot $\Delta$ NiFeCm containing a *mob-sac* cassette from pMob2 in the NotI site; Suc<sup>S</sup>, Cm<sup>R</sup>, Ap<sup>R</sup> (this study).
- pNotMNiFeN      pNot19 containing the N- terminal [NiFe] hydrogenase gene of DvMF on a 774 bp HindIII-BamHI fragment; Ap<sup>R</sup> (this study).
- pNot $\Delta$ MNiFe      Ligation of a 776bp BamHI-KpnI C- terminal fragment of [NiFe] hydrogenase gene, following N- terminal of pNotMNiFeN; Ap<sup>R</sup> (this study). Resulting in deletion of 1.9 kb gene fragment.

---

pNotΔMNiFeCm	pNotΔMNiFe with a <i>cat</i> gene inserted at BamHI site; Cm <sup>R</sup> , Ap <sup>R</sup> (this study).
pNotΔMNiFeCmMob	A mobilizable derivative of pNotΔMNiFeCm containing a <i>mob-sac</i> cassette from pMob2 in the NotI site; Suc <sup>S</sup> , Cm <sup>R</sup> , Ap <sup>R</sup> (this study).
pNFC	pUC19 containing the 2kb SphI fragment of DvMF chromosomal DNA, coding for [NiFe] hydrogenase operon, downstream of <i>hynA</i> and <i>hynB</i> (this study).
pNFAB	pUC19 containing <i>hynA</i> and <i>hynB</i> of DvMF [NiFe] hydrogenase gene on a 3.1 kb HindIII fragment (this study).
pMBAD	pMosBlue containing DvMF [NiFe] hydrogenase operon on a 4.1 kb HindIII fragment (this study).
pJRDAB	pJRD215 containing <i>hynA</i> and <i>hynB</i> of DvMF [NiFe] hydrogenase operon on a 2.9 kb HindIII fragment (this study).
pETC	pET28a containing <i>hynC</i> from DvMF [NiFe] hydrogenase operon on a 550 bp NdeI- HindIII fragment (this study)

## 3.2 Chemicals and Enzymes

### 3.2.1 Chemicals

All chemicals and reagents used throughout this work were of analytical grade or of maximal purity available and were obtained from Merck (Darmstadt), Sigma (Deisenhofen), Serva (Heidelberg), DIFCO (Detroit, USA), Gibco/BRL (Eggenstein), Biomol (Hamburg), Pharmacia (Freiburg), ICN Biomedicals (Aurora, USA) and BioRad (München). Chelex resin (used for metal exchange/removal from buffer and media for minimal medium preparation for labeling experiments) was from Biorad.

### 3.2.2 Enzymes

Restriction enzymes and DNA-modifying enzymes were from AGS (Heidelberg), Boehringer Mannheim (Mannheim), Pharmacia (Freiburg), Stratagene (Heidelberg),

USB (Cleveland, USA) and NEB (New England Biolabs) (Schwalbach/Taunus). Oligonucleotides were custom-synthesized by Metabion (Martinsried).

### 3.2.3 Antibodies

Primary Antibody: - DvMF [NiFe] hydrogenase specific polyclonal antibody was prepared by Eurogenetec (Belgium).

Secondary Antibody: - Antirabbit immunoglobulins were from DAKO (Hamburg).

### 3.2.4 Isotopes

#### 3.2.4.1 Radioactive Isotope

[ $\alpha$ -<sup>32</sup>P]dCTP was from ICN Biomedicals (Canada).

#### 3.2.4.2 Non-Radioactive Isotope

<sup>61</sup>Ni metal (92%):- Campro Scientific, Veenendaal, Netherlands.

<sup>15</sup>N His (<sup>15</sup>N3, 98%):- Cambridge Isotope Laboratories, Inc. USA

### 3.2.5 Kits

QIAquick® PCR purification kit	QIAGEN
QIAquick® Gel extraction kit	QIAGEN
Dneasy® Tissue kit	QIAGEN
Perfectprep® Plasmid Mini	Eppendorf
Perfectprep® Plasmid Midi	Eppendorf
Bradford assay kit	Biorad

### 3.3 Media and Solutions

Media were sterilized by autoclaving. Filtration, if necessary, was done through 0.22  $\mu\text{m}$  filter, to sterilise heat labile components. Millipore distilled threefold deionised water was used for preparing media and buffers. For the minimal medium preparation for *Desulfovibrio* cultures, chelex-cleaned-water was prepared by using a chelex resin column. Chelex resin binds metal ions selectively and thus cleans the solution, of any metal contamination.

#### *E. coli* medium

<b>LB:</b>	10 g/l NaCl, 5 g/l yeast extract, 10 g/l tryptone
<b>LB-agar:</b>	10 g/l NaCl, 5 g/l yeast extract, 10 g/l tryptone, 15 g/l agar
<b>TBY:</b>	16 g/l tryptone, 10 g/l yeast extract, 5 g/l NaCl
<b>TBY-agar:</b>	16 g/l tryptone, 10 g/l yeast extract, 5 g/l NaCl, 15 g/l agar
<b>SOC:</b>	20 g/l tryptone, 5 g/l yeast extract, 1% (v/v) 1 M NaCl, 0.25% (v/v) 1 M KCl, 1% (v/v) filter sterilized 2 M $\text{Mg}^{2+}$ stock (1 M $\text{MgCl}_2$ ; 1 M $\text{MgSO}_4$ ), 1% (v/v) filter sterilized 2 M glucose stock.

#### *Desulfovibrio* Medium

<b>PB</b>	0.5 g/l $\text{KH}_2\text{PO}_4$ , 1 g/l $\text{NH}_4\text{Cl}$ , 1 g/l $\text{CaSO}_4$ , 2 g/l $\text{MgSO}_4 \cdot 7\text{H}_2\text{O}$ , 3.5 g/l sodium lactate (70%), 1 g/l yeast extract, 0.1 g/l ascorbic acid, 0.1 g/l thioglycolate, 0.5 g/l $\text{FeSO}_4 \cdot 7\text{H}_2\text{O}$ (adjusted to pH 7.0-7.4) Purpose: preparation of stock cultures.
<b>PC</b>	0.5 g/l $\text{KH}_2\text{PO}_4$ , 1 g/l $\text{NH}_4\text{Cl}$ , 4.5 g/l $\text{Na}_2\text{SO}_4$ , 0.06 g/l $\text{CaCl}_2 \cdot 6\text{H}_2\text{O}$ , 0.06 g/l $\text{MgSO}_4 \cdot 7\text{H}_2\text{O}$ , 6 g/l sodium lactate (70%), 1 g/l yeast extract, 0.004 g/l $\text{FeSO}_4 \cdot 7\text{H}_2\text{O}$ , 0.3 g/l sodium citrate (adjusted to pH 7.5) Purpose: routine DvH culture growth broth.
<b>PE</b>	0.5 g/l $\text{KH}_2\text{PO}_4$ , 1 g/l $\text{NH}_4\text{Cl}$ , 1 g/l $\text{Na}_2\text{SO}_4$ , 1 g/l $\text{CaCl}_2 \cdot 6\text{H}_2\text{O}$ , 2 g/l $\text{MgCl}_2 \cdot 7\text{H}_2\text{O}$ , 3.5 g/l sodium lactate (70%), 1 g/l yeast extract, 0.5 g/l $\text{FeSO}_4 \cdot 7\text{H}_2\text{O}$ , 15 g/l agar (adjusted to pH 7.6)

	Purpose: routine culture growth plates.
<b>PE/KNO3</b>	500 ml PE, 1.5 g KNO <sub>3</sub> , 7.5 g agar Purpose: plates for conjugation.
<b>FM</b>	4 g/l Na <sub>2</sub> SO <sub>4</sub> , 0.6 g/l MgSO <sub>4</sub> ·7H <sub>2</sub> O, 0.4 g/l KH <sub>2</sub> PO <sub>4</sub> , 3 g/l tryptone, 0.8 g/l yeast extract, 10ml sodium lactate (50%), 0.01 g/l FeSO <sub>4</sub> ·7H <sub>2</sub> O, 5ml 10% antifoam to 8L media Purpose: fermentation in 10L flask, for DvMF: 8L media, 1.5L culture as inoculum.
<b>MM</b>	0.5 g/l KH <sub>2</sub> PO <sub>4</sub> , 4.5 g/l Na <sub>2</sub> SO <sub>4</sub> , 0.04 g/l CaCl <sub>2</sub> ·2H <sub>2</sub> O, 0.06 g/l MgSO <sub>4</sub> ·7H <sub>2</sub> O, 0.3 g/l sodium citrate, 20 ml sodium lactate (25%, chelexed), 0.01 g/l FeSO <sub>4</sub> (1 ml of the stock solution (to be added after autoclaving)), 5 ml of “each amino acid stock” (to be added after autoclaving, chelexed), 1 ml trace element stock (to be added after autoclaving), 1.3 mg/l NiCl <sub>2</sub> (to be added after autoclaving), 5 ml 10% antifoam to 8 L media Purpose: isotope labeling of protein.
<b>AA stock I</b>	10 g/l Ala, 4 g/l Arg, 2 g/l Cys, 4 g/l Gly, 1 g/l Lys, 4 g/l Met, 6 g/l Pro, 6 g/l Ser, 8 g/l Thr, 2 g/l Trp
<b>AA stock II</b>	8 g/l Asp, 16 g/l Glu, 2 g/l His, 8 g/l Leu, 6 g/l Phe, 8 g/l Tyr, 8 g/l Val
<b>Trace Elements -Stock</b>	1.5 g/l FeCl <sub>2</sub> ·4H <sub>2</sub> O, 60 mg/l H <sub>3</sub> BO <sub>3</sub> , 120 mg/l CoCl <sub>2</sub> ·6H <sub>2</sub> O, 70 mg/l ZnCl <sub>2</sub> , 15 mg/l CuCl <sub>2</sub> ·2H <sub>2</sub> O, 25 mg/l NaMoO <sub>4</sub> ·2H <sub>2</sub> O

### Antibiotic Solutions

All water-soluble antibiotics were filter sterilized.

<b>Ampicillin</b>	25 mg/ml in H <sub>2</sub> O
<b>Chloramphenicol</b>	20 mg/ml in ethanol
<b>Kanamycin</b>	10 mg/ml in H <sub>2</sub> O
<b>Streptomycin</b>	10 mg/ml in H <sub>2</sub> O

**Southern Blot**

<b>20xSSC</b>	88.2 g/l sodium citrate, 175.4 g/l NaCl (pH 7.2)
<b>SSC/ SDS</b>	50 ml 20xSSC, 20 ml 10% SDS, adjust volume to 1 L.
<b>Prehybridization- -fluid</b>	60 ml 20xSSC, 50 ml 10% SDS, 100 ml 50*DH, 5 ml ss DNA, adjust volume to 1 L.
<b>DH</b>	10 g/l Ficoll, 10 g/l polyvinyl pyrrolidone, 10 g/l BSA, to be stirred O/N for complete dissolution.

**SDS-PAGE and Western Blot**

<b>2x Laemmli Buffer</b>	100 mM tris HCl (pH 6.8), 200 mM DTT, 4 % (w/v) SDS, 0.2 % (w/v) bromophenol Blue, 20 % (v/v) glycerol
<b>Coomassie Stock</b>	1 tablet of phastgel blue R in 200 ml 60 % (v/v) methanol (gives a 0.2% coomassie blue R solution)
<b>Coomassie staining</b>	1 volume coomassie stock, 1 volume 20 % acetic acid
<b>Tank Buffer</b>	25 mM tris base, 150 mM glycine, 20 % methanol
<b>TBS</b>	10 mM tris HCl (pH 7.5), 150 mM NaCl
<b>TBST</b>	20 mM tris HCl (pH 7.5), 500 mM NaCl, 0.05 % (v/v) tween-20
<b>Block Buffer</b>	3 % (w/v) BSA in TBS buffer
<b>NBT stock</b>	5 % NBT in 70 % DMF
<b>BCIP stock</b>	5 % BCIP in 100 % DMF
<b>Buffer A</b>	100 mM tris HCl (pH 9.5), 100 mM NaCl, 5 mM MgCl <sub>2</sub>
<b>Buffer AP</b>	44 µl NBT stock, 33 µl BCIP stock in 10 ml Buffer A

**Native PAGE**

<b>TBE</b>	10 mM tris borate EDTA (pH 8.3)
<b>Phosphate buffer</b>	50 mM phosphate buffer (pH 7.0)
<b>Triton detergent</b>	2% triton X-117
<b>Loading buffer (5X)</b>	60 mM tris HCl (pH 6.8), 25% glycerol, 0.1% bromo phenol blue

**Hydrogenase activity assay**

<b>PMS</b>	0.09 mM Phenazine methosulfate
------------	--------------------------------



<b>NBT</b>	0.06 mM Nitroblue Tetrazolium
<b>BV</b>	0.5 mM Benzyl viologen
<b>DTT</b>	60 mM Sodium dithionite/ Sodium hydrosulfite
<b>TTC</b>	1 mM Triphenyl tetrazolium chloride

### **Electrochemical analysis buffers**

<b>For H<sub>2</sub> uptake</b>	100 mM TrisCl (pH 8.5), 0.1 mM MV
<b>For H<sub>2</sub> production</b>	100 mM (CH <sub>3</sub> COO)Na (pH 5.6), 0.1 mM MV

### **Other Solutions**

<b>EP</b>	0.5 mM HEPES (pH 7.6), 10 % glycerol
<b>6*Loading Buffer</b>	0.25 % (w/v) bromophenol blue, 0.25 % (w/v) xylene cyanol FF, 30% (v/v) glycerol
<b>TE</b>	10 mM tris HCl (pH 8.0), 1 mM EDTA
<b>TAE</b>	50 mM tris acetate, 1 mM EDTA (pH 8.0)

## **3.4 Microbiology and molecular biology techniques**

### **3.4.1 Cell cultures**

#### **3.4.1.1 *E. coli* cell culture**

*E. coli* cell cultures were grown in LB with appropriate antibiotics, at 37°C, 180 rpm, O/N. A single isolated colony was used to inoculate culture volumes up to 150 ml. For large-scale cultures, 1% inoculum was used.

#### **3.4.1.2 *Desulfovibrio* cell culture**

10 ml agar cultures, or 5 ml PB stock cultures were used as inoculum to start in parallel three 50 ml cell cultures. Screw-capped glass bottles with the center of the lid replaced by a septum for gas exchange were used for all culture growth. Cultures of 50 ml, grown for two days were used to inoculate 500 ml medium. All inoculations were done in

anaerobic glove boxes. Three 500 ml cultures, grown for two days were used to inoculate one 10 L glass bottle fermentor, containing 8 L medium.



Fig. 3.1 Home built 10-litre glass fermentor. Water bath is used to maintain the temperature at 37°C. pH is maintained in a range of 7.0-7.4, with 1M H<sub>2</sub>SO<sub>4</sub> connected via a manually controlled pump. Fermentor is maintained anaerobic by bubbling with N<sub>2</sub>. Inoculum is added through the same pump as for acid.

The fermentor was maintained anaerobic by constantly bubbling with nitrogen. 1 M H<sub>2</sub>SO<sub>4</sub> was added during growth, in order to maintain the pH around 7-7.4. Cells were allowed to grow for three days in the fermentor with an addition of 400 ml of 25 % sodium lactate (chelexed, autoclaved) on the second and the third day morning. Cells were harvested by centrifugation at 6000 rpm, 4°C, and 30 minutes. Wet cell-yield with minimal medium was standardised to be 15-20 g per 10 L fermentor, which was comparable to the yield from the full medium. Cells were kept frozen at -80°C, until lysed for protein purification. 60-80 g wet cell mass were used for one protein purification.

### **3.4.2 Chromosomal DNA isolation**

#### **3.4.2.1 Dneasy® Tissue kit**

One ml of an O/N grown culture in an Eppendorf tube was spun down for a minute (13,000 rpm), and subjected to the protocol of the manufacturer. Yields were comparably less than the other protocol (chapter 3.4.2.2), but still sufficient for most purposes.

#### **3.4.2.2 Chromosomal DNA isolation protocol**

Cells from a 1.5- 5 ml of an O/N grown culture were harvested through centrifugation, washed with 500  $\mu$ l 0.1M NaCl/0.15 M EDTA. Cells were resuspended in 280  $\mu$ l 0.1 M NaCl/0.15 M EDTA, followed by the addition of 20  $\mu$ l lysozyme solution (5 mg/ml), and incubated for 10 minutes at 37°C. To this cell suspension, 24  $\mu$ l SDS (25%) were added, and incubated for 5 minutes at 60°C. Then 72  $\mu$ l of 5 M NaClO<sub>4</sub> and 420  $\mu$ l iso-amyl alcohol were added and kept on a moving wheel for one hour to denature and precipitate proteins. After centrifugation (10,000 rpm, 3.5 minutes, at RT), the upper clear phase was collected in a new Eppendorf tube and twice the volume of 95% ethanol (-20°C) was added and mixed by inverting the tube several times. DNA was pelleted by centrifugation (15 minute, 13,000 rpm, 4°C). The DNA pellet was dissolved in 200  $\mu$ l TE. 20  $\mu$ l RNase (1 mg/ml) were added to this solution, which was incubated at RT for one hour, followed by addition of 10  $\mu$ l of ProteinaseK (10 mg/ml), and another incubation at RT for one hour. To this solution, 80  $\mu$ l of phenol were added, followed by incubation at RT for 10 minute. The incubation mixture was then centrifuged for 3 minutes. The supernatant was collected, and 500  $\mu$ l of DNA precipitation mix (2.5-times the volume) were added. It was then centrifuged for 10 minutes at 4°C.

The DNA pellet was resuspended in 50-200  $\mu$ l TE, depending on the size of the pellet. The concentration of DNA was determined (see 3.4.7) and stored at 4°C until further use.

### 3.4.3 Plasmid DNA isolation

Perfectprep® Plasmid Mini and Perfectprep® Plasmid Midi kits from Eppendorf were used for small and large-scale plasmid preparations, respectively, according to the manufacturer's protocol.

### 3.4.4 Polymerase chain reaction

Two different DNA polymerase enzymes, Taq and Pfx (providers Promega and Invitrogen, respectively) were used, and the manufacturer's protocol was followed for concentration and volume of the reaction mix, with only little modifications.

Taq procedure: - for one 50 µl reaction, 5 µl of amplification buffer, 4 µl MgCl<sub>2</sub>, 1 µl dNTP mix (10 µM each), 2 µl of each primer (25 pmol/µl), 1-200 ng of template DNA and 1.25 U (0.5 µl) Taq were mixed and brought, to a final volume of 50 µl with tri-distilled autoclaved H<sub>2</sub>O.

Pfx procedure:- for one 50 µl reaction, 5 µl of amplification buffer, 1.5 µl MgSO<sub>4</sub>, 1.5 µl dNTP mix (10 µM each), 2 µl of each primer (25 pmol/µl), 1-200 ng of template DNA, and 1.25 U (0.5 µl) Pfx were mixed and brought, to a final volume of 50 µl with tri-distilled autoclaved H<sub>2</sub>O.

A three step cycling PCR reaction was performed to amplify the target DNA. A DNA denaturation step (94°C, 2 minutes) was followed by 30 amplification cycles. Each cycle consisted of denaturation (94°C, 1 minute), annealing (50-65°C, 30-40 seconds, depending on the T<sub>m</sub> of the primers) and amplification (69°C for Pfx or 74°C for Taq) for 30 seconds to 4 minutes, depending on the template DNA to be amplified (1 kb/minute). The amplified DNA was controlled on agarose gel by loading 5 µl of the reaction mix.

### **3.4.5 Agarose gel electrophoresis**

Agarose gels of 0.8-1.3 % were used to resolve DNA fragments of 10 kb to 0.5 kb, respectively. Gels were prepared and run in TAE buffer. 0.2 volumes of 6x loading buffer were added to the DNA and run at 5 V/cm. A 1 kb DNA ladder (NEB) or HindIII-digested  $\lambda$  was used as a size standard. DNA was visualized by illumination with UV light.

### **3.4.6 Isolation of DNA from agarose**

After separation by agarose gel electrophoresis, DNA fragments were cut out from the gel and extracted by using the QIAquick® Gel extraction kit following the manufacturer's protocol.

### **3.4.7 Determination of DNA concentrations in aqueous solution**

The most accurate method is the measurement of the absorbance at 260 nm, using for a pure DNA sample ( $A_{260}/A_{280} = 1.8-2.0$ ) a value of,  $A_{260} = 1$  for 50  $\mu\text{g/ml}$ .

Since the 1 kb ladder size marker from NEB has defined concentrations for each band of different size, the DNA concentration can be estimated by comparison.

Another method for evaluating the amount of DNA is based on the spotting of various dilutions of known concentration of a standard solution along with the unknown sample on an ethidium bromide agar plate followed by incubation in the dark for one hour. When viewed in UV illumination, the respective intensities of bands can be used for concentration determination.

### **3.4.8 Restriction digestion**

Various restriction enzymes were used for digesting PCR-amplified DNA or plasmids for preparing them for ligations, for checking the correctness of a given gene fragment with the restriction sites derived from computation. Temperature and buffer were used

according to the manufacturer's protocol for each restriction enzyme, reactions lasting 30 minutes to O/N. Restriction digestions were controlled by checking the reaction product on an agarose gel.

### **3.4.9 Dephosphorylation**

Vectors that are restriction-digested with a single restriction enzyme can religate. To avoid this, they can be dephosphorylated with calf intestinal phosphatase (CIP) (provider Invitrogen) following the manufacturer's instructions. The digested and dephosphorylated vector was purified using agarose gel extraction or PCR purification kit chapter 3.4.10).

### **3.4.10 Desalting of DNA solutions**

Desalting of DNA reaction mixtures for subsequent enzymatic reactions and to remove primers from PCR reactions was accomplished by QIAquick PCR purification kit (Qiagen) using manufacturer's protocol.

### **3.4.11 Ligation reactions**

Restriction-digested and dephosphorylated plasmid DNA and restriction digested insert-DNA were desalted using QIAquick® PCR purification kit before ligation. A molar ratio of roughly 1:2.5 was used between linearised plasmid and insert-DNA. Ligase with buffer (provided with enzyme) and H<sub>2</sub>O was added to a final volume of 10-20 µl. The ligation reaction was allowed to run for five hours or up to O/N, 3-4 µl of ligation mixture was used for transformation purposes.

### **3.4.12 Preparation of *E. coli* competent cells and DNA transformation**

#### **3.4.12.1 Preparation of CaCl<sub>2</sub> competent *E. coli* cells**

From an O/N grown culture, 0.2 ml were used to inoculate 5 ml TBY medium. The culture was allowed to grow in a shaker for 2-3 hours (37°C, 180 rpm), to an OD<sub>600</sub> of

0.6-0.8. The cells were harvested by centrifugation (5 minutes, 3,000 rpm, 4°C). The cell pellet was resuspended in 3 ml of ice-cold CaCl<sub>2</sub> solution (0.1 M). After incubating in ice for 20 minutes, cells were again pelleted, and resuspended in 1 ml of ice-cold CaCl<sub>2</sub> solution (0.1 M). 35 µl of DMSO were added to this solution. After gently mixing, the cells were incubated on ice for another 15 minutes. Finally, 35 µl of DMSO were added and aliquots of 200 µl were dispensed in the Eppendorf tubes. These were immediately frozen in liquid N<sub>2</sub> and stored at -70°C, until used.

#### **3.4.12.2 Transformation of CaCl<sub>2</sub> competent *E. coli* cells**

Competent cells were thawed on ice, and the DNA to be transformed was added, mixed gently, and incubated on ice for 30 minutes. The cells were then subjected to a heat shock at 42°C for 90 seconds and immediately transferred back to ice. 200 µl of SOC were added and the transformed cells were incubated at 37°C for one hour. Three dilutions (10<sup>-2</sup>, 10<sup>-4</sup>, 10<sup>-6</sup>) of the cells were plated on appropriate antibiotics-containing LB plates and incubated O/N at 37°C.

#### **3.4.12.3 Preparation of electrocompetent *E. coli* cells**

Electrocompetent *E. coli* cells were prepared according to Dower *et al.*, (1988). One liter of TBY medium was inoculated with 10 ml of an overnight culture of *E. coli* DH5α or *E. coli* S17-1 cells, and grown in a rotary shaker at 37°C and 180 rpm to an OD<sub>600</sub> of 1.0. After cooling the cells on ice for 15 minutes, they were centrifuged for 10 minutes (5000 rpm, 4°C). The cell pellet thus obtained was resuspended in a total of 450 ml of ice-cold EP-medium, and was centrifuged three more times under the same conditions as described. After the first centrifugation they were resuspended in 350 ml EP-medium, after the second turn in 200 ml EP-medium and after the last centrifugation step in 2 ml EP-medium, resulting in a final volume of about 3.5 ml. The cells were either used directly or frozen in liquid nitrogen in aliquots of 200 µl and stored at -70°C.

#### 3.4.12.4 Transformation of electrocompetent *E. coli* cells

After thawing the electrocompetent cells on ice, 100  $\mu$ l of the cells were mixed with 0.5 to 4  $\mu$ l of DNA and again placed on ice. The mixture of cells and DNA was pipetted onto the bottom of a pre-chilled electroporation cuvette. The cuvette was then placed in the cuvette holder of the Gene Pulser (BioRad) and a pulse was applied (2.4 kV, 200  $\Omega$ , 25  $\mu$ F). Immediately after the pulse, the cuvette was removed from the cuvette holder and 1 ml of SOC-medium was added to the cells. The cells were transferred to an Eppendorf tube and incubated in a rotary shaker for one hour at 37°C and 180 rpm. A maximum of 200  $\mu$ l of the cells was plated on LB plates with the appropriate antibiotic. After drying, the plates were incubated at 37°C overnight.

#### 3.4.13 Sucrose sensitivity assay

The plasmids ready for conjugation pNot $\Delta$ NiFeCmMob, pNot $\Delta$ MniFeCmMob (chapter 5.1) were transformed in-to *E. coli* S17-1 and the sensitivity to sucrose in the cultures was checked, before proceeding for conjugation with *Desulfovibrio* species. Fresh O/N cultures were prepared in 5 ml TBY medium with Cm. One ml aliquots of each overnight culture were split to inoculate in parallel two glass tubes each with caps, containing 5 ml of TBY medium with Cm and TBY medium with Cm and sucrose 5% (w/v) respectively. Tubes were closed and incubated at 37°C, while monitoring the start of growth (medium getting turbid). Cultures in TBY Cm start growing within 6-8 hours, while cultures in TBY Cm suc take longer. The TBY Cm suc cultures that take longest, or do not grow at all were selected for isolating the plasmid to be used for conjugation.

#### 3.4.14 Conjugation

Conjugation is the process whereby DNA is transferred from one bacterial cell (donor) to another (recipient) by a mechanism that requires cell-to-cell contact (Willetts and Wilkins 1984; Willetts, 1988). This process requires the gene *oriT* (for origin of transfer) or *mob* (for mobilization) in the plasmid to be transferred as well as a set of *trans*-acting *tra* genes. Plasmids containing both the *oriT* or *mob* and the *tra* genes are self-transmissible. Plasmids containing only the *oriT* or *mob* are mobilizable but non-



conjugative, which requires the function of *tra* genes to be provided either by a co-existing conjugative plasmid (helper plasmid) or by the donor cell genome with integrated *tra* genes (mobilizer strain).

To transfer the suicide plasmid (chapter 5) from *E. coli* to *Desulfovibrio*, a filter-mating method was used for conjugation. Briefly, 1 ml of an O/N culture of *D. vulgaris* in medium C was mixed with 0.2 ml of an O/N culture of the *E. coli* donor cells in a 1.5 ml microfuge tube under anaerobic conditions (work performed inside the anaerobic hood). The cell mixture was spun down, resuspended in ~20 µl medium C, spread onto a membrane filter (Millipore, 0.22 µm, Ø =25 mm) placed on a Medium E-nitrate mating plate which has been pre-dried to facilitate absorption of the liquid medium. The plates were incubated anaerobically at 37°C for 1 day. The mating filter was then transferred into a microfuge tube and the cells were resuspended in 1 ml of medium C. Aliquots of the cell suspension were plated onto medium E plates containing Km and Cm. The plates were incubated at 37°C for four to seven days to select for the Cm<sup>R</sup> Km<sup>R</sup> transconjugants or transconjugal integrants and against the Km<sup>S</sup> *E. coli* donor cells and Cm<sup>S</sup> wild type *D. vulgaris*.

The Cm<sup>R</sup> colonies that emerged were colony purified by growing them to saturation in medium C containing Cm and by plating dilutions (10<sup>-2</sup>, 10<sup>-4</sup>, and 10<sup>-6</sup>), onto medium E agar plates with Cm. The purified isolates were further analyzed by Southern hybridization of chromosomal DNA to verify and map plasmid integration.

### 3.4.15 Southern Hybridization

This technique is designed to detect a specific sequence of DNA in a complex mixture. In this study, it was used during the downstream sequencing of an operon starting from a known sequence into the unknown 3' region, for verification of plasmid integration, and for integration mapping.

Chromosomal or plasmid DNA was restriction digested with specific restriction enzyme/s, followed by agarose gel electrophoresis and blotting. After the agarose gel separation, the gel was shaken gently in 0.5 M NaOH/ 1.5 M NaCl for 30 minute and washed 2-3 times with water. The gel was then shaken with 1 M Tris/ 1.5 M NaCl (pH

8) for 20 minute. The arrangement for the blotting procedure was from bottom to top: - a glass stack in a tray with 3mm filter paper wrapped around the glass, followed by the gel with the first sample to the right (special care was given for the avoidance of any air bubble on either side), followed by a Hybond membrane of the same size as the gel (labeled and wet), two of the 3 mm filter paper (also wet), a stack of paper towels, and finally a heavy weight on top to facilitate the diffusion to the top. This arrangement was left O/N for blotting the DNA on Hybond.

After 12 hours the Hybond membrane is washed once in SSC and UV irradiated for 3 minutes after drying. A prehybridization mixture was added to the dried membrane, followed by incubation at 68°C for 3-4 hrs. The DNA mixture for labeling was prepared by adding 5 µl of λ DNA (40 ng), 5 µl of the DNA probe and 10 µl H<sub>2</sub>O, to make a final volume of 20 µl. This labeling mix was boiled and ice cooled for 3 minutes to denature the DNA. Following this, 6 µl PE mix, 2 µl of DNA polymerase (Klenow fragment) and 2 µl α-<sup>32</sup>P dCTP were added in order to label the DNA probe and λ DNA with α-<sup>32</sup>P dCTP and incubated at RT for 2-3 hrs. This labeling mix was then added to the Hybond membrane at 68°C and incubation was continued at 68°C O/N. Next day, the membrane was again washed once in SSC and then incubated once in SSC/ SDS at 68°C for one hour. It was then taken out and air dried (5-10 minutes). After wrapping the dried Hybond in Saran foil, it was developed on an Image plate for 2-4 hrs and scanned on an Imaging Plate Reader to obtain the image.

### **3.5 Protein Chemistry Methods**

#### **3.5.1 Extraction of hydrogenase protein from DvMF cells**

Harvested cells were thawed and washed (1g in 2ml) with ice-cold 25 mM TrisCl, pH 7.0 in JA 25.5 rotor (10,000 rpm, 30 minutes, 4°C). The cell pellet thus obtained was resuspended in the same buffer and 0.2 mg/ml Dnase-I was added to it. The cell membrane was lysed by sonification or using the French press. For sonification, 50 ml aliquots were sonicated; each aliquot was subjected to 3 rounds of 2.5 sec cycles, at 70% output, with 5-10 minutes of cooling in between. To collect the membrane fraction, broken cells were centrifuged at 50,000 rpm, 4°C, for 90 minutes. The pellet thus

obtained was resuspended in 25 mM TrisCl, pH 7.5 (1 g of wet pellet/ 4 ml buffer), and trypsin digested O/N at 4°C under argon atmosphere to release the hydrogenase from the membrane. A centrifugation (50,000 rpm, 4°C, 90 minutes) followed to separate the hydrogenase from the membrane fraction. The supernatant thus obtained contained the protein and was concentrated if required before loading on ion exchange column for purification.

### 3.5.2 Protein purification

For protein purification, Äctabasic 10/100 from Amersham Pharmacia Biotech (now General Electric) was used. Äcta<sup>TM</sup>basic is an automated liquid chromatography system designed for method development and research applications. It consists of a compact separation unit and a personal computer running the UNICORN<sup>TM</sup> control system version 3.0. DvMF hydrogenase was purified from the cell free extract using a DEAE Toyopearl 650 S ion-exchange column (350 ml (XK 50/20 cm)), washed and run at a flow rate of 5ml/minute with buffer A i.e. 25 mM TrisCl (pH 7.4), containing 10 mM NaCl. A sample volume of 20-100 ml was injected and the adsorbed hydrogenase was eluted by a linear gradient of buffer B i.e. 1 M NaCl in H<sub>2</sub>O from 0-20%. The peaks obtained were assayed for presence of the hydrogenase by activity assay (chapter 3.5.4) and SDS-PAGE (chapter 3.5.6). The active fractions were pooled, and concentrated using AMICON filters (PM 30) to a final volume of 5-50 ml and applied on a second column of Sephacryl S 200HR (480 ml (XK 26/100)). Buffer A was used to run the column with a flow rate of 2 ml/minute. The peaks thus obtained were subjected to another ion-exchange column DEAE Toyopearl 650 S (74 ml (XK 2.6/14 cm)), run with buffer A with a flow rate of 1 ml/minute and eluted with a gradient of buffer B from 0-22.5%. This was followed by a Hi-Load column (318 ml (XK 26/60 cm)), run with 25 mM TrisCl (pH 7.4) with a flow rate of 1 ml/minute, to desalt the sample besides further purifying the protein.

The purity of the protein was determined by SDS-PAGE and Maldi-TOF (chapter 3.5.7). The concentration of the protein was determined by Bradford assay (chapter 3.5.3) and appropriate aliquots were kept frozen in liquid N<sub>2</sub> till used for spectroscopic measurements.

### 3.5.3 Determination of protein concentration

The concentration of the protein was determined using the Bradford assay kit from Biorad. Protein dilutions ranging from 0-1.5 mg/ml, with assay buffers, were measured with a spectrophotometer at 700 nm. The spectrophotometer reading of the protein dilutions, in the range of BSA standard was used to calculate the protein concentration.

### 3.5.4 Methyl Viologen activity assay

For hydrogenase activity assay, 50  $\mu$ l of hydrogenase were added to 1 ml of a 25 mM TrisCl buffer (pH 7.4), containing 3 mM methyl viologen. This mixture was incubated at 37°C for 5-10 minutes with constant bubbling with H<sub>2</sub>. A strong blue color indicates the reduction of methyl viologen and the presence of active hydrogenase.

### 3.5.5 Modified Clark electrode assay

Hydrogen production was measured using the modified Clark Electrode assay. An AgCl electrode was washed with ammonia solution (25% NH<sub>3</sub> + H<sub>2</sub>O 1:1) and run in oxygen mode (several minutes) in saturated KCl + HCl (17.5 g KCl/100ml H<sub>2</sub>O + 10 mM HCl), followed by a washing with H<sub>2</sub>O, and drying. Onto the Pt-electrode, one drop of AgCl solution (3 M KCl saturated with AgCl) was applied, covered by a piece of cigarette paper and a piece of the P.T.F.E. (polytetrafluoroethylene) membrane (Hansatech instruments), followed by the O-ring with the applicator.

After installation of the reaction chamber, the electrode was equilibrated with enzyme buffer O/N and the buffer was bubbled with H<sub>2</sub> until a stable output signal was recorded.

For calibrating the electrode, a stable potential with 0% H<sub>2</sub> and 100% H<sub>2</sub> saturation was measured respectively. To obtain the stable potential, the reaction chamber with buffer was bubbled with argon and hydrogen respectively for ~10 minutes.

For performing the measurement, the reaction chamber was filled with 1.75 ml argon saturated enzyme buffer (25 mM Tris/HCl, pH 7.4), 30  $\mu$ l methyl viologen solution (163 mM), 150  $\mu$ l glucose solution (1M) and 30  $\mu$ l glucose oxidase (30 mg/ml in buffer).

After closing the reaction chamber, 100  $\mu$ l sodium dithionite solution (1M Na<sub>2</sub>S<sub>2</sub>O<sub>4</sub>) was added, and incubated for complete oxygen removal by glucose oxidase (5-10 minutes). Then the potential was recorded and 50  $\mu$ l of the crude cell lysate was added. Due to H<sub>2</sub> production, the potential increases and this drift is recorded.

Hydrogen production was calculated by the conversion formula:

$(X \text{ cm} * a \text{ } \mu\text{mol H}_2)/(\text{minute} * Y \text{ cm} * b \text{ mg protein})$ , where

X = slope (as measured in recorder, with increase of H<sub>2</sub> production) in cm/minute

a =  $\mu$ mol H<sub>2</sub> in saturated buffer (780  $\mu$ M at 25 °C)

Y = potential at 100% H<sub>2</sub> in cm

b = used amount of protein in mg

### **3.5.6 SDS-PAGE and coomassie staining**

The Pharmacia phast gel system was used with 4-20% gradient gels and New England Biolabs gel system with 10% and 12% homogeneous gels. To 25  $\mu$ l of the cell pellet suspension, 25  $\mu$ l of the Laemmli buffer was added, boiled for 10 minutes, and centrifuged for 5 minutes. The supernatant was loaded and electrophoresed at 10 V/cm. The gels were then stained with Coomassie or used for western blot.

For Coomassie staining, the gel was fixed with two incubations of 5 minutes each in a solution of 40% ethanol and 10% acetic acid. It was then stained for 2-3 hours in Coomassie staining solution, followed by destaining in the same solution as for fixing to remove background staining. To preserve the gels, they were washed in 10% glycerol for 5 minutes and allowed to dry.

### **3.5.7 Western blot**

To transfer the proteins from the gel to a PVDF membrane, it was blotted using electrophoretic transfer system (NEB). The transfer sandwich was assembled under transfer buffer in the following way: starting from cathode, 2 pieces of soaking pads, 1 piece of filter paper (of same size as gel and membrane), gel, membrane (immersed in methanol till it does not float, followed by transfer to transfer buffer till used for blotting), filter paper and soaking pads. All air bubbles were carefully removed from

both sides of the gel. This sandwich was placed into a transfer cassette, which was then inserted in-to the tank, and filled inside with transfer buffer. The proteins were transferred at a constant current of 25 V for 80-90 minutes. Pre-stained marker was used to control the completion of transfer.

Blotted membrane was washed twice in TBS for 10 minutes, followed by incubation in blocking buffer to saturate non-specific protein binding sites. After washing two times for 10 minutes in TBST, and one time for 10 minutes in TBS, the membrane was incubated with the primary antibody (1:1000 diluted in blocking buffer) for one hour at RT. To remove unspecifically bound antibody, the blot was then washed two times for 10 minutes in TBST, and one time for 10 minutes in TBS. It was then incubated with the secondary antibody (1:1000 diluted in blocking buffer) for one hour at RT. Before developing the blot it was again washed four times for 10 minutes with TBST. To develop the blot, it was stained in freshly prepared AP buffer, and the color was allowed to develop in dark. To stop the chromogenic reaction, it was washed twice in water.

### **3.5.8 Native PAGE and in-gel activity assay**

*Desulfovibrio sp.* cells grown in medium C for 2 days were harvested and equal wet cell weight (1 g) was used for the experiment. Cells were washed with 50 mM phosphate buffer (pH 7.0) and lysed using the French press. Cell debris was separated from crude cell lysate by a slow spin at 4000 rpm, for 15 minutes, 4°C. The supernatant was centrifuged in ultracentrifuge at  $4 \times 10^4$  rpm, 4°C, for 90 minutes to separate the soluble fraction from membrane fraction. The pellet was solubilised in 2% Triton X-117 at 4°C for an hour to get the membrane proteins in solution. The suspension was centrifuged at 4000 rpm for 15 minutes at 4°C to separate the membrane extract from the debris. Total protein content in each sample was quantified using the Bradford assay, and 200 µg of protein was loaded in a well.

Pre-prepared 3-15% native gels were run for 3000 Volt-hour at 4°C to achieve separation of proteins on the gels. Molecular weight marker was stained in CBB separately.

Gels were subsequently incubated in either 50 mM phosphate buffer (pH 7.0) or (pH 5.5) that were  $H_2$  saturated by evacuating and refilling with  $H_2$  three times. After incubating at RT for 2 hours under  $H_2$  bubbling, the gels were activity-stained with PMS/NBT and BV/TTC, respectively. For the PMS/NBT assay, 1 ml each of PMS and NBT stock solutions were mixed and injected in a rubber-tight bottle, containing the gel in 200 ml phosphate buffer. The hydrogenase reacts with  $H_2$ , the electrons are transferred to PMS, and the reduced Phenazine Methosulfate ( $PMSH_2$ ) reacts with NBT to give a blue color. The bottles were incubated at  $37^\circ C$  till the blue color developed. In case of *Desulfovibrio sp.* it took ~ 10-20 minutes. To stop the reaction, gels were washed in excess water.

For the BV/TTC assay, 0.5 ml of  $H_2$ -saturated BV solution was added to 1 ml of sodium dithionite (60 mM). 200  $\mu l$  of this solution were injected into a rubber-tight bottle containing the gel in 200 ml phosphate buffer. Almost immediately, the blue color development could be seen. To fix the bands, 100  $\mu l$  of TTC was added to the buffer upon which the color changed into pink. After a uniform color change, washing the gels in excess water stopped the reaction.

### 3.5.9 Preparation of different EPR active redox states

The protein sample (100  $\mu l$ , 700  $\mu M$ ) was transferred in an X-band EPR tube (quartz tube, outer diameter 3.85 mm, inner diameter 2.75 mm) and connected to an anaerobe line, with the sample part dipped in a stirred water bath adjusted at  $37^\circ C$ .

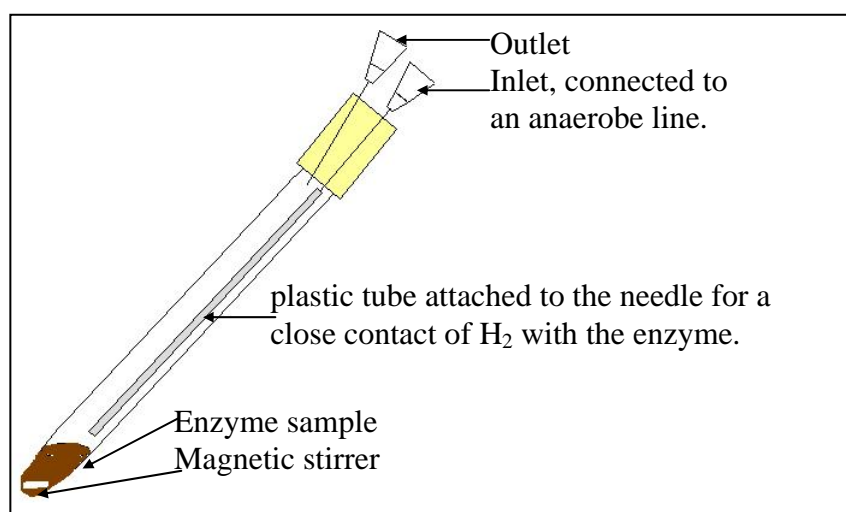


Fig. 3.2 The arrangement used to achieve faster reduction of the sample in the EPR tube.

A small magnet was put in the EPR tube as well. The angle of the EPR tube was adjusted in the water bath such that the small magnet is moving up and down as well as rotating to ensure uniform mixing of the solution. The opening of the tube was sealed with rubber tubing having a glass/ plastic seal on the other end. Needle/(s) (0.8x 90mm) were passed through the rubber tube to connect the EPR tube with the anaerobe line and/ or the atmosphere. A small plastic tube was attached to the first needle hanging in the EPR tube to enable the H<sub>2</sub> flow to be in better contact with the sample. The sample was evacuated and flushed with H<sub>2</sub> for three times through the single needle. A continuous stream of H<sub>2</sub> flowing over the sample through the first needle followed this and a second needle was attached after opening the H<sub>2</sub> flow, for outlet. With this construction, the time required for reducing the sample reproducibly to Ni-C, was found to be decreased from 6 hours (as used in previous work) to only 10 minutes. It took about 20 minutes to generate the fully reduced state Ni-R.

**Optimisation of Ni-B protocol:** The time for reduction has been optimised to be 20 minutes. To optimise the conversion to Ni-B and to quantify the reduced states/dead protein generated in the oxidation of the reduced sample, the time for oxidation was studied with different samples in parallel.

The formation of Ni-B from the completely reduced state by oxidation is reproducible, and oxidation for 15 seconds gave best results, as shown in fig. 3.3. But the signal intensity of Ni-B compared to that of the as-isolated sample was found to be only 1:100. It has to be kept in mind, however, that this significant amount of the protein (99%) is completely damaged and does not convert into an EPR silent state. This is evident from a comparison of the back-oxidised sample with the as-isolated state, from the beginning.



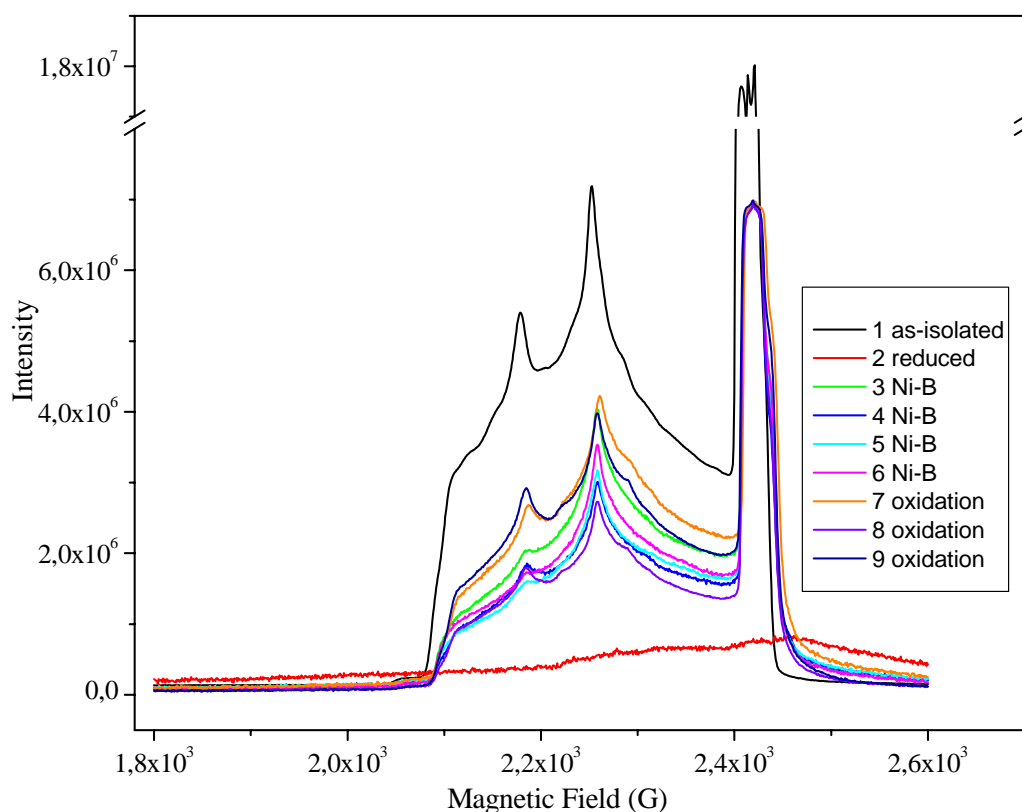


Fig.3.3 Absorption EPR spectrum of [NiFe] hydrogenase from DvMF, showing the effect of oxidation on the completely reduced sample with respect to time. The different labeled samples from 1 to 9 in fig 3.2 represents (1) the as-isolated sample (Ni-A and Ni-B), (2) completely reduced sample (Ni-R), (3) 10 seconds oxidization of reduced sample (Ni-B ~80%), (4) 15 seconds oxidization of reduced sample (Ni-B ~85%), (5) 20 seconds oxidization of reduced sample (Ni-B ~80%), (6) 30 seconds oxidization of reduced sample (Ni-B ~80%), (7) 20 minutes oxidation of 85% Ni-B in ice (Ni-A increases), (8) 25 minutes of oxidation of 85% Ni-B at RT, (9) 30 minutes of oxidation of 85% Ni-B at RT.

Based on these standardisations, the following protocols were used for obtaining all four redox states of the enzyme: -

**Ni-C:** - 10 minutes of reduction, followed by disconnecting the needle, removal of the small magnet and the plastic tube halfway in the tube, and freezing the sample immediately in liquid N<sub>2</sub>. The transfer to Q-band tube following thawing of the sample was done in the anaerobic glove box to avoid any contact with air. The stirring of the sample is required to have homogeneity in the solution, which is not possible to achieve in Q-band tube.

**Ni-L:** - A Ni-C sample was illuminated with strong light for 5 minutes keeping it still in liquid N<sub>2</sub>.

**Ni-B:** - 20 minutes of reduction followed by similar procedure as for Ni-C. The frozen sample was thawed and oxidised at RT for 15 seconds. After this procedure, the sample was carefully frozen in liquid N<sub>2</sub>.

**Ni-A:** - no clear protocol was established. Best results (70% Ni-A, compared to 45-50% Ni-A in the as-isolated sample) were obtained after a short reduction for 5 minutes, followed by oxidation by exposure to air for about 5 minutes.

### **3.5.10 MALDI-TOF MS molecular weight analysis (matrix assisted laser desorption/ ionisation-time of flight mass spectrometry)**

MALDI involves embedding the analyte in a solid matrix, which absorbs the energy of the laser. The laser energy absorbed by the matrix, typically on the order of 10<sup>6</sup> watts/cm<sup>2</sup>, leads to intense heating and generation of a plume of ejected material that rapidly expands and undergoes cooling, and is then separated according to its apparent mass to charge ratio, within the mass spectrophotometer.

For the experiments conducted, a Voyager-DE PRO Workstation and Voyager-DE<sup>TM</sup> PRO Biospectrometry Workstation from Applied Biosystems (USA) were used. The matrices used were  $\alpha$ -cyano-4-hydroxycinnamic acid (CHCA)(M1), 2,5-dihydroxybenzoic acid (2,5-DHB)(M2), Sinapinic acid and a mixture of 2,5-dihydroxybenzoic acid and 5-methoxysalicylic acid (DHBs).

## **3.6 Spectroscopy Methods**

### **3.6.1 Ultraviolet/Visible (UV/VIS) spectroscopy**

UV-VIS spectroscopy is the measurement of the wavelength and intensity of absorption of near-ultraviolet and visible light by a sample. The concentration of an analyte in

solution can be determined by measuring the absorbance at some wavelength and applying the Beer-Lambert law (or Beer's law).

$$A = \epsilon * c * d$$

where  $A$  is the measured absorbance,  $\epsilon$  is a wavelength-dependent absorptivity coefficient,  $c$  is the analyte concentration, and  $d$  is the path length.

All the measurements were done with a Shimadzu UV-140 spectrophotometer. Before starting to measure, the buffer (also the salts solutions, if any) used to make the dilution of the sample was used to set the blank.

### 3.6.2 EPR

Hydrogenase sample aliquots of 100  $\mu\text{l}$ , each with 700  $\mu\text{M}$  concentration were used for most X-band measurements. For Q-band, samples with similar concentration and 30  $\mu\text{l}$  volume were used.

EPR measurements were performed with Bruker E500 Eleksys (cw X-band), ESP200E (cw Q-band), ESP380E (pulsed X-band) and Eleksys E580 (pulsed Q-band) spectrometers equipped with an Oxford liquid helium cryostats (ESR 910). The field was calibrated with a Bruker ER035 teslameter, and the microwave frequency was measured with a Hewlett-Packard 5352B frequency counter. The temperature setting was chosen differently depending on which redox state was studied and which spectrometer was used. For the oxidized Ni-A and Ni-B states, the cw-EPR experiments were done at 120 K, using a modulation amplitude of 5 G and 2 mW microwave power. Pulse EPR experiments were performed at 5 or 10 K, in which the length of the 90 degree pulse was 16 ns. The Ni-C redox state was measured at 40 K or 80 K and with a modulation amplitude of 5 G and 2 mW microwave power. Modulation experiments, like three pulse ESEEM or HYSCORE were performed at 5 K using 90 degrees microwave pulses with a length of 16 ns.

### 3.7 DFT calculations

Density functional theory uses the electron density to calculate the electronic structure. Taking care of important factors affecting the environment of the electronic species, it is possible to calculate the structure quite close to the experimental data.

The work reported here was done with the ORCA programming package (Neese F, 2003). The B3LYP functional was used within a spin-unrestricted formalism. Two model systems were considered. The large model system of the active site consists of Ni, Fe, four (SCH<sub>2</sub>CH<sub>3</sub>) groups to model the cysteines, the diatomic ligands of iron (2CN<sup>-</sup> and CO), a methylimidazole group (CH<sub>3</sub>C<sub>2</sub>NCNH<sub>3</sub>) to model His-88 and the bridging ligand (OH<sup>-</sup> for Ni-B, van Gastel *et al.*, to be published). In the small model system, the methylimidazole group is not present. After geometry optimization, the Ni-S distances were manually adjusted to 2.22 Å, based on data from EXAFS measurements (Davidson G *et al.*, 2000). The split-valence basis set of Ahlrichs was used (Schaefer A *et al.*, 1992), augmented with a set of polarization functions on all heavy atoms. The g tensor and hyperfine tensor calculations were all performed with ORCA and the large 'CP' basis set (Neese F, 2002) was used for Ni and Fe augmented with two polarization functions (Wachters AJ, 1970) and one diffuse function. The accuracy of the DFT method with respect to calculating g values is about 30 % in the g shift (Stadler C *et al.*, 2002; Neese F, 2001). The accuracy is about 20% for ligand hyperfine interactions (Neese F, 2003). For the central metal, however, especially the isotropic hyperfine interaction is difficult to calculate (Neese F, 2003).

### 3.8 Electrochemistry

Cyclic voltammograms trace the transfer of electrons during a redox reaction.

Experimentally, three electrodes dip into a solution which contains at least one compound which can exchange electrons with the working electrode and an excess of supporting electrolyte (0.1 M KCl) to provide a high electric conductance of the solution. The primary redox reactions themselves take place on the surface of the working electrode, a glassy carbon disk of 2 mm diameter. Its potential (vs. the

reference electrode) can be adjusted or scanned within a suitable range by means of a potentiostat (model M 273 by EG&G, operated with electrochemical software M 270). When the working electrode's potential is more *negative* than the redox potential of the electrochemically active compound (methyl viologen in our case), electrons are donated from the electrode to methyl viologen, i.e. reduction occurs. *Vice versa*, if the potential is more *positive* than the redox potential, oxidation takes place. The electric currents that accompany oxidations and reductions flow through the third electrode, the platinum disk counter electrode. The currents are recorded and displayed by the potentiostat, and they are a measure for the activity of the respective sample under investigation. The reference electrode was of the type Ag/AgCl-NaCl with known potential (at + 0.210 V vs. the standard hydrogen electrode, SHE).

The system starts off at an initial potential at which no redox reaction can take place. As the redox potential is approached critical potential during the forward scan, the methylviologen will begin to be reduced. In cyclic voltammetry, the direction of the potential is reversed at the end of the first scan. After reversal of the potential, depletion of the oxidised species occurs and it gets re-oxidised.

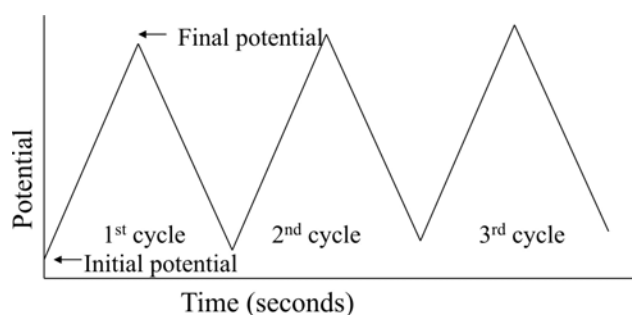


Fig. 3.4 Redox cycling in cyclic voltammetry, with potential plotted as function of time.

The basic shape of the current response for a cyclic voltammetry experiment is shown in fig. 3.5. At the start of the experiment at point A, the bulk solution contains only the reduced form (R) of the electrolyte. As the redox potential is approached, R starts getting converted into its oxidized form (O). At point B, redox potential is positive enough that any R that reaches the electrode surface is immediately oxidized to O. Upon reversal of the scan (point C), the current continues to decay until the potential reaches the redox potential. At this point, a net reduction of O to R occurs which eventually produces a peak shaped response (point D).

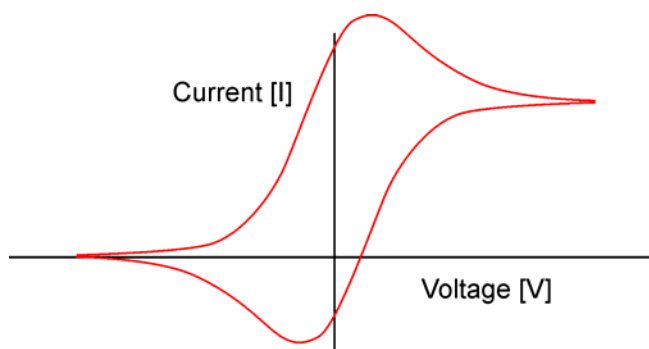


Fig. 3.5 Typical cyclic voltammetry curve, obtained when plotting current versus potential.

Equal amounts of wet cell weight was used for all samples. Cells were washed with 25 mM TrisCl (pH 7.4), and lysed by ultrasonication with a pulse cycle of a 2 sec pulse and 2 sec pause for 2 minutes. The substrate used was immobilised on the surface of the working electrode (Lojou E and Bianco P, 2004), by pipetting 2  $\mu$ l of the sample on the electrode and allowed to dry under  $N_2$  stream. A piece of a dialysis membrane (cutoff 10 kDa) was fitted against the dried sample and fixed with an O-ring. In case of pure protein, 2  $\mu$ l of a 600  $\mu$ M protein solution was used.

The activity was measured every 3 minutes at constant bubbling with argon and hydrogen, respectively, to see the differences in different set of experiments. A scan rate of 10  $mVs^{-1}$  was used. For measurements under argon-saturation, the sample in the electrochemical cell was kept under constant bubbling with argon for 10 min before starting the measurements, to achieve a completely anaerobic atmosphere. When changing to hydrogen (performed together with a buffer change), the samples were bubbled with argon for 20 minutes to obtain an oxygen-free environment, and were then switched to hydrogen bubbling for 5 minutes before starting the potential scan. Constant bubbling was found advantageous and thus was used for all the measurements done.

### 3.9 Software

Multiple sequence alignments were performed using Clustal W (Thompson JD *et al.*, 1994). Phylogenetic and molecular evolutionary analyses were conducted using MEGA version 2.1 (Kumar *et al.*, 2001). Sequence alignments for comparing known proteins to the newly sequenced gene (coding for hynC protein), GeneDoc multiple Sequence Alignment Editor and Shading Utility version 2.6.002 (Nicholas KB and Nicholas HB Jr 1997) was used. The *hynC* gene sequence was translated using ORF Finder at NCBI

website (<http://www.ncbi.nlm.nih.gov/gorf/gorf.html>), and the molecular weight of the translated protein in dalton was calculated using the Scansite software at Expasy ([http://scansite.mit.edu/calc\\_mw\\_pi.html](http://scansite.mit.edu/calc_mw_pi.html)).

The PSIPRED secondary structure prediction method (Jones DT, 1999) was used to predict the secondary structure of hynC. A one vs. one secondary structure alignment of hynC with the sequence homolog, crystallized protein hybD from *Escherichia coli* (Fritsche *et al.*, 1999), was prepared using the SSEA server (<http://protein.cribi.unipd.it/ssea/>) (Fontana *et al.*, 2005). The three-dimensional structure of hynC was modelled, based on homology to hybD, obtained from the Brookhaven Protein Data Bank (entry: 1cfz). The hynC sequence was aligned to the template using the tools available in the SwissPdbViewer (Guex and Peitsch 1997). Energy minimization was carried out with the MAB all-atom force field implementation of the MOLOC molecular modelling and simulation software (Gerber and Müller 1995; Gerber 1998).

Simulations of EPR spectra were performed with home-written software. ESEEM and HYSCORE spectra were simulated according to procedures given in references van Gastel M. *et al.*, 1998 and Brecht M. *et al.*, 2003, respectively.

## Chapter 4

# DvMF [NiFe] Hydrogenase: Complete Operon Sequence

The [NiFe] hydrogenase protein consists of a small and a large subunit, encoded by the structural genes *hynA* and *hynB* (commonly used nomenclature for *Desulfovibrio*) respectively. As can be deduced from the available genome structures of other organisms, *hynA* and *hynB* are usually present at the 5'-end of an operon. They are followed by a set of accessory genes present on the same operon (*in cis*) encoding maturation and regulatory proteins. Besides, there are many genes organised in several transcription units (*in trans*) scattered in the genome of the organism, as known from the studies on various species. A comparison of genes known to be involved in maturation of the [NiFe] hydrogenase of the most studied organisms is given in table 9.1 in the appendix. In case of DvMF, only the structural genes (*hynA* and *hynB*) were known before this study (Deckers HM *et al.*, 1990), however, the genome of a very closely related species, DvH was recently published (Heidelberg JF *et al.*, 2004). All the accessory genes for the maturation of [NiFe] hydrogenase present in DvH were reported from the sequence comparisons of several strains with known gene sequences. For a closer look at the genes now known in [NiFe] hydrogenase operon in DvH and DvMF as compared to other well known *Desulfovibrio* species and *E. coli* refer to table 4.1.

From various mutants studied, mostly in case of *E. coli* (Menon NK *et al.*, 1994; Blokesch M *et al.*, 2001; Blokesch M *et al.*, 2002; Blokesch M *et al.*, 2004), *Ralstonia eutropha* (Massanz, C *et al.*, 1997; Lenz O *et al.*, 1998; Buhrke T *et al.*, 2001; Jones,



AK *et al.*, 2004) and a few other species, the roles of various maturation genes has been ascribed in the specific maturation pathway. It turned out that complex pathways are required in order to ensure that nascent hydrogenases mature into physiologically competent enzymes (Casalot L *et al.*, 2001). The formation and insertion of the bimetallic Ni-Fe center are specific for hydrogenases, but other aspects, e.g. the formation of [4Fe-4S] clusters and the membrane translocation pathway, are shared with other metalloproteins. There is much evidence that the additional proteins, the so-called ‘accessory proteins’, are required to insert the metal centers in a manner which must be coordinated with the folding pathway. The complexity of these processes explains in part the usually high number of genes specifically required for hydrogenase activity.

Function	<i>Escherichia coli</i>			<i>Desulfovibrio</i>			
				<i>gigas</i>	<i>fructosovorans</i>	Miyazaki F	Hildenborough
	Hyd 1	Hyd 2	Hyd 3				
Small Subunit (SSU)	hyaA	hybO	hycG	hynA	hynA	hynA	hynA
Large Subunit (LSU)	hyaB	hybC	hycE	hynB	hynB	hynB	hynB
C-terminal peptidase	hyaD	hybD	hycI	hynC	hynC		hynC
Ni incorporation/maturation	hybF	hybF	hypA				hypA
Ni insertion	hypB	hypB	hypB				hypB
Chaperone/maturation	hypC hybG	hybG	hypC	hynD			hynD
Ni incorporation/maturation	hypD	hypD	hypD				hypD
Purine derivative binding	hypE	hypE	hypE				hypE
CN/CO delivery	hypF	hypF	hypF				hypF

Table 4.1 The [NiFe] hydrogenase structural and maturation genes. In case of DvH the complete list is shown as it was deduced from the genome sequence. The genes shaded in same color are present in the same operon. SSU and LSU code for structural genes, the rest for maturation genes with their respective functions described on the left hand side.

In one reported experiment expression of [NiFe] hydrogenase operon from *D. gigas* in *D. fructosovorans* led to one-sixth expression, where all the *in trans* located maturation

genes were from *D. fructosovorans* (Rousset M *et al.*, 1998). Similar studies have also led to a better understanding of the specificity of the various genes products. One particular example was found in case of *E. coli*. In *E. coli* three different [NiFe] hydrogenases are present. It was demonstrated that these three [NiFe] hydrogenases consists of distinct sets of genes, which encode structural and maturation proteins. The function of these maturation proteins is very specific and the function of one cannot be replaced by another, with the exception of the gene product of *hybG*, which belongs to the *E. coli* hydrogenase 2 operon and is involved in both hydrogenase 1 and 2 maturation (Menon NK *et al.*, 1994).

In most cases, especially amongst the Proteobactereaceae, e.g. *R. eutropha*, *Azotobacter* sp., *Rhizobium leguminosorum*, *Bradyrhizobium japonicum*, the hyp genes are clustered in operons with a conserved gene order similar to that found in *E. coli*. The function for all the genes present in all the operons for various bacteria is not known completely, but the ones shown in table 4.1 and those present in DvH (derived from the genome sequence) are the best studied ones. In case of DvH they are scattered in the genome unlike others where all these genes are found in one operon.

The generation of mutants and the analysis of the function affected, or the identification of the step of maturation where the cycle stops due to unavailability of an altered protein, have ascribed the functions of these genes. For a more detailed description of the maturation pathway and the role played by genes involved refer to the introduction.

#### **4.1 Rational for sequencing the operon**

When this work was started, only the structural genes coding for [NiFe] hydrogenase of DvMF and a small stretch of the 5'-UTR were known (Deckers HM *et al.*, 1990). However, as outlined above, any work aiming at the expression of hydrogenase activity in any particular organism, e.g. *E. coli*, requires not only the structural genes but has to utilize also all those factors that are involved in maturation. This was found from an expression of only the structural genes with the native promoter in *E. coli* (chapter 4.4) showing that the protein formed was neither matured nor functional.

The expression of *D. gigas* in the related organism *D. fructosovorans* was possible albeit with lower yields (Rousset M *et al.*, 1998). With the above-discussed studies it is well certain that the expression of both structural and functional genes is required to get the fully functional hydrogenase. As shown in table 4.1, the presence of maturation genes is of universal nature and their high specificity makes it very probable that they are also present in DvMF. At least some of the maturation genes should be present downstream of the structural genes in the same operon. Thus, keeping these probabilities in mind, the sequencing of the [NiFe] hydrogenase operon of DvMF with already known structural genes, was attempted.

### **4.2 Sequencing Strategy I**

Since the 5'-end of the operon encoding the structural genes was known, PCR was used to amplify the 3'-end of LSU. This method implied the use of specific forward primers and degenerate non-specific reverse primers. Latter ones were generated from sequence alignments for the *hynC* between 31 different organisms with related gene sequences, as seen from NCBI blast and choosing the most conserved regions for designing the primer (fig. 4.1 and fig. 4.2).

1	Dv Hildenborough HynC	-----	-----MSENTSIL	VLGVGNILYTDEGIG	VRAVERLSAG
2	D gigas HynC	-----	-----MSNDSPRIL	VMGVGNILYTDEGLG	VRLVEHLEAR
3	D fructosovorans HynC	-----	-----MSDTPPKIL	ILGVGNILYTDEGVG	VRAVERLLET
4	NostocspPCC7120alr1423	-----	-----MLT	IIGCGNLRSDDAVG	VIIAQRLQKY
5	BradyrhizobiumjaponicumHupD	-----	----MPTSSQDNRI	VLGIGNILWADEGFG	VRAVEEFHRR
6	Rhizobium_leguminosarumbv.Vici	-----M	TIPYPLGPPPAPRIL	VLGIGNILWADEGFG	VRAVEAFHKA
7	RhodobactercapsulatusHupD	-----	----MPAFKPERVL	VLGIGNVLWADEGFG	VRCVERMAET
8	AzotobacterchroococcumHup	-----	----MTGSSPNIL	ILGIGNLLWADEGFG	VRCVELLNER
9	AzotobactervinelandiiHox	-----	----MTAPNIL	ILGIGNLLWADEGFG	VRCVELLNER
10	Thiocapsa_roseopersicinaHupD	-----	----MRSDPEIL	VLGIGNLLWADEGFG	VRAVEALQRH
11	PseudomonashydrogenovoraHupD	-----MHSQPF	VNPRPQPTEAAGPII	VLGIGNVLWADEGLG	VRCVELLQQR
12	RalstoniaeutrophaHoxM	-----	-----MVV	AMGIGNVLWADEGFG	VRCIETLQQR
13	EscherichiacoliK12Hyad	-----	-----MSEQRVV	VMGLGNLLWADEGFG	VRVAERLYAH
14	Salmonellaentericaspenterica	-----	-----MNAQRVV	VMGLGNLLWADEGFG	IRVAERLYAR
15	SalmonellatyphimuriumLT2	-----	-----MAEVT	ILGLGNLLWADEGFG	VRAAEKLFEQ
16	MethylococcuscapsulatusHupD	-----	-----MPPRVL	ILGIGNLLWADEGFG	VRVAQALQRD
17	Salmonellaentericasubspenteric	-----	-----MRIL	VLGVGNILLTDEAIG	VRIVEALEQR
18	SalmonellatyphimuriumLT2HybD	-----	-----MRIL	VLGVGNILLTDEAIG	VRIVEALEQR
19	EscherichiacoliK12HybD	-----	-----MRIL	VLGVGNILLTDEAIG	VRIVEALEQR
20	MethanosarcinaacetivoransC2Avh	-----	----MPILQAPIR	ILGCGSPLMGDDGVG	LKVIEALKKT
21	MethanosarcinamazeiGoelvhTD	-----	----MTILHSPIR	ILGFGSPIMGNDGVG	LKVIEILKKE
22	Aquifex_aeolicusHupD	-----	-----MIT	VLGIGNILLSDEGLG	VRTVEELQRR
23	Desulfitobacteriumdehalogenans	-----	-----MLQPKIM	VMGVGNVLLSDEGLG	VQFLTLLSQE
24	ArchaeoglobusfulgidusvhtD-2	-----	-----MSRIL	VVGVGNPLMGDDGLG	IRVVEELKRR
25	Helicobacterpylori26695HP0634	-----	-----MSQKIL	ILGIGNILFGDEGIG	VHLAHYLKKN
26	CampylobacterjejuniHydD	-----	-----MKFL	VLGIGNIMFADEGLG	VHLCKQLEKN
27	MethanocaldococcusjannaschiiMJ	-----	-----MKKKDIL	IVGCGNLLFGDDGFG	CEVVSCKLEKM
28	Methanococcusvoltae	-----	----MPGYLNKEIL	VLGCGNILFGDDGFG	YHMIKRLNEL
29	MethanosarcinamazeiGoelMM3044	-----	---MKEMDKLYSEIV	VAGCGNPLYADDGFG	PAVVERLKGM
30	Methanothermobacterthermautotr	-----	-----MPYDAEIL	VVCGGNILFKDDGFG	PEVIKALEEY
31	MethanopyruskandleriAV19Hyad_2	MSKDSVRAASTGHTH	GAGVGLLRFLQRRVL	IVGCGNELFGDDGFG	PAVIKEIERR

Fig. 4.1 HynC protein sequence alignment graph of different organisms for the comparison of 5' end of the endopeptidase sequence. The sequence part marked in red was used to design the reverse primer. Also shown is the comparison for the known *Desulfovibrio* species (shown in red), in the beginning of the figure.

Based on this sequence alignment the complete sequences for the C- and the D-subunit of DvMF could be obtained (Fig. 4.2). This figure shows also the strategy that was applied and the designed primers.

```

3241 tttccaaccc  tatagtacac  cccacATGag  caatcgcccc  aacatcctcg  tccttggcgt
3301 gGGCAACATC  CTGTACACCG  ACGAAGGCAT  CGGCGTGCGc  gccgtggagg  gctgcaaaag
      CCGTTGTAG  GAWATGTGVC  TGCTYCCGNA  NCCGCAMGC  Epep001down (RP) worked
      CCGTTRTAW  GAWAYWYGVC  TGCTYCCGNA  NCCGCAMGC  Epep000down (RP)
3361 gccccatgcct  tcagcgacaa  cgttttcgctc  atggatggcg  gcacgctggg  catcgcgctc
3421 atggacgcca  tcatggactg  cgaccacctg  atcgtggtgg  acgccgtgct  tgcgggggac
3481 gaaccggcg  ccatctaccg  cctgaccggc  gaagacctgc  gcaagagcct  cggcttcaac
3541 gactccatgc  accagaccga  cctcgtggac  accctgatct  tctgcgaact  ggtgggcaaa
3601 cggccagaag  cagtgatcat  cggcatggag  ccgcacgact  accagtccct  gggcaccgaa
3661 ctttcccccg  tggcaggcca  ggcctgcca  ctgctgtgcg  atgccgtggt  cgccgaggta
3721 cgccgcgcgg  gcggcgacag  cgccccgacc  gacaacggac  accccgccTG  Agcgatcagg
3781 ccgtacaacc  cgctgaaac  gatcaggctg  gccaaaccga  cggagcagac  ccgATGtgcc
3841 tcgccattcc  cgccgagatc  gtggaaatca  atgatgccgg  catggccaag  tgccgtgtgg
3901 gcaagagcga  aacctacctc  aacgtctcgg  ccatgtgct  gcccgaaacgc  cccgccatcg
3961 gcgaatacgt  catcGTGCAC  GCCGGGTTTG  CCCTGCGCGT  GCTGGACaag  gcagaggcag
      CASGTA  CGGCCMAAYC  GGGACGCGTT  CMASCTG  hynDup worked
4021 aggaaaccct  gcggctgctg  cgcgaaatgt  ccgaggccgt  ggaaggccag  cccgccgggt
4081 tcTGAatccgc  gccgggtttg  cgcggtacgc  agcccgtgct  cgggcacacc  agatttaatg

```

Fig. 4.2 DNA sequence of the C- and D- subunit genes of DvMF [NiFe] hydrogenase operon (this work). The numbers on the left hand side are taken as such from the operon (ref. appendix). ATG and TGA in blue marks, the start and stop codons respectively, for *hynC* and *hynD*. Sequences marked in red are the ones to design the primer, based on sequence alignment of different organisms for the same region with high sequence similarity. Primer sequences are written below the DNA sequence, with their specific names. FP stands for forward, and RP for reverse primer. Specific forward primers were used from the known sequence for the PCR. For degeneracies in the primers, wobble IUPAC-IUB symbols were used: **R** (A or G), **Y** (C or T), **M** (A or C), **K** (G or T), **S** (G or C), **W** (A or T), **H** (A or C or T), **B** (G or T or C), **V** (G or C or A), **D** (G or T or A), **N** (G or A or T or C) (ref. www.metabion.com).

The first designed primers, Epep000down and Epep001down (fig. 4.2), had different degrees of degeneracy. The former one was more non-specific as compared with all 31 different endopeptidases sequences, while the latter was more specifically designed from a comparison with other *Desulfovibrio* species. The first PCR results showed the

amplification with Epep001down (fig. 4.3). Negative controls with no template and positive controls with *lsu* FP (ATG ACT CTA GAA AGG AGA ATA CCA TGA GCG GCT, binding at 1219 bp of the operon) and *lsu* RP (TGA CGA AGC TTT TAC AGG ATG CGG AAC TTG T, binding at 2915 bp of the operon) were always used under identical conditions. Restriction sites for XbaI and HindIII are underlined in the primer sequence of *lsu* FP and *lsu* RP, respectively.

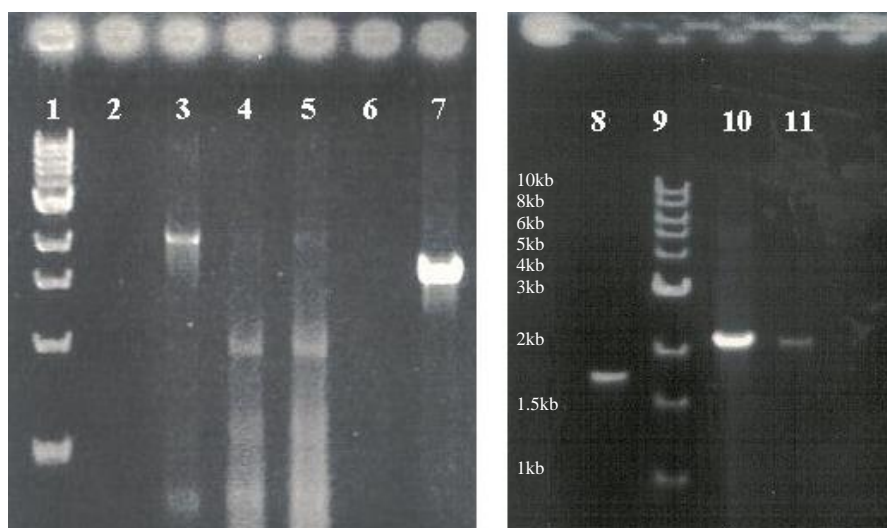


Fig. 4.3 Agarose gel showing PCR results with Epep001 and *lsu* FP. Lane 1, 1kb molecular weight ladder (NEB), lanes 2, 3, 4, 5, PCR product for the test (see text), lane 6, negative control, lane 7, positive control, lane 8, positive control, lane 9, same as lane 1, lane 10, test product amplified, lane 11, 1:10 dilution of lane 10. Molecular weight range of the ladder used present on the right hand side.

For PCR, the forward primer *lsu* FP was used with the reverse primer Epep001 down (fig. 4.2) with chromosomal DNA of DvMF as template. A PCR product of ~2100 bp was obtained and sequenced. The large sub-unit was used as positive control for the PCR. Reverse primer *lsu* RP was used together with *lsu* FP. The operon sequence upto 3100 bp was already known from the earlier work of Voordouw *et al* (1990). The sequencing results from this experiment added another 250 bp to the sequence and marked the start of *hynC*.

Continuing with this result, another conserved region was found downstream in the operon. For this work, primer *hynDup* (fig. 4.2 and fig. 4.4) was generated, comparing the sequences of *D. gigas*, *D. desulfuricans*, and *D. vulgaris* Hildenborough. Again, the PCR product was sequenced and resulted in the gene sequence upto position 4000.

These results completed the sequence of *hynC* and gave a partial sequence of *hynD*. Another set of degenerate primers namely *hynD2* (GWC GCC TTC AKC NVC CKC GGC CA) and *hynD3* (AGA ABV BCR CGK WGW CGC CTT C) were designed downstream of the sequenced operon, but did not lead to specific results, making another approach necessary.

	1	15	16	30	31	45	
1	Azotobacter_vinelandii_hypC	MCLAIPVRIEELLDE	Q-SAVACIGG--LRK	TINVALLDDLKV	GDY		
2	Rhizobium_leguminosarum_hypC	MCLAIPVQVKELLPD	N-MAKVTLDG--VSK	IVSTALVDDVKV	GDY		
3	Thiocapsa_roseopersicina_hypC1	MCLAIPARITSIDVA	ADTAKVALGS--VGK	EISLALIEDAAV	GDY		
4	<i>Desulfovibrio_desulfuricans</i> G20	MCLAIPAEVNELLDG	DMAKCRVGKSDTFVN	VSTMLLEEPAAV	GDF		
5	<i>Desulfovibrio_vulgaris_Hildenb</i>	MCLAIPAEIVEMMDN	DMVRARVGKSETFLT	VSAMLLPEPAAL	GDY		
6	<i>Dgigas_hynD</i>	MCLAIPARIETIEN-	GVATCRVGASDTFVK	ASLLLLLEGQAGP	GDY		
	46	60	61	75	76	90	91 96
1	Azotobacter_vinelandii_hypC	VILHVG	FALQKLDEA	EAQRTLALLAELGRL	AEAEQAAQGEAP---		
2	Rhizobium_leguminosarum_hypC	VVLHVG	YALAKIDPE	EAERTLALIRER---	-----AMGDAA---		
3	Thiocapsa_roseopersicina_hypC1	VLIHVG	YALNKISEE	EAQRTLEMIAQMGLL	ADEQELVPEPTSTVT	GPGGQR	
4	<i>Desulfovibrio_desulfuricans</i> G20	LIVHAG	FALRKLDPA	EAQESLRLLRQMANI	EE-----GTPGGF--	-----	
5	<i>Desulfovibrio_vulgaris_Hildenb</i>	IIVHAG	FALRKLDKA	DAEETLRLLLREVAEA	AE-----GAPAAF--	-----	
6	<i>Dgigas_hynD</i>	LVVHAG	FALRKMDVK	EAEESLQVMRDMAAV	MN-----GGDVRF--	-----	

Fig. 4.4 HynD protein sequence alignment graph of different organisms. The sequence marked in red was used to design the reverse primer. Also the comparison of *Desulfovibrio* species is shown in red.



### 4.3 Sequencing Strategy II

The first results from the initial experiments using PCR gave the complete sequence of *hynC* and the partial sequence of *hynD*. Due to lack of sequence similarities thereafter, it was not possible to complete the sequence of the operon using degenerate primers designed from sequence similarity.

To overcome this problem, another strategy was followed in collaboration during a sojourn with Dr. Voordouw at University of Calgary, Canada.

For this approach, the chromosomal DNA of DvMF was restriction-digested by various endonucleases. The restriction digested chromosomal DNA was run in different wells of analytical agarose gels and blotted. A probe of 425 bp was used for the blot. This probe was generated by PCR using chromosomal DNA as template, p-235f (ACG AAC CCG GCG CCA TCT AC, binding at position 3479) as forward primer and p-236r (GTA GGT TTC GCT CTT GCCCA, binding at position 3898) as reverse primer. A fragment of ~ 2.0 kb was positively identified in SphI-digested sample (lane 5, fig. 4.5), and was selected for further work.

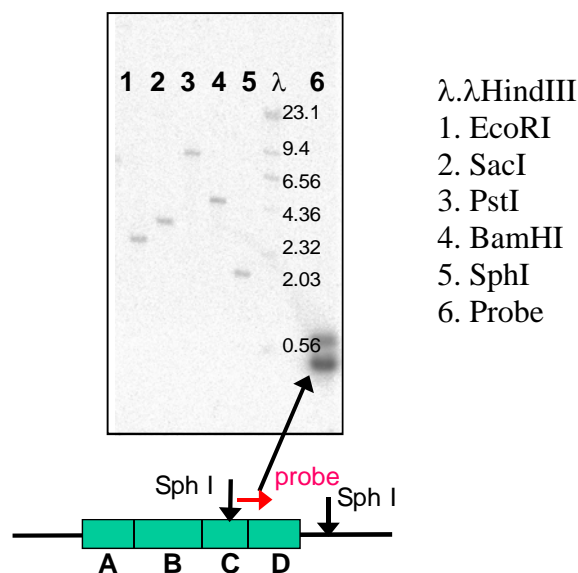


Fig. 4.5 Agarose gel electrophoresis of DvMF chromosomal DNA, restriction digested with EcoRI, SacI, PstI, BamHI and SphI as shown in lanes 1, 2, 3, 4 and 5, respectively. The gel was then southern blotted against a probe shown as red arrow in the schematic figure (probe self blotted in lane 6), complementary to 3'-region of *hynC* and 5' region of *hynD*. The green boxes represent the proposed operon structure of [NiFe] hydrogenase with *hynA*, *hynB*, *hynC* and *hynD* labeled as A, B, C and D, respectively.

Another preparative gel with only SphI digested chromosomal DNA was run to obtain greater amounts of the specific fragment for cloning purposes. The SphI digested chromosomal DNA resulted in a smear due to the presence of DNA fragments of all possible molecular weights depending on the frequency of restriction site occurring in the genome. The part of the smear on the gel in the molecular weight region of the SphI blot ca. 2 kb was cut out and the DNA was gel-extracted. Also the DNA just above and just below the specific molecular weight was cut and eluted in the same way, as shown in fig. 4.6. The three DNA fragments were then again checked for the presence of gene fragment of interest.

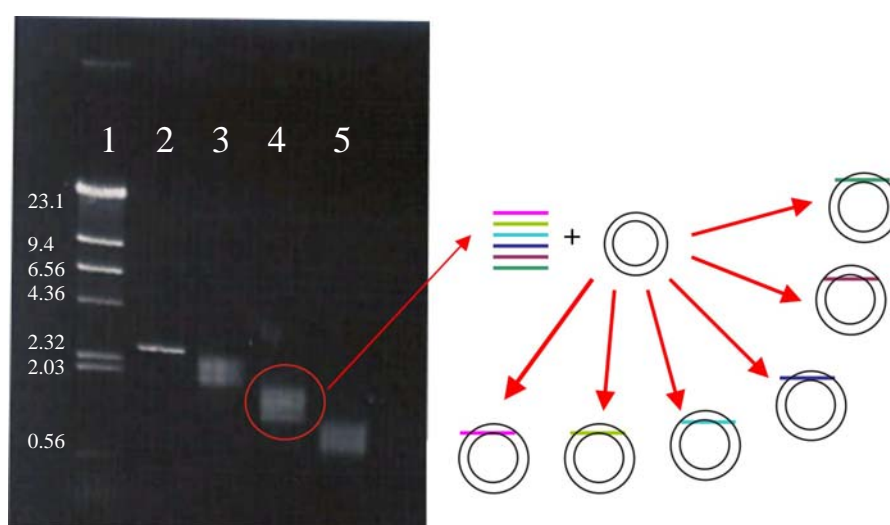


Fig 4.6 SphI digested chromosomal DNA of DvMF (sorted by molecular weight). From left to right, lane 1,  $\lambda$  HindIII, lane 2, SphI digested pUC19. Lanes 3, 4 and 5, are three different molecular weight fractions isolated from SphI digested chromosomal DNA. The excised DNA fragments containing the downstream gene of [NiFe] hydrogenase were randomly cloned in pUC19, and the recombinants were searched for potential positive clones.

The smear fragment was then randomly cloned in the SphI digested and dephosphorylated pUC19 and transformed in *E. coli* TG2, followed by the blue/white colony selection. All the white (recombinant) colonies were checked by pooled colony PCR followed by southern blot with the similar probe (fig. 4.5) to screen for the desired recombinant. The plasmid DNA was then sequenced to generate the complete operon sequence. Thus we now know that [NiFe] hydrogenase operon of DvMF consists of four genes *hynA*, *hynB*, *hynC* and *hynD*, like *D. gigas* and *D. vulgaris* Hildenborough. The 3'-end of the operon was identified by the presence of another gene, probably coding for a lipophospholipase, as derived from sequence comparisons.

*HynC* and *hynD* sequences (this work) were compared with other genes known already (used for designing the degenerate primers) as to place them in the phylogenetic tree (fig. 4.7, 4.8). Software clustal W was used for sequence alignments while mega was used for creating the phylogenetic trees. As seen from the trees, all *Desulfovibrio* species are grouped together and are separated from others to some extent.

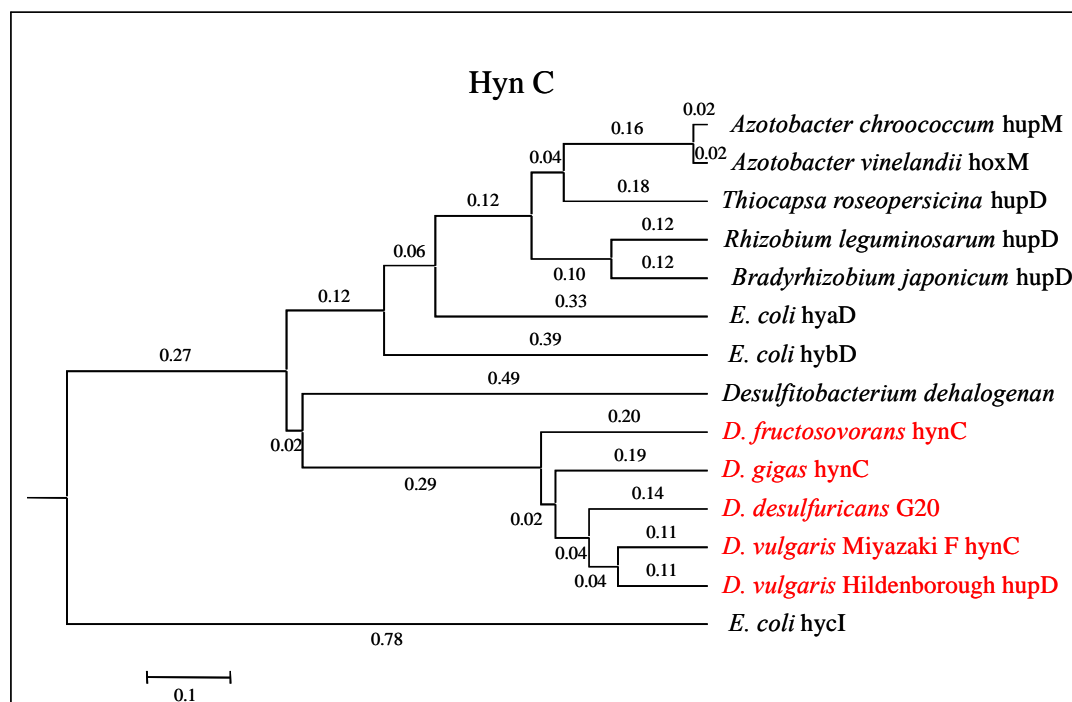


Fig. 4.7 Phylogenetic tree for *hynC*. The numbers shown are Bootstrap number, ranging from 0 to 1, with 0 showing complete identity and no identity by 1. *Desulfovibrio* species pair together in the tree and are marked in red. The respective gi values for the species compared in the tables are: Ac gi:1073096, Av gi:321719, Tr gi:349579, Rl gi:536801, Bj gi:27382050, Ec hyaD gi:13360591, Ec hybD gi:13363350, Dsd gi:9911135, Df gi:538839, Dg gi:3021360, Dde gi:23474622, DvH gi:46580332. First letter of the name of the organism is used for abbreviation for listing the gi values. The order of names used for the list is the same as in tree.

The endopeptidases from two *Azotobacter sp.* pair close together, while two of the three *E.coli* proteins are comparatively closely grouped and much separated from the third. DvMF is most closely related to DvH of the *Desulfovibrio sp.*

The gene for *hynC* (nt 3266-nt 3798) is followed by *hynD* (nt 3825- nt 4086) as in other operons encoding [NiFe] hydrogenases. The *hynC* codes for 168 amino acid residues

(17874.12 Da), while *hynD* codes for 83 amino acid residues (9000.37 Da).

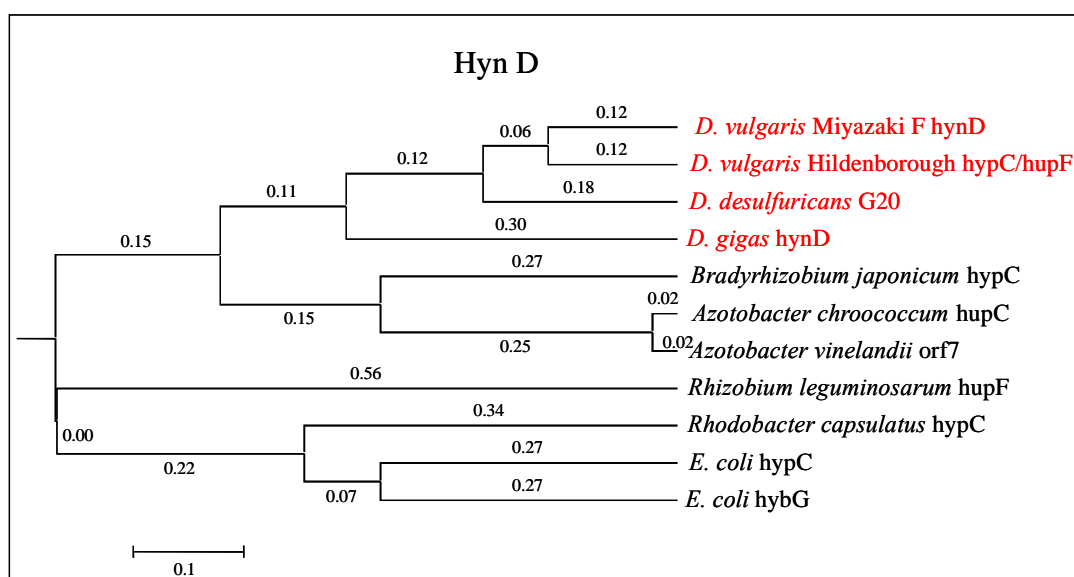


Fig. 4.8 Phylogenetic tree for *hynD*. *Desulfovibrio* species that pair together in the tree are marked in red. The respective gi values for the species compared in the tables are: DvH gi: 46580333, Dde gi:23474621, Dg gi:3021361, Bj gi:27382040, Ac gi:484411, Av gi:39244, RI gi:48726, Rc gi:2126465, Ec *hypC* gi:12517180, Ec *hybG* gi:15833129.

Also in case of *hynD* all *Desulfovibrio* species are grouped close together, with DvMF most closely related to DvH in the phylogeny. Both *Azobacter* species are very closely related for *hynD* too, besides *hynD*. *E. coli* genes are not so closely related, thus in part explaining the inability to substitute for each other in expression studies (Menon NK *et al.*, 1994).

#### 4.4 Expression of the partial and the complete DvMF [NiFe] hydrogenase operon in *E. coli*

The structural genes from DvMF were cloned in pUC19 with **the native promoter** and the expression was studied in *E. coli* DH5 $\alpha$ . Chromosomal DNA from DvMF was used as a template for the PCR with the forward primer DvMF ABCD 001F (AGT CTA AGC TTA TGC GGA AAT GTG TGC CTC A, binding at position 5) and the reverse primer *lsu* RP (TGA CGA AGC TTT TAC AGG ATG CGG AAC TTG T, binding at position 2915) with the HindIII sites underlined. The PCR product was HindIII digested and gel purified, followed by ligation of PCR product with HindIII digested and dephosphorylated pUC19. The recombinants were screened as blue (WT)/ white

(recombinant) colonies against IPTG/ X-gal. Recombinants were confirmed by mini-prep, specific restriction digestion and western blot.

Further identification came from the application of polyclonal antibodies, raised against 90% pure DvMF [NiFe] hydrogenase in rabbit (Eurogenetec, Belgium). It was possible to trace the protein bands with the polyclonal antibodies in western blot. The difference in molecular weight between the WT (the processed form) and recombinant (the unprocessed form) is apparent as seen in fig. 4.9.

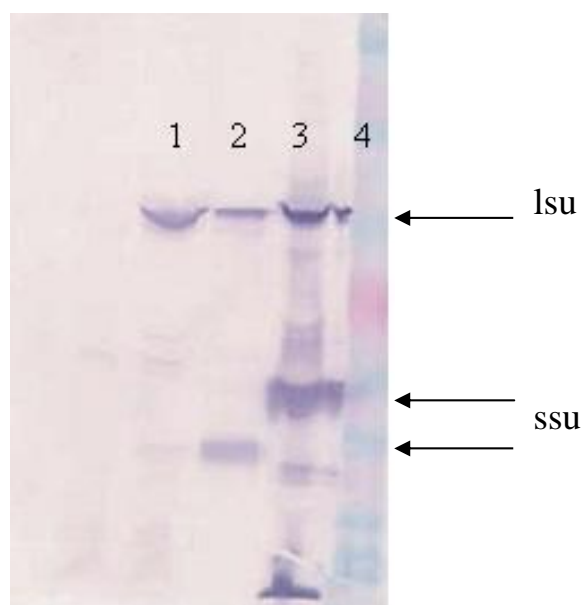


Fig. 4.9 Western blot of native and recombinant [NiFe] hydrogenase. Lane 1 DvH WT, lane 2 DvMF WT, lane 3 recombinant expressed in *E. coli* and lane 4 colored molecular weight marker.

The processed hydrogenase of DvMF has a molecular weight of 60,866 Da for LSU and 28,763 Da for SSU, as compared to the unprocessed one with molecular weight of 62,626 Da and 34,113 Da for LSU and SSU, respectively. The difference in molecular weight between processed and unprocessed SSU is clearly seen comparing lane 2 and lane 3 for the DvMF-derived and recombinant enzyme expressed in *E. coli* that was cloned together with its native promoter. The clone generated by single restriction enzyme HindIII was checked by internal restriction digestion and was found to be in reverse orientation. The expression proves the recognition of the DvMF promoter by *E. coli*. For a detailed account on the maturation pathway, required for a functional, processed enzyme, refer to introduction.

The expression of the complete operon in *E. coli* also leads to similar results stating no maturation of the structural genes in *E. coli*. This again highlights the specificity of the

maturation and the apparent requirement of additional proteins of the maturation pathway (data not shown).

#### **4.5 Cloning of *hynC* in pET28 and expression in *E. coli* BL21**

The endopeptidase gene (*hynC*) from DvMF was cloned in pET 28a (novagen) under the strong T7 promoter to over-express the protein. The gene sequence was amplified using the forward primer FP2 *hynC* NdeI (TGT ACT GAT ACA TAT GAT GAG CAA TCG CCC CA, binding at 3266) and the reverse primer *hynC* HindIII RP ( AAG TAA AGC TTT CAG GCG GGT TGT ACG GCC T, binding at 3778), with the NdeI and HindIII sites underlined, respectively. . The resulting PCR product of ca.520 bp and the plasmid were digested with HindIII and NdeI, buffer exchanged using QIAgen kit, followed by ligation at RT for 5 hours. Ligation was performed for the vector and the gene together with several combination for controls: religating the single cut plasmid with each enzyme separately, religating the double cut plasmid without the gene insert and the main experiment of ligating the double cut plasmid with the gene insert. The ligation mix was transformed in *E. coli* BL21 and selected on LB Cm Kan plates. The number of colonies grown after O/N incubation at 37°C was compared for all the different ligations performed. In case of a marked difference in the number of colonies obtained, between control and main ligation experiment (with the maximum in the main experiment), the colonies were checked by pooled colony PCR. This was followed by miniprep, restriction digesting the gene out of the vector and gene sequencing. Experiments are underway in the group to continue with cell growth, protein isolation and purification, aiming at crystallization of the protein to study the structure and to compare it with other structurally characterized endopeptidases (Fritsche E *et al.*, 1999).

#### **4.6 Secondary structure prediction**

Hydrogenase endopeptidases show a very precise and selected activity. The differences in the various enzyme activities demand the determination of their three-dimensional structure or at least a modelling on the basis of already known crystal structures. Only a single hydrogenase endopeptidase has been characterised up to now in its three dimensional structure, *hybD* from *E. coli* (Fritsche E *et al.*, 1999). A first approach to



#### 4.7 Discussion

With the new sequence obtained in this work, it is now possible to align other sequence information to find similarities for promoters; transcription and translation start sites and termination sequences. The presence of a  $\sigma^{54}$  type of promoter has been proposed for hydrogenase operons (Deckers HM *et al.*, 1990; Rousset, M *et al.*, 1998). In case of DvMF and *D. gigas* (Dg), the presence of a promoter like region was proposed between -190 bp to -181 bp and -159 bp to -148 bp from the translational start site of the small subunit of Miyazaki (Deckers HM *et al.*, 1990).

DvMF CATTTTCAATTGGAATAACGTTTC-----AATGTGTTGTACCTTCCCGG  
 Dg CATTATCAATGCCTTCAATGCACTTCAAGCTGCCGTTGGACCTGCCCCGA  
 DvH CATCATCAAAGGCTATTATTTCCGTATCGAAATAGTCATTATCG

Similar sequences, located -190 bp to -181 bp upstream the translational start site of the small subunit can be seen also for DvH, however, the other conserved region present at -159 bp to -148 bp is missing. In case of *D. fructosovorans* (Df) none of these regions were found.

Species	hynA	hynB	hynD
DvMF	CGAAGGAGGCAG-GGATG	CCAAGGAGAAATA--CCATG	CGACGGAGCAGACCCGATG
DvH	GCAAGGAGGATGCGAATG	AGAAGGAGGAAGCCCATG	TAACGGAGAAAC----ACATG
Df	CAAAGGAGGACGTTTATG	TGACGGAGGAAGCATATG	
Dg	GCCTGGAGCG 20n TCATG	CACAGGAGAA GACCCATG	CCAAGGAGCGCGC--GCATG

Species	hynC
DvMF	TTCCGAC-----CTTGCGCCAGGCCTTTTCCAACCCATATAGTACACCCCACATG
DvH	TTGGCAGACTGCCGCTGTGAAGACGAACCGCA-----CGTCTAGAACCCG----GTATG
Df	TTCGGGCCCCGCTTCGGGCCGGGTTCTTCG-----TTTCTCAAGGAGGTCGCATG
Dg	CCGGCCTTGCCGCCGGGCTCCTGACGCTTATCAAGGTGTT----CATG

Table 4.2 Comparison of ribosome binding regions and promoter regions of *Desulfovibrio* species. The ribosome binding sites (rbs) are marked in dark grey, TATA box (-10) and -35 region is marked in light grey and the translational starts of the genes are marked with ATG. In case of a longer space between rbs and the translational start, the number of nucleotides is indicated, 20n in case of Dg.

A sequence comparison of putative ribosome binding site (rbs) for all the genes present in the [NiFe] hydrogenase operons of the various *Desulfovibrio sp.* reveals that *hynA*, *hynB*, *hynD* have GGAG as conserved rbs, and in a wider context AAGGAGG as shown in the table. However, this motif is not as well conserved for *hynC*. The rbs is a



purine rich region, and as the  $-10$  region of the TATA box is also transcribed, may be the GA sequences present in TATA box add to the rbs for *hynC*. In case of *hynC*, prokaryotic promoter-type sequences  $-10$  and  $-35$  are present as seen from table 4.2. This probably indicates that the structural genes might be expressed separately and that the expression of *hynC* and *hynD* is probably differently regulated. Earlier work involving studies with Df mRNA transcript showed that the sequence containing only *hynA* and *hynB* was maximally present and marginal transcripts were found with higher molecular weight, possibly expressed in conjunction with *hynC* also (Rousset, M *et al.*, 1993). Also the presence of an inverted repeat sequence at the end of *hynB* has been reported for all *Desulfovibrio sp.*, further strengthening the idea of two separate transcription units. For DvMF and DvH, two sequences are found upstream of translational start with similarity to  $-35$  region. Either one of these may be the possible  $-35$  region or probably they both play some role as recognition site for promoter.

The arrangement of other maturation genes present in same operon or in a scattered way in the genome has been described for all the [NiFe] hydrogenases. The recently published genome sequence of DvH (Heidelberg JF *et al.*, 2004) gives the possibility to compare the other maturation genes, besides those present in one operon in *Desulfovibrio*, with the others species. Five genes, namely *hypA*, *hypB*, *hypD*, *hypE*, *hypF* arranged in 3 operons were seen for DvH (table 4.1). They were compared with the known sequences and are presented here in phylogenetic trees.

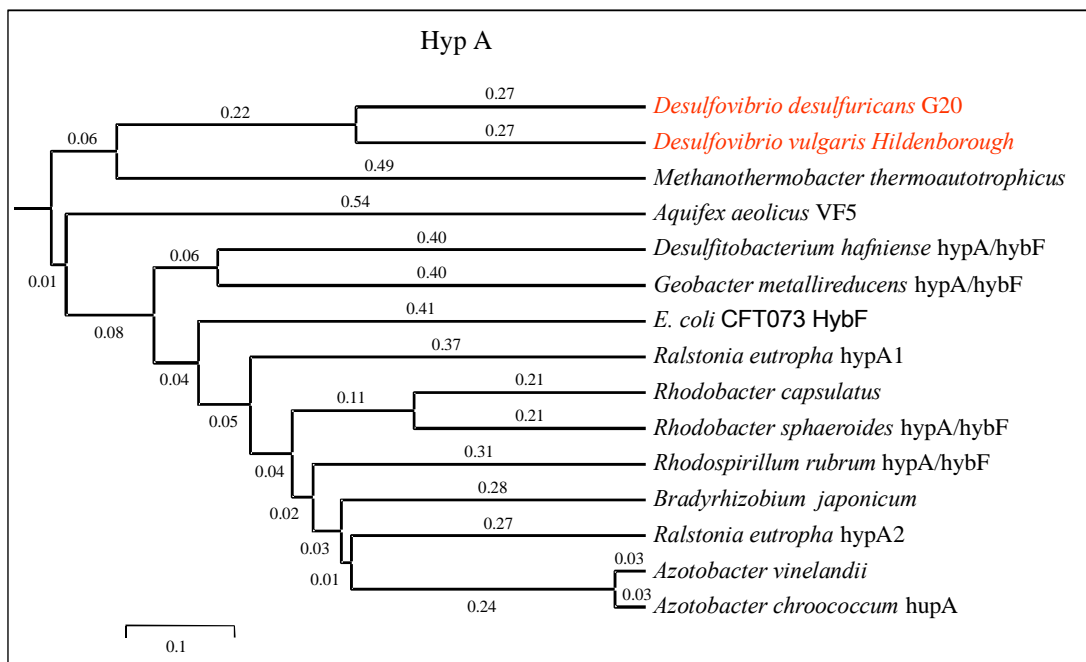


Fig. 4.11 Phylogenetic tree for hypA. The numbers shown are Bootstrap numbers, ranging from 0 to 1, with 0 showing complete identity and no identity by 1. The assignment of “1” and “2” in the species names represents the presence of more than one hydrogenase in the genome, and the number represents the number/name given in the publications. The *Desulfovibrio* species (given in red) pair together in the tree. The respective gi values for the species compared in the tables are: Dde gi|23476007, DvH gi|46580733, Mt gi|14285479, Aa gi|7445131, Dh gi|23120181, Gm gi|23054727, Ec gi|26109967, Re1 gi|38637680, Rc gi|46052, Rs gi|22960018, Rr gi|22968579, Bj gi|27355213, Re2 gi|38637759, Av gi|398007, Ac gi|484408.

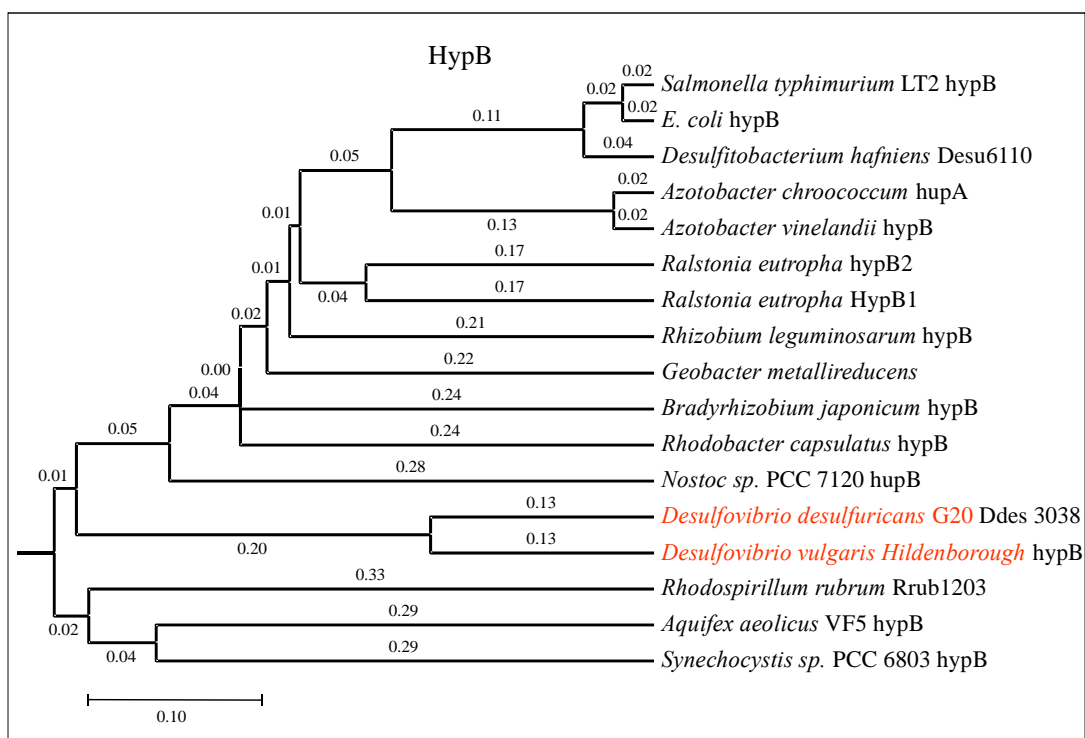


Fig. 4.12 Phylogenetic tree for hypB. The respective gi values for the species compared in the tables are: St gi|16421401, Ec gi|2506574, Dsh gi|23119941, Ac gi|484409, Av gi|23106421, Re2 gi|38637760, Re1 gi|38637681, Rl gi|536810, Gm gi|23055435, Bj gi|30179632, Rc gi|123937, Ns gi|25529708, Dde gi|23476244, DvH gi|46580734, Rr gi|22966604, Aa gi|2983266, Ss gi|1652374.

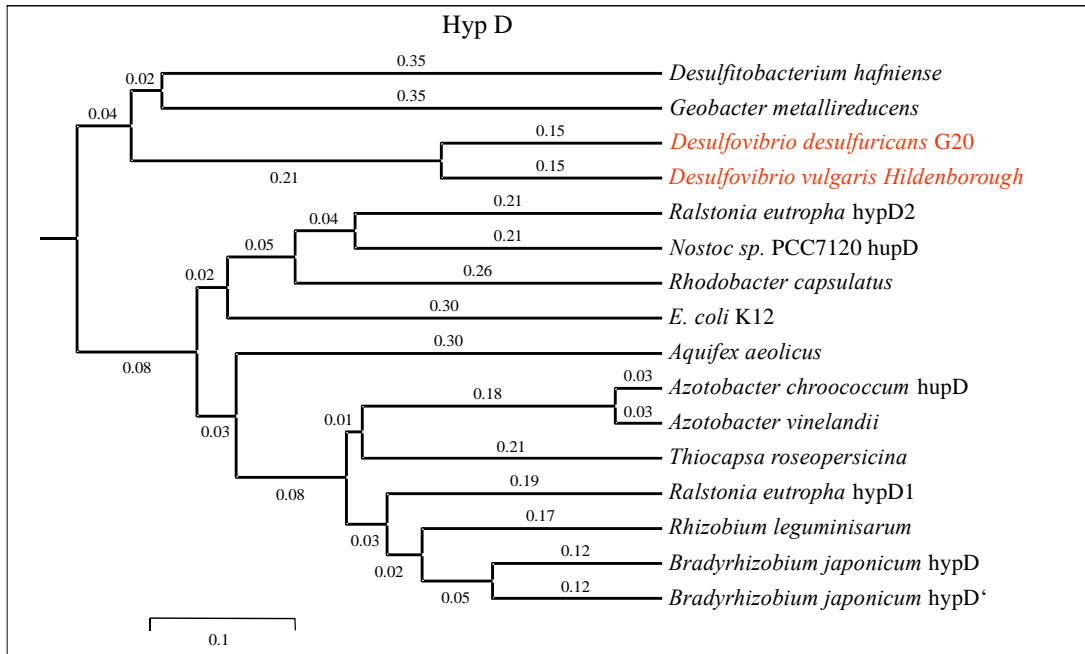


Fig. 4.13 Phylogenetic tree for hypD. The respective gi values for the species compared in the tables are: Dsf gi|23112159, Gm gi|23055431, Dde gi|23474339, DvH gi|46578741, Re2 gi|38637740, Ns gi|17228191, Rc gi|2126466, Ec gi|16130636, Aa gi|15606409, Ac gi|2120752, Av gi|400034, Tr gi|30720165, Re1 gi|38637684, Rl gi|729789, Bj hypD gi|27376847, Bj hypD' gi|27382039.

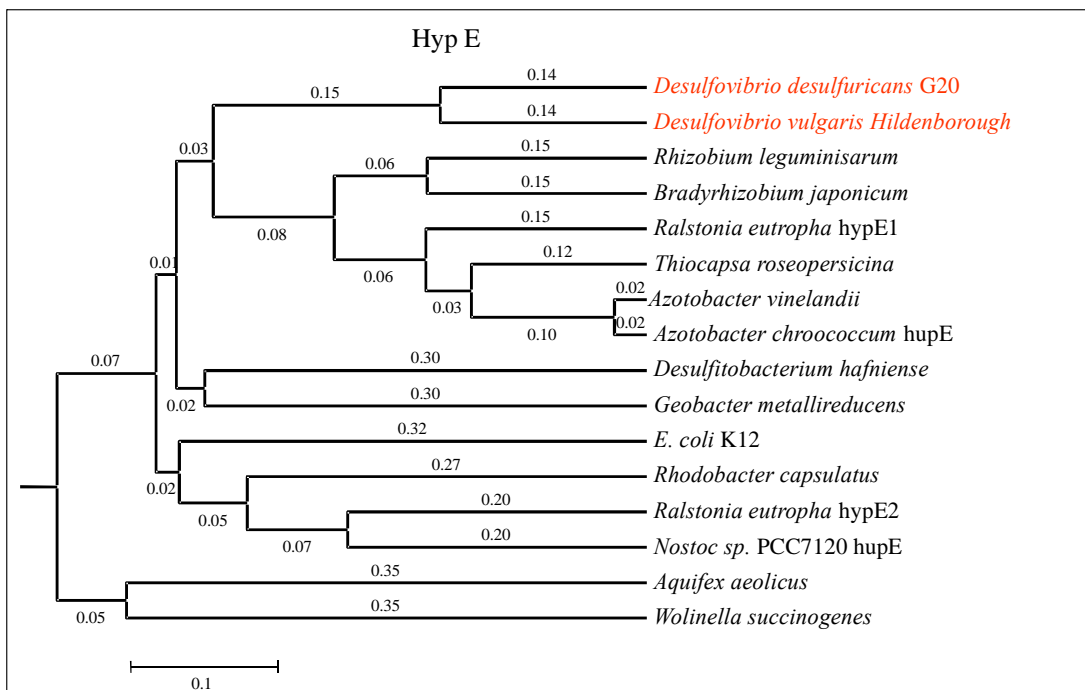


Fig. 4.14 Phylogenetic tree for hypE. The respective gi values for the species compared in the tables are: Dde gi|23474338, DvH gi:46578742, Rl gi|729792, Bj gi|27376848, Re1 gi|38637685, Tr gi|30720166, Av gi|23106417, Ac gi|1170420, Dsf gi|23112158, Gm gi|23055430, Ec gi|16130637, Rc gi|46056, Re2 gi|38637741, Ns gi|17228193, Aa gi|15606316, Ws gi|34557193.

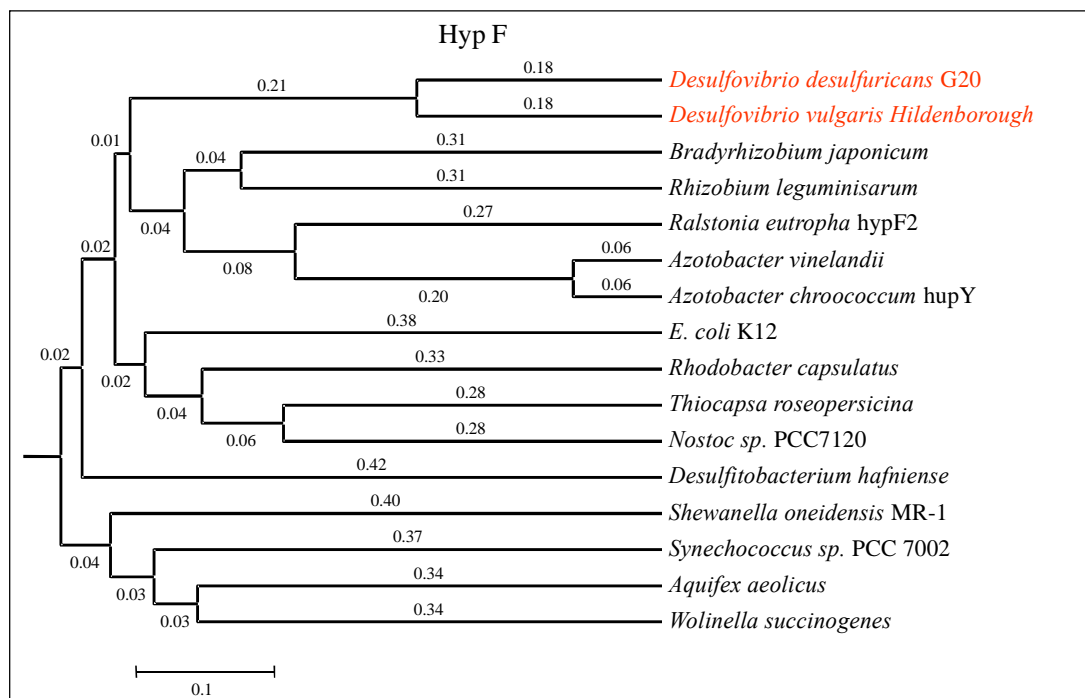


Fig. 4.15 Phylogenetic tree for hypF. The respective gi values for the species compared in the tables are: Dde gi|23475424, DvH gi:46581470, Bj gi|27382041, Rl gi|729795, Re2 gi|38637682, Av gi|3041688, Ac gi|484410, Ec gi|16130619, Rc gi|729796, Tr gi|14209676, Ns gi|17228189, Dsh gi|23112161, So gi|24373654, Ss gi|22652029, Aa gi|15606085, Ws gi|34557188.

The phylogenetic trees demonstrate the relatively close evolutionary relation of all listed species, with *Desulfovibrio sp.* grouped closely together similarly as shown for *hynC* and *hynD* already. Their universal presence in all compared species gives evidence for their importance in the maturation of hydrogenase enzymes. As the attempts to achieve the heterologous expression by cloning only the structural genes of DvMF in *E. coli*, failed, it would thus be important to include all genes in an expression system, as suggested above.

Richest information, also based on a comparison of other proteins of that type, can be obtained for *hynC*. On that basis, a better structural and also functional understanding might be extracted from a comparison of its secondary and predicted tertiary structure with the known one from *hybD* of *E. coli*, which also might shed light on the specificity

of the respective enzymes. The function of the endopeptidases (C- subunit) relates to the last step in the maturation of large subunit, i.e. the removal of 15 amino acid residues from its C-terminal end (Casalot L *et al.*, 2001). It is very interesting that the three different hydrogenase endopeptidases from *E.coli* do not supplement each other in the maturation of the large subunit (Blokesch M *et al.*, 2001). One of the reasons could be the mode of action and requirement of additional gene products. A role for two of these proteins from *E. coli* has been established: *hybD* is a GTPase and facilitates nickel-insertion into pre-hydrogenase (Maier T *et al.*, 1996; Maier T *et al.*, 1993), and *hypC* binds to pre-hydrogenase 3 and keeps it in a conformation accessible for metal incorporation (Drapal N *et al.*, 1998). Another reason for reaction specificity of maturation protein could be related to the molecular structure of the protein and the way in which it interacts with the pre hydrogenase during maturation. Comparison of the secondary structure of *hynC* from DvMF with the known crystal structure of *hybD* from *E. coli* (fig. 4.16), calculated using SSEA Server shows very high homology in the amino acid sequence, secondary structure deducted with the PsiPred, and even the tertiary structure.

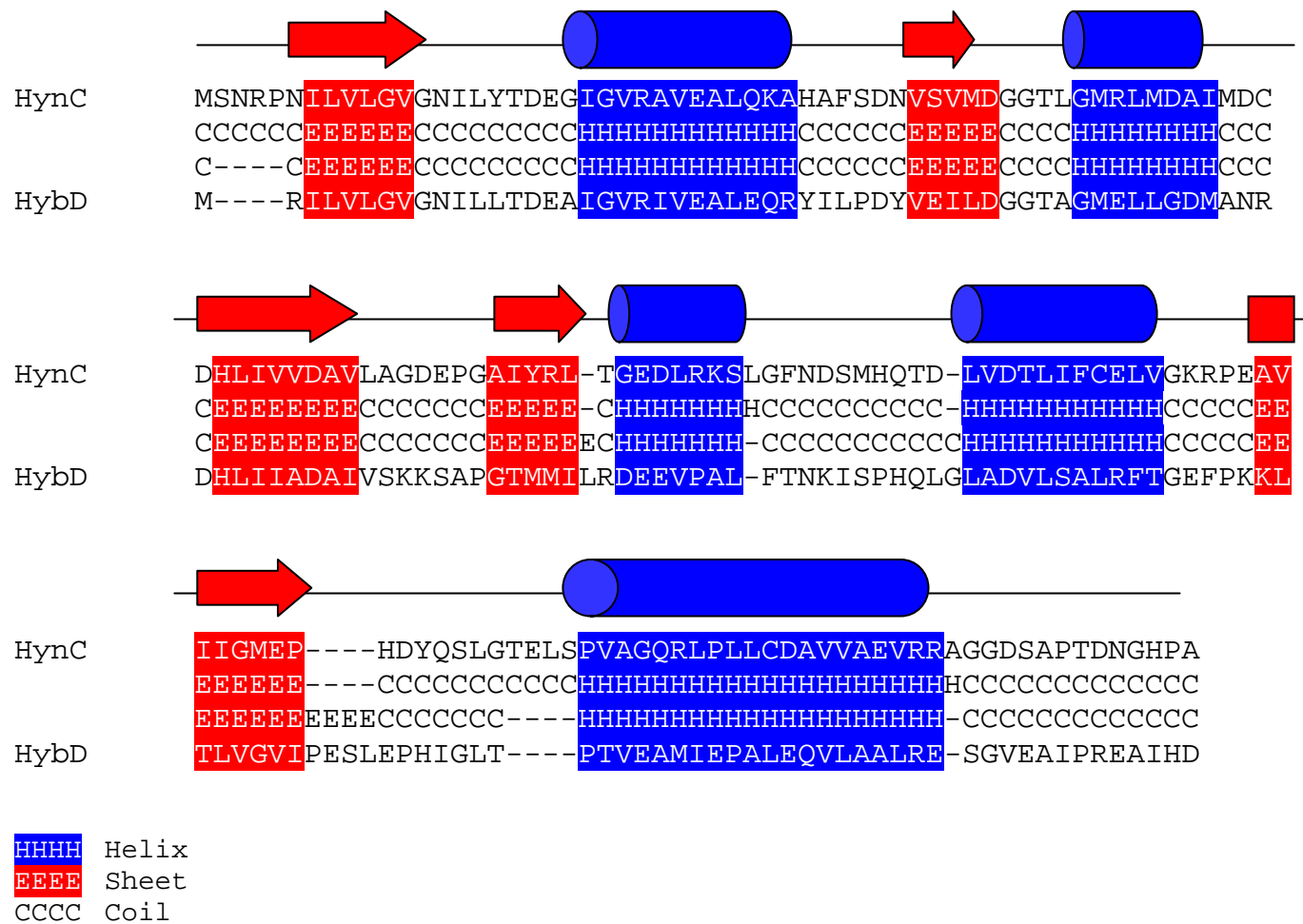


Fig. 4.16 secondary structure comparison hybD vs hynC, SCORE: 94.5783

The sequence alignment and the secondary structure prediction for HynC and HybD indicate the high degree of homology between both proteins. As well the  $\alpha$ -helical parts as also the  $\beta$ -sheets match nearly the same and imply a very similar overall three-dimensional structure.

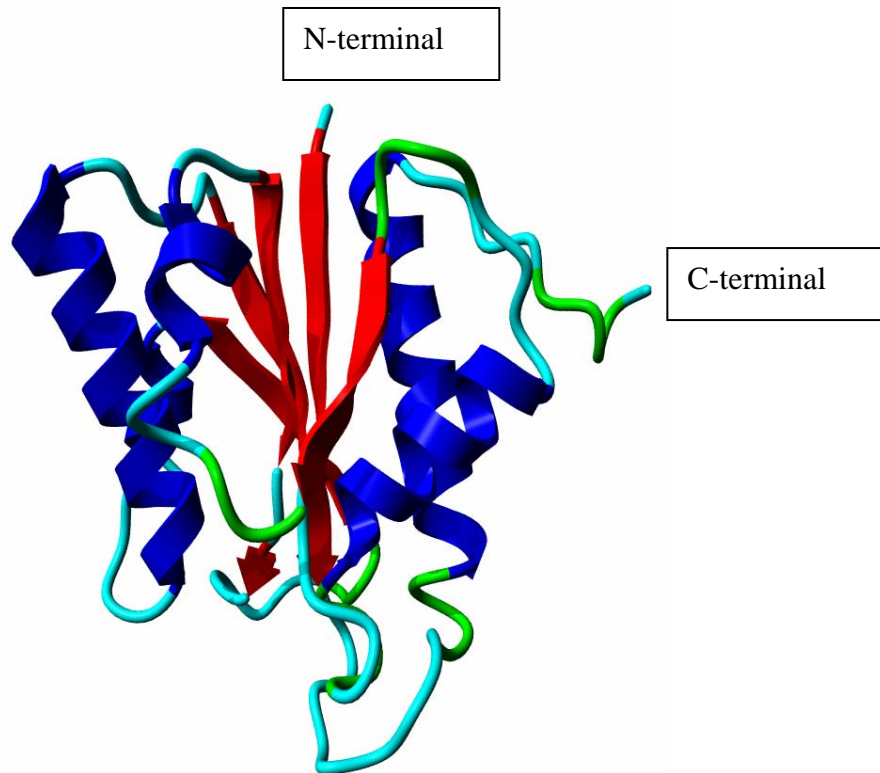


Fig. 4.17 Automatic homology modelling for hynC, using hybD as template. Indicated N- and C-terminus in the figure.

This model was generated using SwissPdbVier with hybD as template. HynC sequence was fitted to the template and energy minimisation was carried out using the MOLOC molecular modelling and simulation software, revealing the putative high similarity of the three-D structure for both proteins.

## Chapter 5

# Construction of a DvH [NiFe] Hydrogenase Deletion Mutant

This part of the thesis was aimed at the controlled expression of the hydrogenase and at the construction of mutants to study the action mechanism of hydrogenase. As outlined above, the maturation of [NiFe] hydrogenase is very complex and very specific. This makes its study difficult in a heterologous system. Furthermore, in case of DvMF the genome sequence is not known. Accordingly, the primary task was the identification of all the maturation genes, at least those being present in the same operon. This was accomplished as described in chapter 4. An alternative to the heterologous expression of the unprocessed form of hydrogenase in a selected host (see above) could be the set-up of a homologous system with deleted endogenous structural genes. Once such a system is established, the expression of the hydrogenase could be restored by reintroducing the structural genes with their native promoter in a cassette in a suitable vector. Accordingly, for the study of functional changes based on mutagenic changes, a cassette, containing the mutated structural genes was prepared.

Various factors were considered and optimized before initiating the construction of the deletion mutant. One important aspect is the employment of selectable markers, which help to identify rare events such as transformants, transconjugants, and mutants from a large background population. Initially, the only reliable selection marker for plasmid transfer to sulfur reducing bacteria was the chloramphenicol resistance gene (*cat*) of Tn9, which renders a slightly higher resistance to chloramphenicol than the background



(5-10 vs. 3  $\mu\text{g/ml}$ ). It had been used for selection of transconjugants with plasmid pSUP104 and its derivatives (van Dongen *et al.*, 1994). Besides, some others have since been used, e.g. kanamycin (Rousset *et al.*, 1991), gentamycin (Casalot L *et al.*, 2002a; Casalot L *et al.*, 2002b).

Plasmid transfer by commonly used chemical treatment protocol has not been documented for *Desulfovibrio*. Transformation by electroporation has been achieved only in case of *D. fructosovorans* (Rousset *et al.*, 1991) and attempts to introduce plasmids into *D. desulfuricans* by electroporation have been reported to be unsuccessful (Wall *et al.*, 1993). The plasmid transfer by conjugation is much less sensitive to nucleases than the transfer by transformation, and is a rather non species-specific process that probably takes place widely throughout the microbial world (Mazodier and Davies, 1991). For *Desulfovibrio* species, a mobilizer strain, *E. coli* S17-1 (Simon *et al.*, 1983), which contains an integrated IncP plasmid RP4 in its genome to provide the *trans*-acting mobilization function, has been used by van der Berg *et al.* (1989) for transfer of pSUP104 ( $\text{Cm}^{\text{R}}$ ) and its derivatives into DvH. Generally for gene replacement mutagenesis, a plasmid is used that is unstable in the target cell (thus also called suicide plasmid or integration plasmid) and that cannot survive unless it is integrated into the target genome by homologous recombination. The suicide vector should lack homology with the target chromosome to ensure that the homologous recombination is limited to the targeting gene sequence. In order to survive, the bacteria have to undergo recombination with the suicide plasmid to incorporate the antibiotic resistance gene used as selection marker, in the genome. The plasmid carries modified gene from the chromosomal DNA. This cloned gene in the plasmid is recognised as homologous to the chromosomal DNA by the bacterial machinery, and at this site recombination takes place between homologous gene sequences of the plasmid and the chromosomal DNA, inserting the complete plasmid into the genome of the bacteria (fig. 5.2).

Homologous recombination-directed mutagenesis could be insertional mutagenesis or replacement mutagenesis. In case of the former, a single recombination event between the targeting sequence introduced into the cell and the targeted homologous chromosomal sequence leads to integration of the circular vector at the target locus on the chromosome (fig. 5.2). The gene sequence in the chromosomal DNA is thus

duplicated, as the primer with the same gene is integrated in the chromosome. Presence of these two identical regions in the chromosome can lead to reversion (of insertion) by a second recombination, leading to losing the integrated plasmid when the proper antibiotic is not maintained in the growth medium. A gene interruption mutant is therefore not very stable without continuous selection. While in case of latter, a double recombination between the targeting sequence introduced into the cell and the targeted homologous chromosomal sequence on both sides of an altered sequence, leads to the replacement of the chromosomal gene with the introduced one (fig. 5.5). Because there are no duplicated sequences in the final construction, replacement mutants are stable and will not revert to wild type by homologous recombination.

Besides the antibiotic as selection marker, replacement mutagenesis requires a counter-selectable marker, for the second crossover. As an example, the *sacB* is used, which confers sucrose sensitivity to the bacterial species. *B. subtilis sacB* is the structural gene for levansucrase (Gay *et al.*, 1983), resulting in hydrolysis of sucrose and synthesis of levans, which are branched fructose polymers of high molecular weight. Cloning and expression studies of the *sacB* gene revealed it to be lethal to the *E. coli* host in the presence of sucrose in the medium (Steinmetz *et al.*, 1983). This lethality was thought to be due to the production of levans, which are retained in the cell envelope structure and block essential transport processes across the membranes (Steinmetz *et al.*, 1983; Jäger *et al.*, 1992). A modified pUC19, containing a unique, rare NotI site was constructed, named as pNOT19, together with several ‘Mob’ cassettes containing *oriT-sacB*, or *oriT-cat-sacB* in a NotI fragment (Schweizer, 1992). This plasmid with the mob-sac cassette can be used to ligate the modified gene of interest with the first selection marker. Then the recombinant plasmid can be transferred into the recipient bacterium, in which the ColE1 replicon is non-replicative, by conjugation from *E. coli* S17-1, a mobilizer strain which contains the *tra* gene required for plasmid transfer (Simon *et al.*, 1983).

## 5.1 Plasmid construction

For the generation of the deletion mutant, a pNOT19-based suicide plasmid was constructed. PCR amplification of DvH DNA with primers p225-f and p226-r (TCG AAA GCT TCG GCG CGG TAA CAC GAT T and TCG AGG TAC CCA GGA GCA

TGG CTG AAA C; HindIII and KpnI sites underlined), gave a 4005-bp PCR product, spanning *hynAB*, and part of *hynC*. Following digestion, this PCR product was ligated to HindIII-KpnI cut pNOT19 to give pNOTNiFe. Another PCR was performed with primers p227-f and p228-r (AGT ACG GAT CCA CGA ACC GGC ACG TCT AG and AGT ACG GAT CCC ATC GTG TGG GTT GGC GAC; BamHI sites underlined). The PCR product thus generated had flanking ends with BamHI sites and a deletion of the 2.5-kb *hynAB*-containing fragment. This product was digested with BamHI and ligated with a 1.4-kb BamHI fragment from plasmid pUC19Cm, containing the *cat* gene encoding a chloramphenicol resistance marker. Insertion of a 4.5-kb NotI fragment from pMOB2 (carrying the *mob-sac* cassette) gave pNotΔNiFeCmMob.

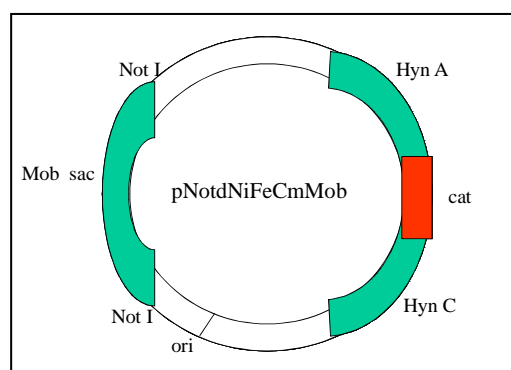


Fig. 5.1 Pictorial representation of suicide plasmid construction. First, the gene fragment spanning *hynA* and *hynB* was ligated to pNot19. This was followed by reverse PCR of the recombinant plasmid generating deletion in the genes, which was replaced by the *cat* gene. Finally, the *mobsac* gene cassette was ligated into the NotI site.

A slightly modified strategy was used for the construction of the suicide plasmid to generate the knockout mutant for DvMF. The upstream region of the operon was amplified using primers p233-f and p224-r (AGT ACA AGC TTA TGC GGA AAT GTG TGC CTC and ATA GGA TCC GCG TCG TTG ACG CCC TT; HindIII and BamHI sites underlined), resulting in a 770 bp PCR product. Following digestion, this PCR product was ligated to HindIII-BamHI cut pNOT19 to give pNOTMNiFeN. Similarly, the downstream region of the operon was amplified using primers p223-f and p222-r (CTG TCG CAC TGG ATC CGC ATC G and AGT ACG GTA CCT GGT CGC AGT CCA TGA TG, BamHI and KpnI sites underlined), resulting in another 775 bp fragment in PCR. Following digestion this was ligated to BamHI-KpnI cut pNOTMNiFeN. This product was digested with BamHI and ligated with a 1.4 kb BamHI fragment from plasmid pUC19Cm, containing the *cat* gene encoding a chloramphenicol resistance marker. Similar to DvH, insertion of a 4.5-kb NotI fragment from pMOB2 (carrying the *mob-sac* cassette) gave pNotΔMNiFeCmMob, where “M” in the name of the suicide plasmid stands for DvMF.

## 5.2 First cross over mutant

The mobilizable, suicide plasmid was transferred by conjugation (chapter 3.4.13) from *E. coli* S17-1 to DvH and DvMF in separate experiments. Single crossover integrants were selected on medium PE plates, containing kanamycin and chloramphenicol. Homologous recombination was forced by supplementing the growth medium with chloramphenicol. The overlapping region of the plasmid and the chromosomal DNA underwent recombination and the complete plasmid DNA gets integrated in the genome of the bacteria, thus disrupting the [NiFe] hydrogenase operon (chapter 5.1). The scheme here considers the downstream region of the operon as crossed over (which was the case for the experiments done), however, also the upstream region could be targeted as well.

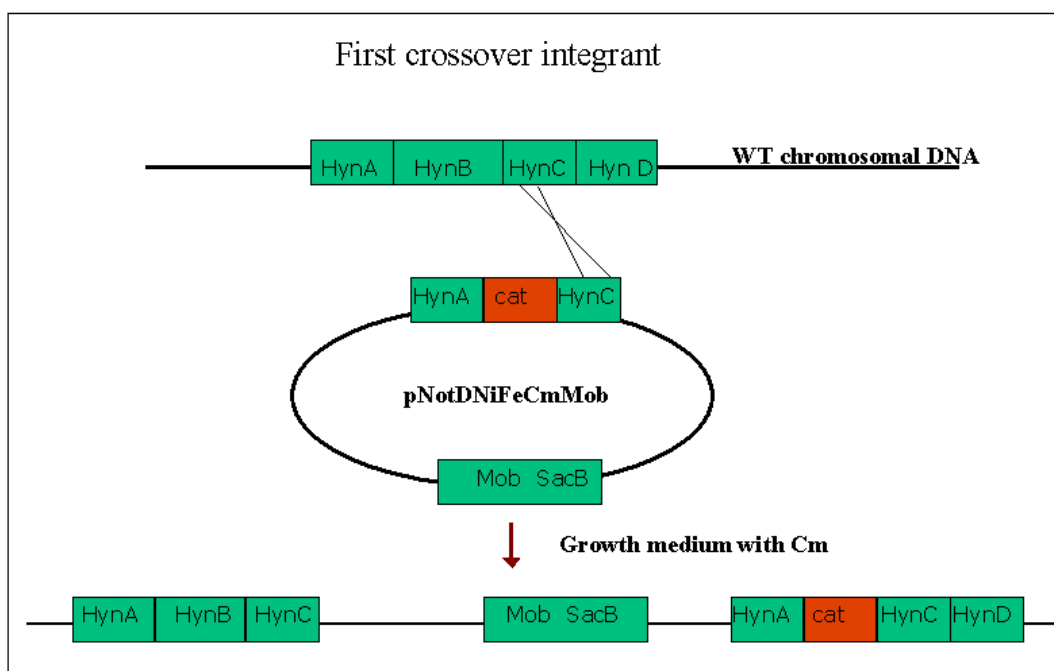


Fig. 5.2 General scheme to show the integration of plasmid DNA in the chromosomal DNA following the homologous region crossover. Following the crossover, the complete vector is inserted in the genomic DNA.

The integrants were screened by PCR (Fig. 5.6) using the primers p225-f and p226-r for DvH, and p233-f and p222-r for DvMF, respectively. Following, this was confirmed with Southern blotting (chapter 3.4.14) (Fig. 5.3), using a 750-bp PCR-derived fragment corresponding to the upstream region of the homologous region used for crossover, as the probe. In case of WT, single bands are obtained in southern blots, while the

integrant shows a band from the WT, besides an extra band from the genes introduced by the integrated plasmid (fig. 5.3), as the restriction pattern of the gene is modified. For KpnI, the digestion results in a high molecular weight product, as the restriction site is present less frequently. In this case, the plasmid integration alters the digestion pattern also for the WT band.

The restriction pattern was also calculated and was found to be: for WT, HindIII >29643 bp, SalI 2469 bp, PstI 2687 bp, KpnI 6551 bp, EcoRI 3906 bp. For the integrant, besides the similar band as obtained for the WT, an extra band was observed with restriction pattern, HindIII 8813 bp, SalI 7892 bp, PstI 6909 bp, KpnI 10549 bp and 4070 bp, and EcoRI 3900 bp.

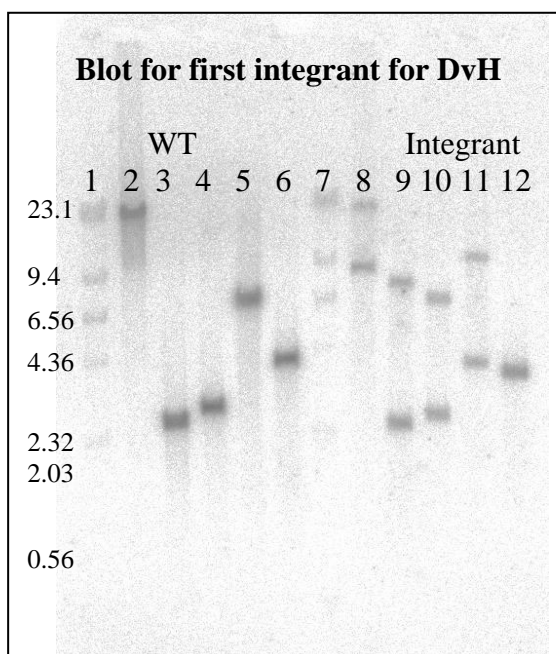


Fig. 5.3 Southern blot, comparing the WT and the integrant for [NiFe] hydrogenase of DvH. Lane 1,  $\lambda$  cut with HindIII, lane 2 to lane 6, WT DNA restriction digested with HindIII, SalI, PstI, KpnI and EcoRI, respectively, lane 7, same as lane 1, lane 8 to lane 12, integrant DNA restriction digested with HindIII, SalI, PstI, KpnI and EcoRI, respectively.

As seen in fig. 5.3, chromosomal DNA from WT and integrant has been restriction digested with a similar set of endonucleases. There are two bands in case of integrants, as compared to a single band from WT. In case of EcoRI, both the bands are of related molecular weights thus an overlapping strong band is observed.

In case of DvMF, a calculation of the exact molecular weight of the restriction digestion pattern was not possible, as the genomic sequence is not known. From the calculation, we could find the possibility of SalI digested chromosomal DNA, which produces a band of >1309 bp, and an extra band for the integrant of 7562 bp. The SalI digested band from the WT was found to be 4.5 kb from the experiments as shown in the fig. 5.4.

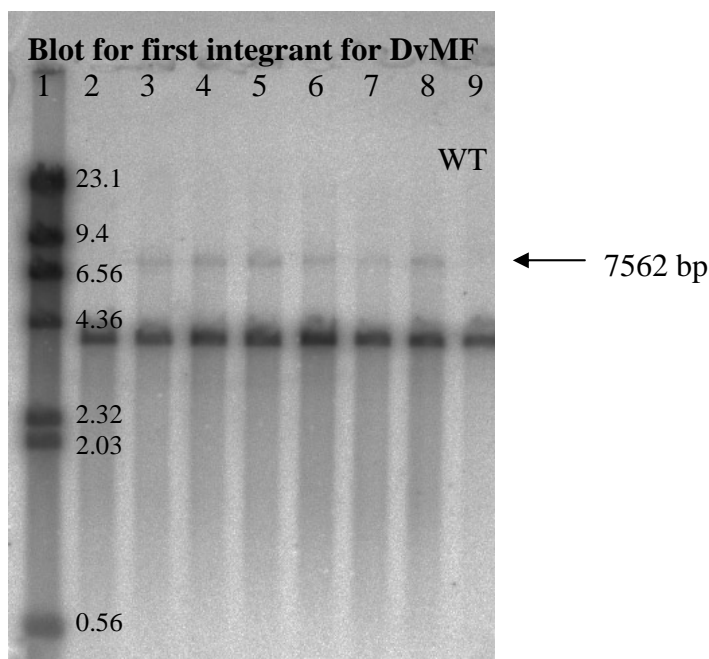


Fig. 5.4 Southern blot comparing the WT and the integrant for [NiFe] hydrogenase of DvMF. Lane 1,  $\lambda$  cut with HindIII, lane 2 to lane 8, integrant DNA restriction digested with SalI, lane 9, WT DNA, restriction digested with SalI.

In case of the integrant (fig. 5.4), an extra band of molecular weight ~7.5 kb is expected. Such band was visible in case of each integrant tested but shows very low intensity, unlike in DvH. Isolated single cell colonies of the integrant were cultured and DNA was blotted to check the intensity of two bands representing the WT and the integrant. However, all the colonies tested did not show equally intense bands. This indicates that probably the integrant cannot grow and survive on its own, probably as a result of the mutation introduced, and thus can only survive in mixed cultures.

### 5.3 Second cross over mutant

A double crossover replacement mutant (DvH NiFe100) was obtained from the cultures of the integrant grown in medium C in presence of sucrose and chloramphenicol. With

the presence of sucrose in the medium, the *sacB* gene causes lethality, thus rendering the bacteria unable to grow while retaining the plasmid. The bacteria can undergo a second crossover, resulting in deletion of the part of the plasmid coding for *sacB* gene, but still retaining the chloramphenicol resistance gene, which then enables them to survive. However, the selection is not absolute as found from observing the growth of the mutant. Apparently, the sucrose gets consumed which could result in the growth of WT.

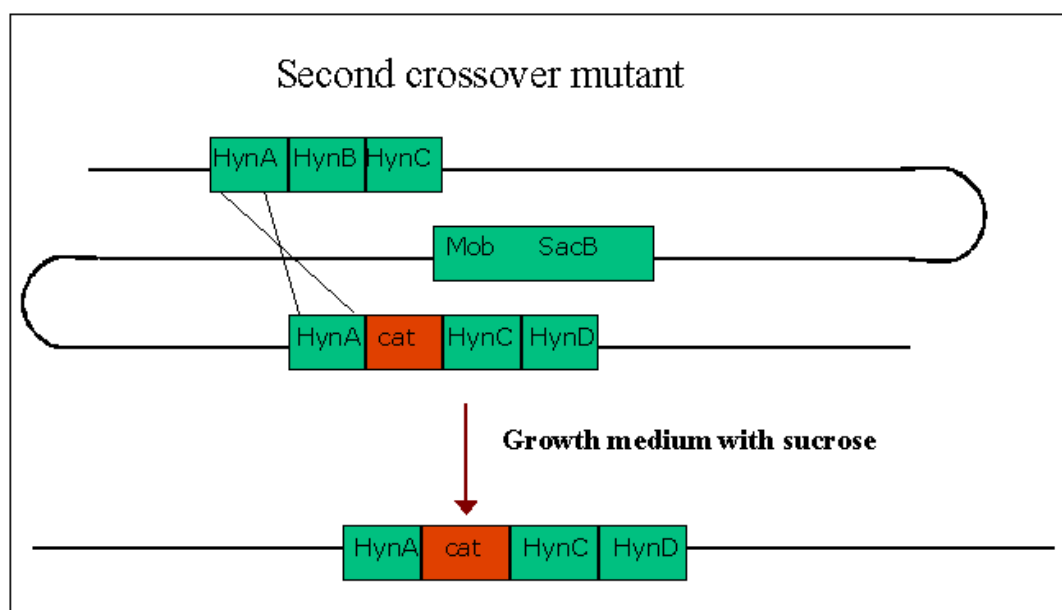


Fig. 5.5 General scheme to show the deletion of the integrated plasmid from the chromosomal DNA after the second homologous crossover.

Replacement mutagenesis was confirmed by PCR (fig. 5.6), Southern blotting and Western blotting (fig. 5.7). The latter two techniques showed a hybridization pattern consistent with gene replacement and absence of *hynAB* in DvH NiFe100, respectively.

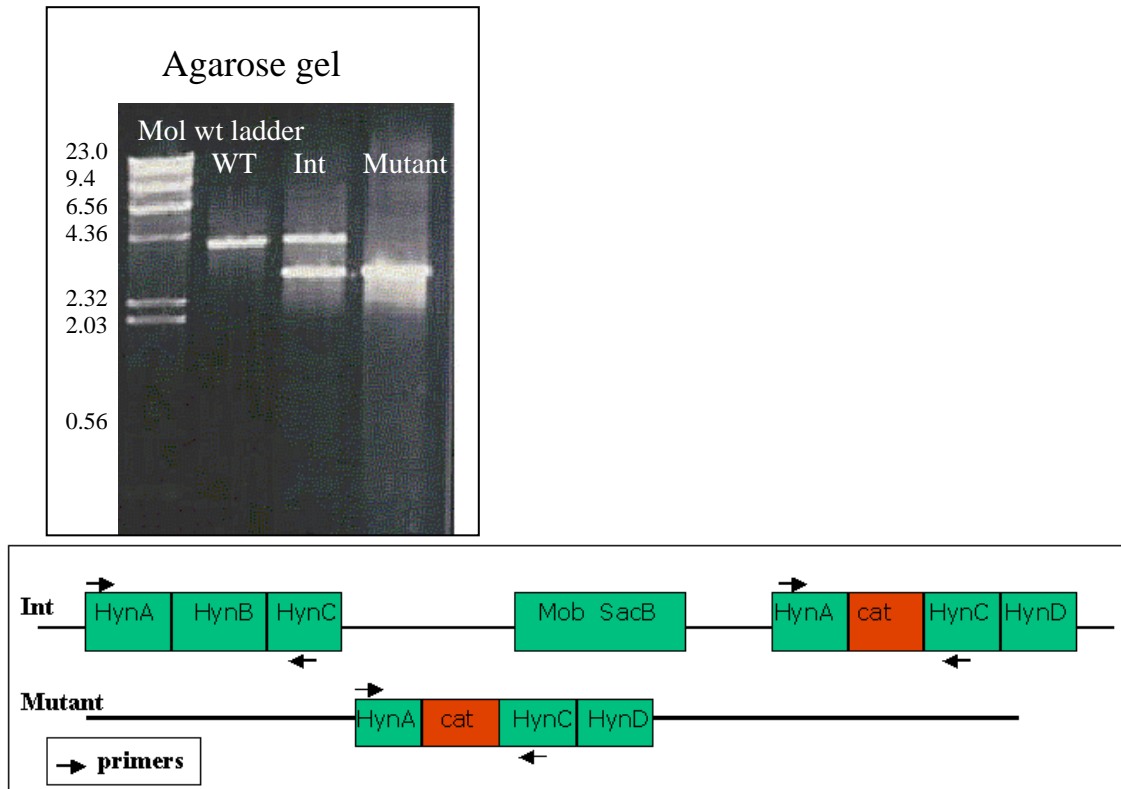


Fig. 5.6 PCR, using the same set of forward and reverse primers for WT, integrant and mutant, respectively result in a different pattern on agarose gel. The scheme shows the primers binding sites on the operon (arrows) in case of integrant and mutant. As there are two primer-binding sites in case of the integrant, two bands result in PCR. For WT, the pattern is the same as the upstream region of the integrant.

The gene deleted from the [NiFe] hydrogenase operon was of 2.5 kb, which is larger by 1.1 kb as compared to the *cat* gene insert of 1.4 kb. Thus, the PCR shows a clear difference in the WT and the mutant, due to the molecular weight difference in the deleted gene and the replacing gene.



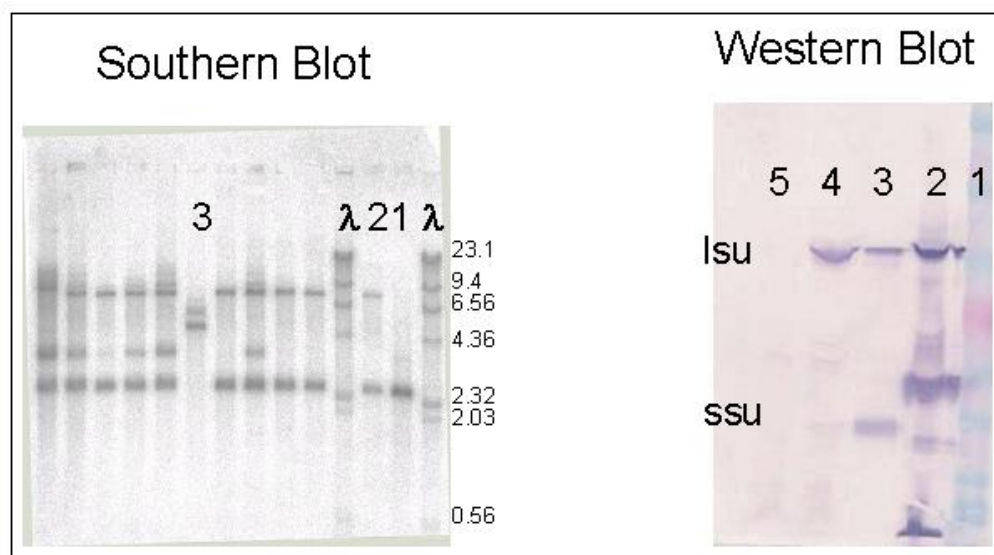


Fig. 5.7 Southern blot and Western blot to confirm the construction of deletion mutant. (Southern blot) Lane  $\lambda$  is  $\lambda$  DNA cleaved with HindIII (molecular weight marker, fragment sizes in kb); lanes 1, 2 and 3 represent hybridizing Sall fragments for the wild type, the integrant and the replacement mutant, respectively. The unmarked lanes are screens for other possible mutants. (Western blot) Lane 1 represents molecular weight markers, lane 2 is DvMF HynAB expressed in *E. coli*, lane 3 is DvMF HynAB purified from DvMF, lane 4 is protein extracted from DvH wild type, lane 5 is protein extracted from replacement mutant DvH NiFe100. Positions for the large (Isu) and the small (ssu) subunit of NiFe hydrogenase (61 and 28 kDa in processed form) are indicated. Polyclonal antibodies recognizing DvMF [NiFe] hydrogenase (Eurogentec, Belgium) were used for detection.

The growth of the probable DvH [NiFe] hydrogenase deletion mutant culture was started in 8 flasks, which were monitored for the growth, everyday. After 8-12 days (Klett meter gave a reading of 50; 150 Klett units correspond to 1 OD<sub>600</sub>), the cultures were diluted and plated on PE kanamycin chloramphenicol plates to obtain isolated colonies. Also, the cell culture was analyzed by DNA blot to check the presence of mutant. Of all the cultures and plates analyzed there was one mutant present (fig. 5.7) (on last day of my stay in Dr. Voordouw's lab in Canada!!), which clearly revealed the absence of [NiFe] hydrogenase protein in DvH in the western blot (fig. 5.7).

## 5.4 Expression Studies

Comparative growth studies were performed for a preliminary characterization of the mutant phenotype. The wild type and  $\Delta hynAB$  mutant strains were grown in Postgate medium C (lactate and H<sub>2</sub> as electron donors) or in DMM acetate medium (only H<sub>2</sub> as the electron donor). Growth is compared in Fig. 5.8. The time courses of growth were

very similar, except that the *hynAB* deletion mutant did not reach the same cell density (medium C) or died more quickly in the stationary growth phase (DMM acetate).

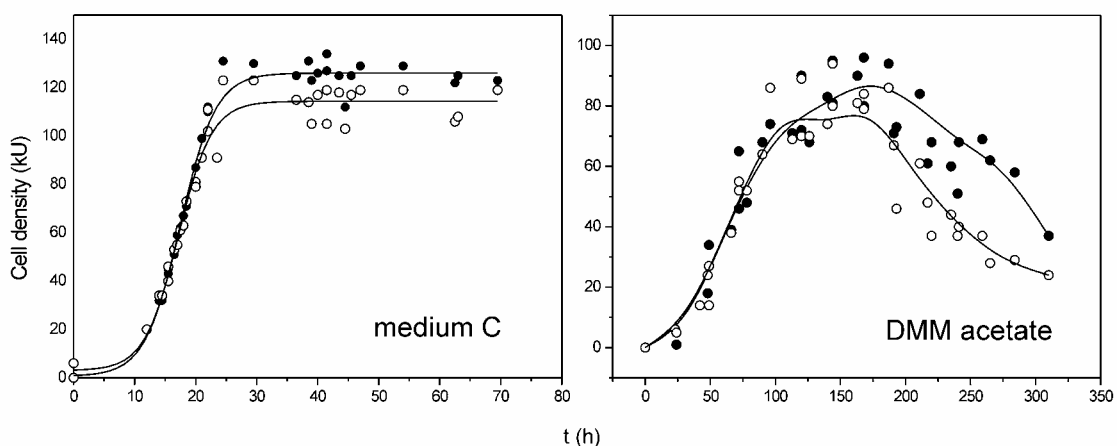


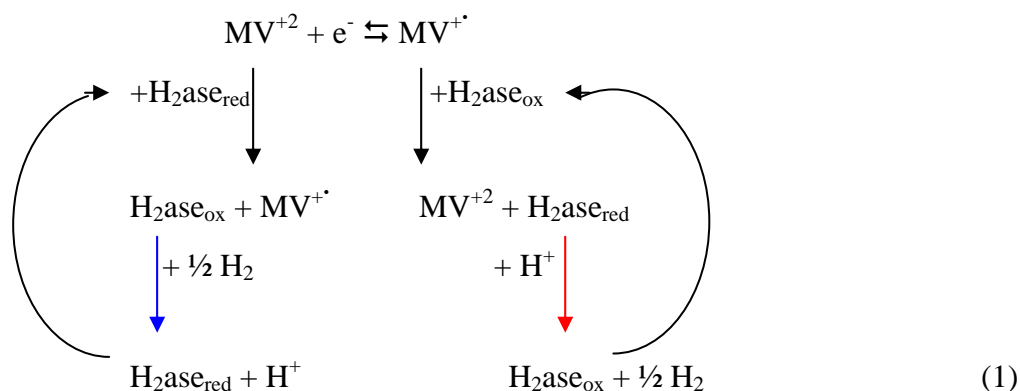
Fig. 5.8 Growth in medium C and in DMM acetate for the wild type (closed circles) and NiFe100 (open circles) strains. The cell density (Klett units; 150 Klett units correspond to 1 OD<sub>600</sub>) is plotted against time (h). Cell density data are averages for 3 independently determined growth curves.

## 5.5 Electrochemical Studies

The efficiency of H<sub>2</sub> production/ consumption was compared between DvH WT and DvHdNiFe, to analyze the effect of deletion of [NiFe] hydrogenase gene on the overall catalytic efficiency of the organism. DvMF's activity was measured under similar conditions for comparisons, in direction to understand the differences causing difficulty in generating its knock-out for [NiFe] hydrogenase gene.

Hydrogenases do not directly exchange electrons with a polished glassy carbon surface. Methyl viologen (MV) was therefore used as a mediator to shuttle electrons between working electrode and protein. It was noted that the mediator compound (MV<sup>2+</sup> or BV<sup>2+</sup>) is immediately reduced by dithionite to produce the mono-cationic radical MV<sup>•+</sup> or BV<sup>•+</sup>, which in turn function as an electron donor to the *D. vulgaris* cells (whole cells suspension used), catalyzing the reduction of H<sup>+</sup> to H<sub>2</sub>. Dithionite itself is not effective as an electron donor in a hydrogenase-catalyzed hydrogen evolution reaction. The catalytic constant of the H<sub>2</sub> evolution reaction was independent of pH up to 7.7 and 6.4 with MV<sup>•+</sup> and BV<sup>•+</sup>, respectively. At higher pH a decrease with increase in pH is

observed. The opposite pH effect was observed on the rates of H<sub>2</sub> consumption (Sakaguchi S *et al.*, 2004).



As outlined in the above scheme (1), it was suggested that H<sub>2</sub> oxidation and proton reduction involves separate catalytic cycles. The rate-determining step in H<sub>2</sub> oxidation is independent on the pH value, whereas proton reduction is controlled by at least two protonation equilibria (Leger C *et al.*, 2002). The reaction shown in blue is slower than the reaction shown in red. The difference in the reaction rates can lead to an accumulation of the end product of the slow reaction in the system, i.e. the reduced hydrogenase. This shifts the equilibria, resulting in accumulation of a reduced state of hydrogenase, termed as hydrogen inhibited. A similar observation was reported where it was suggested that the consumption of protons during the first reduction step causes a local pH increase in the close vicinity of the electrode, thus diminishing the number of H<sup>+</sup> cations available for further reduction (Brugna, MG. *et al.*, 2001). ). This leads to similar end-effect that is the accumulation of reduced product, because of different reaction rates on either side of the equilibrium.

A membrane electrode with dried, immobilized protein/ cell-lysate was used for the electrochemical studies. Experiments done with cytochrome c3 of *D. novuginum*, comparing the conventional and membrane electrodes showed that they both work in a similar manner. Though the membranes are charged, thus modifying the electric environment of the trapped protein (Lojou E. and Bianco P. 2004), it can be very well used to compare the behavior of different samples in the same environment. This publication also reviews work done using membrane electrodes. Work has been

reported on *D. fructosovorans* (Lojou E. and Bianco P. 2004) using also whole cells immobilized on an electrode, leading to very similar results.

Voltammograms numbered from (1) to (5) as shown in fig. 5.9a were recorded in time intervals of 3 minutes. The plateau current at potentials lower than  $-0.5\text{V}$  is taken as a measure for the activity of the protein. The increase in activity with the time of activation is decreasing, when comparing the different voltammograms in fig. 5.9a. The increase in current between the first and the second, the second and the third voltammogram measured, reduces progressively, following the direction of black arrow. After 15 minutes (curves (1)-(5)) curves started to overlap. Thus after curve (5), the curves plotted are at longer time intervals (see figure 5.9a legend). This demonstrates a fast activation step in the beginning, followed by a slower activation and then by saturation, where there is no more increase in current with time of hydrogen bubbling.

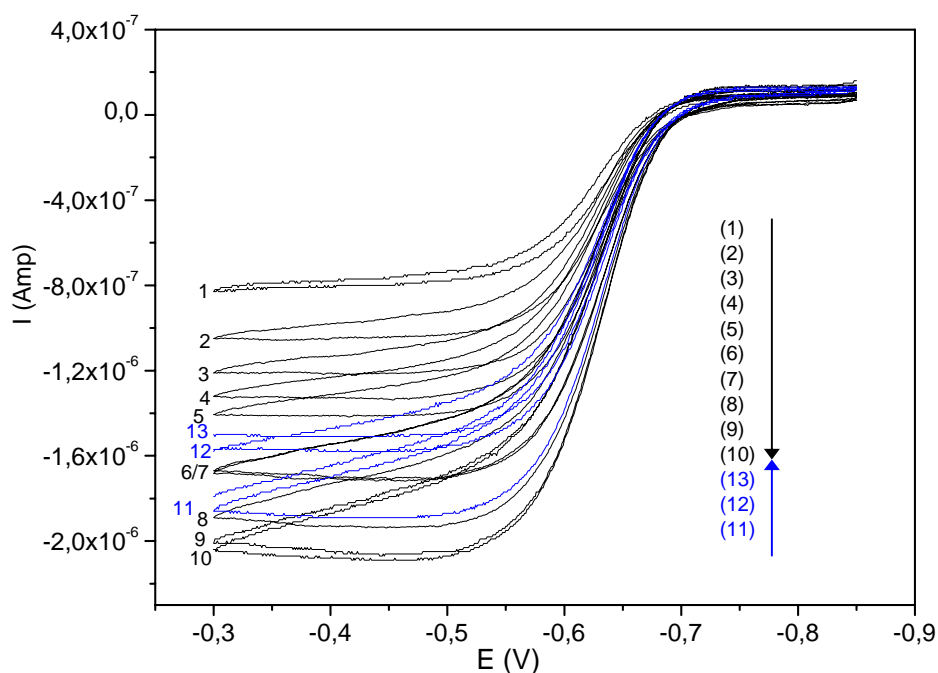


Fig. 5.9 (a) Cyclic voltammograms showing the activation of pure [NiFe] hydrogenase of DvMF in presence of hydrogen. Activation is shown in black and deactivation in blue. The direction of activation and inactivation is shown by arrows. From voltammogram 1 to 10 the sample is getting activated with time, but after some time, the sample starts to deactivate under constantly similar conditions. Voltammograms (1) to (5) were measured at 3 minutes time interval each. With the slow change in current, progressively, other measurements were done with longer time intervals. Voltammograms (1) to (5) were measured in a time span of 15 minutes, and the rest 6 to 10 measurements of activation were measured in following 40 minutes. After this

increase, the voltammograms measured during another hour show that the current does not increase anymore. After this stagnant behavior, current starts to decrease rapidly.

Experiments were done using pure [NiFe] hydrogenase from DvMF, and whole cell lysates of DvH WT, DvH d NiFe and DvMF. The results are outlined in figs. 5.9 – 5.12. For details on sample preparation and experimental set up, refer to materials and methods.

The activation of all samples in presence of hydrogen follow a similar pattern: there is a very fast activation step during the first 15 minutes, followed by a slower activation step for about 40 minutes, it stays most active on this level for an hour and starts to decay thereafter irreversibly. Complete activity is then lost within following 30 minutes. The change with time for hydrogen activation can be easily monitored comparing the distances between different voltammograms on the current axis. Each voltammogram was measured with a time difference of three minutes, but the increase in the current between them progressively reduces. The blue voltammogram with the lowest current value has a fork shape on the current axis, with the two points representing begin and end of the voltammogram crossing each other during the course of run. This is due to the fast reduction in current within a two-minute cycle of one voltammogram.

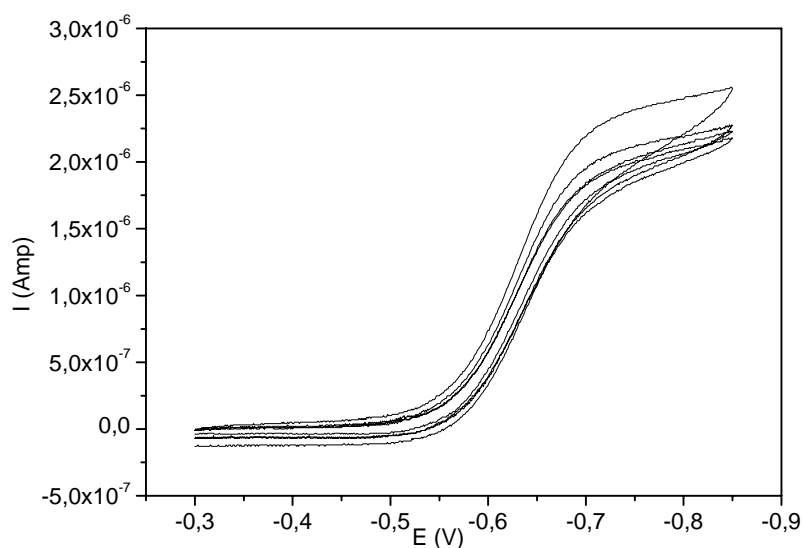


Fig. 5.9b Cyclic voltammograms showing the activation of pure [NiFe] hydrogenase of DvMF in presence of argon. The activation in presence of argon is stabilized within 5 minutes and stays the same for hours.

In presence of argon, all the samples show a fast activation, and stay at the activated level for more than two hours as checked in the measurements done for this work. After the argon activation, same sample could be used with another buffer for hydrogen activation studies, showing the similar results.

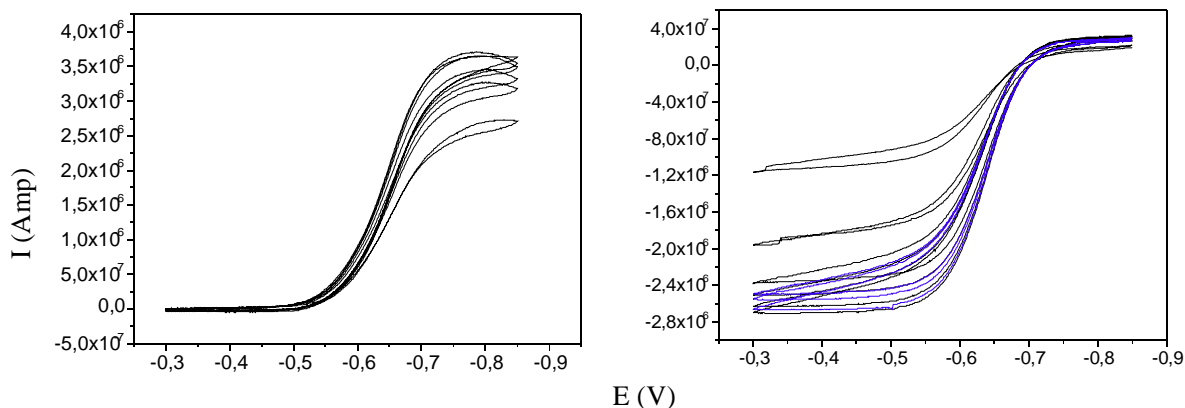


Fig. 5.10 Voltammograms showing DvH WT activation with argon (left) and H<sub>2</sub> (right). The details are the same as described for figure 5.9a and 5.9b.

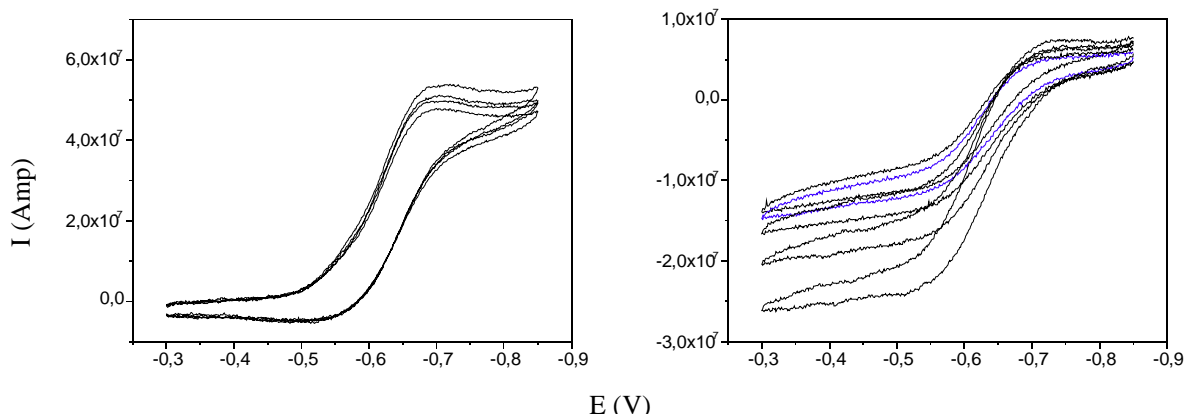


Fig. 5.11 Voltammograms showing DvH d NiFe activation with argon (left) and H<sub>2</sub> (right). The details are the same as described for figure 5.9a and 5.9b.

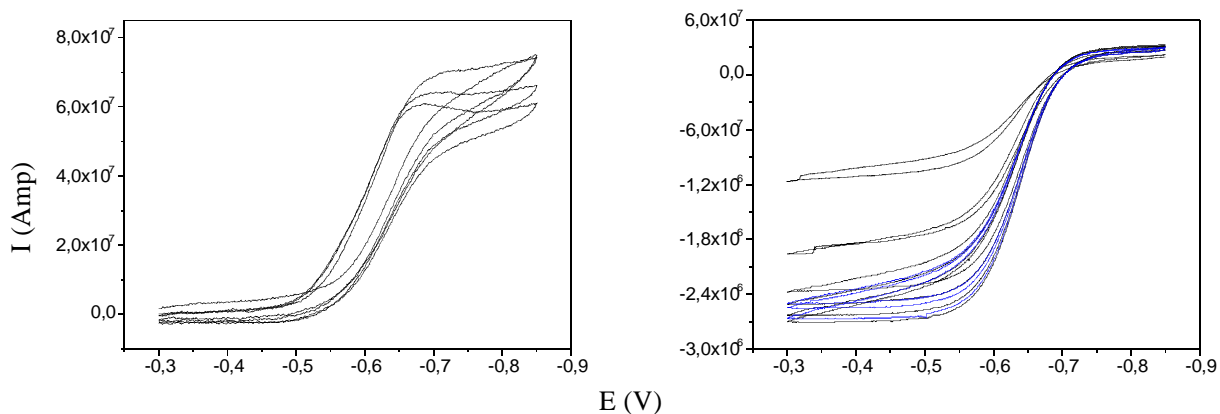


Fig. 5.12 Voltammogram showing DvMF activation with argon (left) and H<sub>2</sub> (right). The details are the same as described for figure 5.9a and 5.9b.

The pattern of the curves observed for all the samples is the same, however there is a remarkable difference in the maximum current attained. The DvMF cell extract and the DvH mutant reach almost similar maxima, which are only one-eighth of the current maxima of the DvH WT.

## 5.6 Native PAGE in-gel activity assay

The presence of six hydrogenases in DvH is known from the recently published genome sequence (Heidelberg JF *et al.*, 2002). In case of DvMF, the [NiFe] hydrogenase is the only hydrogenase known. Thus the in-gel activity assay for DvMF was done as to check the active hydrogenases present, after running the crude cell lysate on a native gel.

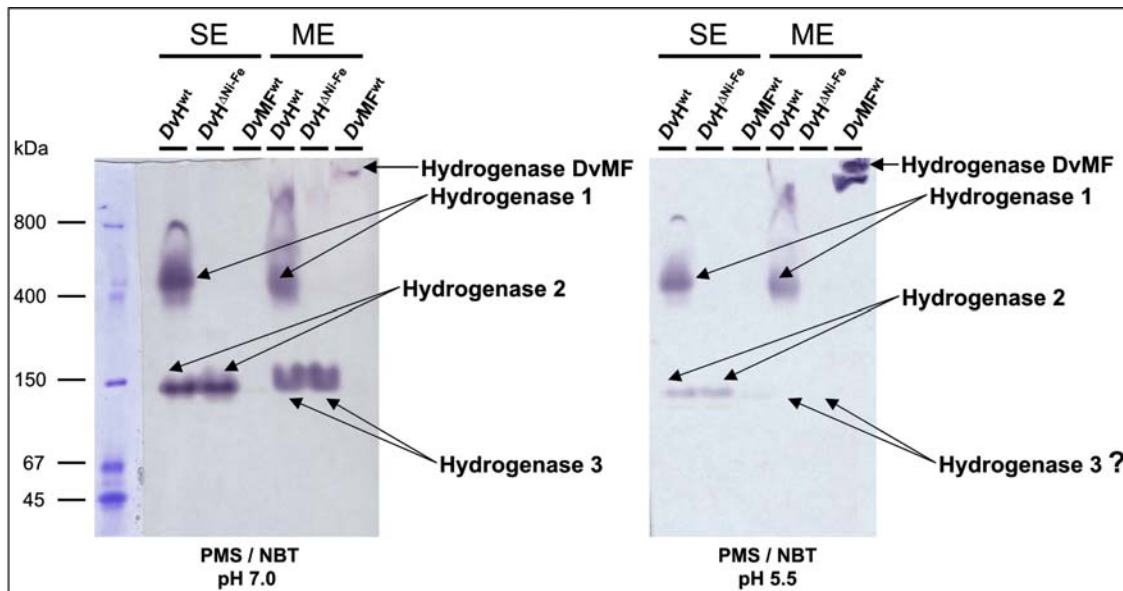


Fig. 5.13 In-gel activity assay to see the hydrogenases present in DvH and DvMF. A total of 200  $\mu$ g of proteins were separated by native PAGE. Purple bands occurred upon incubation with PMS and NBT at 30°C in the dark, indicating H<sub>2</sub>-oxidizing activity of the hydrogenases by the PMS-mediated reduction of NBT. SE: soluble extract, ME: membrane extract.

Three different [NiFe] hydrogenases can be identified in DvH. Hydrogenase 1 (the numbering is arbitrary, as shown on the gels) runs at a position of about 400 kDa and can be detected in the soluble and membrane extracts at both pH values. This indicates that this hydrogenase is loosely attached to the membrane. Hydrogenase 1 is deleted in the DvH mutant. Hydrogenase 2 is a soluble enzyme, which runs at a usual position for a standard dimer (shortly below 150 kDa). Hydrogenase 3 runs a bit slower and is

restricted to the membrane. Although hydrogenase 2 and 3 are roughly at the same position, they are obviously different enzymes because hydrogenase 3 does not react with PMS at pH 5.5, than at pH 7.0, whereas hydrogenase 2 does. Hydrogenases 2 and 3 are distinct from hydrogenase 1, because they are present in the DvH deletion mutant.

In DvMF there was only one membrane-associated hydrogenase reacting with PMS. The band intensity was higher at pH 5.5 indicating that the activity of the solubilized protein increases under slightly acidic conditions. Same behavior has been observed for the MBH (membrane bound hydrogenase) of *R. eutropha*. The unusual migration behavior suggests an incomplete solubilisation from the membrane, and probably the presence of a high molecular weight protein complex (hydrogenase and other proteins), or an unfavorable pI.

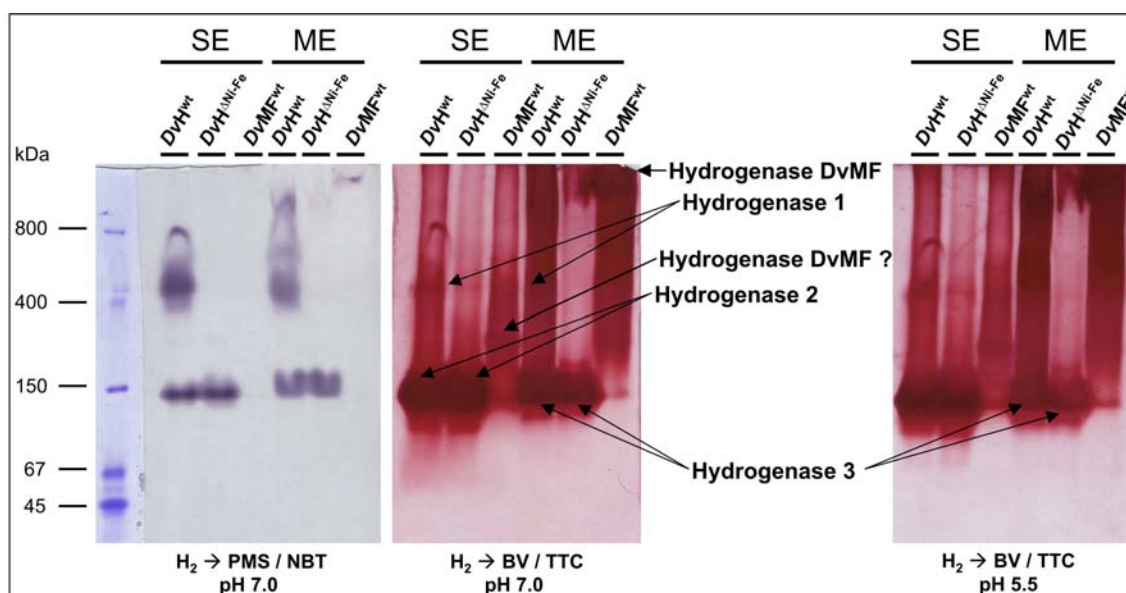


Fig. 5.14 In-gel activity assay comparing the results with PMS/ NBT and BV/ TTC. The labels used are similar to fig. 5.13.

The BV/TTC staining underlines the PMS/NBT results with the exception that hydrogenase 3 of DvH reacts with BV/TTC at pH 5.5. Also, the BV/TTC staining shows the presence of a very faint second hydrogenase band in the DvMF WT soluble extract fraction. Maybe there is an additional soluble hydrogenase activity in DvMF, though its nature needs to be verified by further experiments. Even if it promises to be another relative of the hydrogenase family, its activity in normal conditions is almost negligible as compared to other hydrogenases.



## 5.7 Discussion

The construction of a deletion mutant of [NiFe] hydrogenase in DvH was successful, but the same approach in DvMF did not work. The presence of a plasmid integrant was well visible with the exact molecular band as calculated, but even the isolated colonies did not grow as pure culture to continue work on it. Comparison of growth behavior with lactate and hydrogen as electron donor or only hydrogen as electron donor showed unimpaired growth activity, though the mutant had a lower final cell density and died more quickly.

Presence of other hydrogenases was checked with the native gel assay, confirming the [NiFe] hydrogenase as the only hydrogenase present in case of DvMF. The other protein present in DvMF native gel assay showed a much lower activity.

The reason for not being able to mutate DvMF [NiFe] hydrogenase could probably be due to the fact that only one hydrogenase is present in the organism and its deletion proves lethal for the growth, especially for the growth conditions used for the experiments. Presence of only one hydrogenase, [NiFe] hydrogenase, is known for other species as well (Voordouw *et al.*, 1990; Hatchikian EC *et al.*, 1995), though an attempt for introducing mutation has never been reported. Also the single hydrogenase present has been reported to function both in oxidation and reduction (Hatchikian EC *et al.*, 1995). Recent electrochemical studies have shown that the H<sub>2</sub> oxidation activity of [NiFe] hydrogenase is much higher than previously believed (Armstrong FA, 2004). This is also interesting because of the observation that the activity of the crude cell extract of DvH mutant shows almost eight fold less activity than the DvH WT as compared in fig. 5.16. The deletion of [Fe] hydrogenase from DvH caused only a two-fold decrease in the activity of the cell, as compared to the WT (Pohorelic BK. *et al.*, 2002).

Furthermore, the activity of DvMF whole cell lysate is comparable to that of DvH mutant (fig. 5.15, 5.16), stating a fewer number of hydrogenases or a less active hydrogenase (in PMS/NBT at pH 7.0; fig. 5.13, though equally strong in the rest of the experimental conditions; fig. 5.14) in case of DvMF.

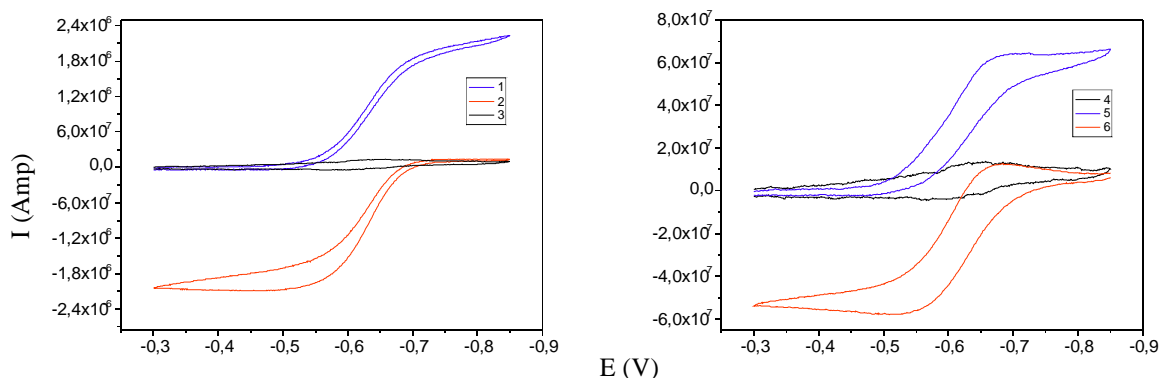


Fig. 5.15 Voltammograms comparing pure [NiFe] hydrogenase from DvMF (left) and DvMF crude cell extract (right). **1** and **4** represents the argon activated sample, while **2** and **6** represents the hydrogen activated sample. The baseline with buffer containing MV and no enzyme or cell extract is represented by **3** and **4**, respectively.

With the use of pure protein, higher current maxima was reached for DvMF. But when used the same wet-cell-weight for DvMF and DvH wild type species, a considerable eight fold reduced current maxima was observed in case of DvMF.

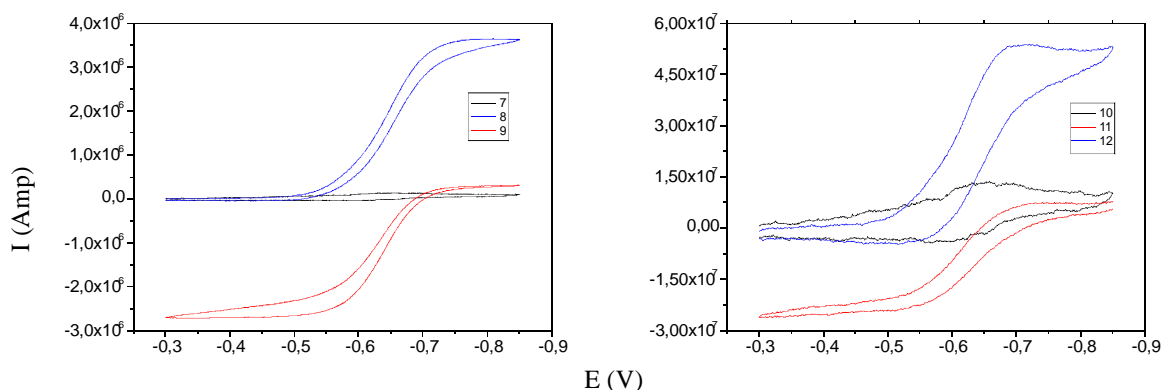


Fig. 5.16 Voltammograms comparing activities in crude cell extract from DvH (left) and DvHdNiFe crude cell extract (right). Same color code as fig. 5.15 has been used for hydrogen activated, argon activated and baseline voltammograms.

The reversal of activity from the active protein to inactive protein (see blue voltammograms in fig. 5.9a), while bubbling with hydrogen could be caused by irreversible inactivation of the reduced active site by trace amounts of oxygen. Such behavior has been reported, as the enzyme is more sensitive when it is in the active state. Probably, in the experimental conditions used for this work, the constant bubbling with  $H_2$  was not enough to keep the reaction conditions totally anaerobic over hours. Experiments done in our group with the method of ‘Protein Film Voltammetry’ without  $MV^{2+}$  (C. Fichtner, PhD thesis) with the whole set up in a glove box did not lead to inactivation of the enzyme. This saturated sample could be activated again under

appropriate conditions. Nevertheless, a similar activation behaviour with time was observed in terms of a fast and a slow component in activation kinetics. Despite these problems which occur only on a longer time scale, the experiments provide important information about the comparative redox activity of the different species.

## Chapter 6

# Isotope Labeling of DvMF [NiFe] Hydrogenase by $^{61}\text{Ni}$ and $^{15}\text{N}$ Histidine

$^{61}\text{Ni}$  is the only stable isotope of Ni with a nuclear spin larger than 0 ( $I = 3/2$ ) and has a natural abundance of 1.14%. Owing to the nuclear spin, a hyperfine structure, which consists of four lines, can be observed in the EPR spectrum of a paramagnetic Ni-complex. Studies of  $^{61}\text{Ni}$ -enriched hydrogenase samples may provide information on the wave function of the unpaired electron near the active site Ni ion. For these studies the nuclear spin of  $^{61}\text{Ni}$  functions as an ideal spin probe.

Lancaster first reported the detection of a natural-abundance nickel EPR signal in biological systems in membrane preparations of *Methanobacterium bryantii* (Lancaster JR Jr 1980). The first unequivocal assignment of the rhombic EPR signal to Ni(III) was obtained from isotope-enriched  $^{61}\text{Ni}$  preparations of *Mb. bryantii* membranes (Lancaster JR. 1982) and *Mb. thermoautotrophicum* hydrogenase (Albracht SP *et al.*, 1982). The earliest results published for the genus *Desulfovibrio* includes the work by (Moura JJG *et al.*, 1982) and by (Krüger HJ *et al.*, 1982). Various other hydrogenases have been studied using  $^{61}\text{Ni}$  enriched preparations as described in (Moura JJG *et al.*, 1988) and (Erkens A. *et al.*, 1996). In these studies, the  $^{61}\text{Ni}$  isotope was used solely for the identification of Ni as the central metal. So far, no interpretation of the information contained in the  $^{61}\text{Ni}$  hyperfine coupling constants at the electronic level has been performed.

It has already been attempted in our research group to enrich the [NiFe] hydrogenase from DvMF with  $^{61}\text{Ni}$  (S. Foerster PhD thesis). As the labeling was done by using an excess amount of the isotope in a standard medium in a steel fermentor (which could provide Ni ions to the bacteria), the extent of labeling was found not to be sufficient ( $40\pm 5\%$ ). To have a better ratio of  $^{61}\text{Ni}$  in the protein, another, specially designed medium was established in this study (chapter 3.3). For this purpose, all solutions and water were passed through a chelex resin column to remove natural abundance Ni, and the enriched Ni was added in a concentration as was found to be optimum for cell growth (see chapter 6.2). Cell growth was performed in 10-liter homemade glass bottle fermentors (see chapter 3.4.1.2), filled with a volume of 8 L, and one liter was used as inoculum. These growth conditions yielded more than 90%-enriched protein (see chapter 3.2.4.2).

## 6.1 Spectroscopy Theory

An elaborate description of all EPR related techniques used in this work can be found in the book of Schweiger and Jeschke. In the following sections, a brief summary of the techniques is given with emphasis on how they are used in this work to extract information about the electronic structure.

### 6.1.1 EPR

Electron Paramagnetic Resonance is a spectroscopy that deals with microwave-induced transitions between magnetic energy levels of systems that contain unpaired electrons for which the net spin and orbital angular momentum is larger than zero.

The energy differences that are studied by EPR are predominantly due to the interaction of unpaired electrons in the sample with an external magnetic field. This effect is called the Zeeman effect. The electron will have a state of lowest energy when the moment of the electron,  $\vec{\mu}$ , is aligned parallel with the magnetic field and a state of highest energy when  $\vec{\mu}$  is aligned antiparallel to the magnetic field. The energy of an electron with

spin  $\langle S_z \rangle / \hbar \equiv M_S = \pm \frac{1}{2}$  is given by

$$E = g\mu_B B_0 M_S = \pm 1/2 g\mu_B B_0$$

and the energy difference  $\Delta E$  is defined by

$$\Delta E = g\mu_B B_0 = h\nu$$

where  $g$  is the  $g$ -factor, which is a proportionality constant approximately equal to 2 for free electrons, but which may vary depending on the electronic configuration when the unpaired electrons are coupled to metal ions,  $\mu_B$  is the Bohr magneton, which is the natural unit of electronic magnetic moment,  $B_0$  is the static magnetic field.

The elucidation of parameters like the electronic Zeeman interaction ( $g$ ), hyperfine ( $A$ ), nuclear quadrupole ( $Q$ ) and zero-field splitting ( $D$ ) tensors, which characterize the interactions between an electron and its surrounding, can lead to an understanding at the electronic level of the atomic and molecular structure at the paramagnetic sites.

The interaction of a magnetic moment with an external magnetic field is called **Zeeman interaction**. The interaction of spin  $S$  with the magnetic field  $B$  is given by a symmetric tensor called the  $g$ -tensor which has three principal values,  $g_x$ ,  $g_y$  and  $g_z$ .

For a free electron, the principal values are equal, i.e. there is no dependence on the relative orientation of the magnetic field and the electron spin; the tensor reduces to a simple value, the free electron  $g$ -value  $g_e$  (2.0023). When the wavefunction of the unpaired electron is largely localized on a metal ion, the spin-orbit coupling interaction between the electron spin and the orbital angular momentum of the electron in the metal  $d$  orbital causes the tensor components to become anisotropic and  $g_x \neq g_y \neq g_z$ . Vice versa, by studying this anisotropy, information about the underlying electronic structure can in principle be obtained.

Moreover, if the metal has a nuclear spin, the magnetic interaction of the unpaired electron spin and the nuclear spin ( $I > 0$ ) causes additional structure in the EPR spectrum and is called **nuclear hyperfine interaction**.

**Nuclear quadrupole interaction** is the interaction between the nuclear quadrupole moment and the electric field gradient caused by all electrons. All nuclei with a nuclear spin  $I > 1/2$  have a quadrupole moment. The negatively charged electrons, which include

in this case not only the unpaired electrons but also the paired electrons present near the nucleus create an electric field present at and around the nucleus, which is determined by the wavefunction of all electrons. When spherical symmetry is absent, i.e., if the orbital of the electrons that surround the nucleus are not the same in every direction, the first derivative of the electric field at the nucleus becomes non-zero, i.e., a gradient is present. The electric field gradient interacts with the nuclear quadrupole moment to split the nuclear spin levels even at zero field. Spectroscopically, by measuring the quadrupole interaction, information about the asymmetry of the electron distribution in the surrounding of the nucleus can in principle be obtained.

### 6.1.2 ENDOR

Electron-Nuclear Double Resonance (ENDOR) proposed by G. Feher in 1956, combines EPR with NMR spectroscopy. During an ENDOR experiment NMR transitions are induced by applying an additional rf-field (1-100 MHz) to the sample. The effect of these induced NMR transitions upon a saturated EPR signal comprises the ENDOR spectrum. The exact frequency positions of the ENDOR signals depend on the relative size of the nuclear Zeeman energy and the hyperfine coupling term.

ENDOR significantly increases the spectral resolution of the EPR experiments so that hyperfine and quadrupole coupling constants may be determined which are not resolved in conventional EPR spectra. It also offers a unique tool to identify the specific type of nuclei interacting with the paramagnetic center.

### 6.1.3 ELDOR-detected NMR

ELDOR-detected NMR (EDNMR) is a pulsed EPR technique which, like ENDOR, allows the resolution of hyperfine interactions and which does not require additional rf fields. The general idea of this method is to apply a strong pumping microwave pulse, which varies the microwave frequency. A normal Hahn echo pulse sequence is used for EPR detection at a fixed microwave frequency. When the frequency of the pump pulse equals an EPR forbidden transition ( $\Delta M_S = \pm 1$ ,  $\Delta M_I = \pm 1$ ), a small decrease of the echo signal can be observed. From the difference of the microwave frequencies of the pump and probe pulses, the hyperfine interaction can be obtained. The significant

disadvantage of EDNMR lies in the fact that a lower resolution is obtained with respect to ENDOR, because of the larger excitation bandwidth of the pump pulse as compared to the rf pulse, but it has the advantage over ENDOR that large hyperfine interactions can be detected with superior sensitivity.

This property makes the EDNMR technique especially suited to detect the hyperfine interaction of a central metal in a complex, which holds a large part of spin density. The metal hyperfine coupling constants obtained from EDNMR can be obtained with larger accuracy as compared to those obtained by conventional EPR.

#### **6.1.4 ESEEM**

Electron Spin Echo Envelope Modulation (ESEEM) spectroscopy is another technique, which like ENDOR and ELDOR detected NMR can be used to measure hyperfine and quadrupole interactions. With this method the magnetic field is fixed at a position in the EPR resonance line. The frequency of the microwave pulses is also kept fixed. Then three microwave pulses are applied to the system and the resulting echo height is measured. When the time between the second and third pulse is scanned, modulations of the echo height can be observed, which arise from the hyperfine interaction between the unpaired electron and nearby paramagnetic nuclei ( $I > 1/2$ ).

When the modulation pattern (echo height vs time) is Fourier transformed to the frequency domain, the so-called ESEEM spectrum is obtained. The x axis of the ESEEM spectrum (a Fourier transformed time axis) is a frequency axis in the ESEEM spectrum. The amplitudes on the y axis indicate how strong the modulations of a particular frequency present in the experimentally obtained modulation pattern are. By interpreting the signals in the ESEEM spectrum, the nuclear hyperfine interactions responsible for the modulations can be determined. In turn, the wavefunction of the unpaired electron, which determines the hyperfine interaction, can be investigated in this way.



### 6.1.5 HYSCORE

Hyperfine Sublevel Correlation Spectroscopy (HYSCORE) is closely related to ESEEM spectroscopy. It involves four microwave pulses and is a two-dimensional technique. The times between the second and third and the third and fourth pulses are scanned and the intensity of the echo signal is monitored. As in ESEEM spectroscopy modulations can be observed caused by the hyperfine interaction of the unpaired electrons with nearby nuclear spins. By two-dimensional Fourier transformation the HYSCORE spectrum is obtained, which has two frequency axes. HYSCORE spectra are usually presented as contour plots. Similar to correlation spectroscopy in NMR spectroscopy, off-diagonal cross-correlation peaks can be read from the spectrum that relates two frequencies to the same nuclear spin. This allows the identification and assignment of frequencies that belong to one nuclear spin with larger reliability than with the one-dimensional ENDOR, ESEEM and EDNMR techniques. HYSCORE and ESEEM work especially well for paramagnetic nuclei for which the hyperfine interaction is of the same order of magnitude as nuclear Zeeman interaction. In this case, strong modulations are observed.

For DvMF hydrogenase, nuclei observed with this technique at X-band (9 GHz) are  $^1\text{H}$  ( $I=1/2$ ),  $^2\text{H}$  ( $I=1$ ),  $^{14}\text{N}$  ( $I=1$ ) and  $^{15}\text{N}$  ( $I=1/2$ ). The latter is only observable after selective labeling of the enzyme. The labeling of nitrogen with the  $^{15}\text{N}$  isotope allows for an accurate determination of the hyperfine coupling constants. Additionally, if these parameters are used for the analysis of the HYSCORE spectra with the  $^{14}\text{N}$  isotope, accurate nuclear quadrupole coupling constants can be obtained as well.

## 6.2 Optimisation of Required Ni Concentration

A defined minimal medium was designed for this study, with the chelex cleaning procedure to take care of any naturally abundant nickel coming from any of the standard medium components, or water, even if in traces, to get a maximal labeling (chapter 3.3 and chapter 3.4.1.2).

To optimise the concentration of Ni required for DvMF cell growth, cell cultures were grown in the minimal medium with a gradient of Ni concentrations in several batches.

All the experiments were done in triplicates. The cultures were grown in 500 ml following the routine protocols. After two days of growth, cells were pelleted down, and equal wet cell weight was subjected to sonication for cell lysis. The crude cell lysate thus obtained was directly subjected to the hydrogenase activity assay using the modified Clark electrode assay (chapter 3.6.5).

Cultures were grown with Ni concentrations added to the growth medium using 0, 5, 10, 15 and 20  $\mu\text{M}$  Ni, respectively. Equal wet cell weight was resuspended in standard Tris buffer, and sonicated to lyse the cells and release the hydrogenase in the crude cell extract.  $\text{H}_2$  production when more than 15  $\text{mM H}_2/\text{min}$ , was above the limit of instrument used. Therefore dilutions of the sample were used for measurements. Afterwards, the measured  $\text{H}_2$  production was scaled such that it corresponds to the amount produced by 500  $\mu\text{l}$  of cell extract, reported here in fig 6.1.

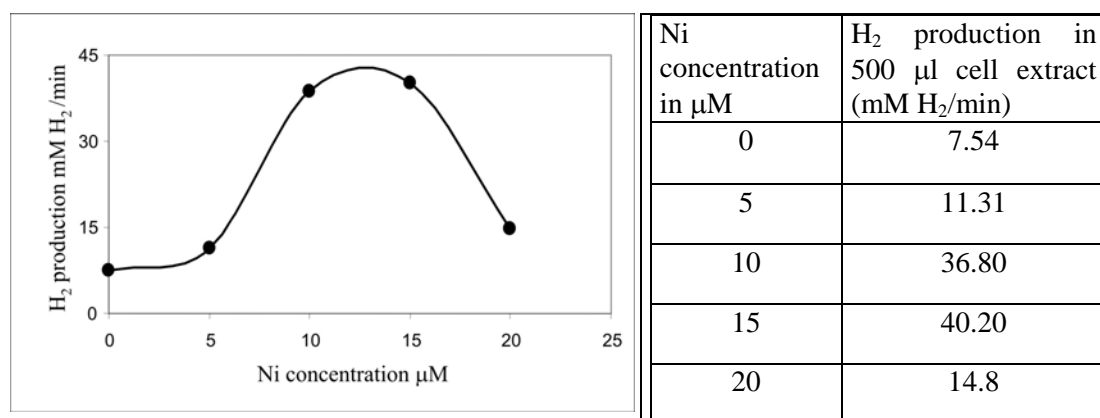


Fig. 6.1 Left, graph comparing the hydrogen production with the concentration of Ni added to the chelex growth medium. Right, table showing the results as obtained for different concentrations of Ni for different volumes of cell extract used.

The amount of  $\text{H}_2$  produced was measured as  $\text{mM H}_2$  produced per minute of the reaction. (chapter 3.6.5). The  $\text{H}_2$  production values thus obtained were used to draw the curve comparing the Ni concentration versus  $\text{H}_2$  production which resulted in a bell shaped curve as shown in figure 6.1. Also, studies were done with growth in a ten liter fermentor without adding Ni to the minimal medium, and the cell pellet was subjected to standard procedure of protein isolation. The results from the first column-purification indicated the presence of negligible [NiFe] hydrogenase in the preparation. Maximum [NiFe] hydrogenase yield (maximum  $\text{H}_2$  production) was achieved at ca. 13  $\mu\text{M}$  Ni. For the labeling experiments, an optimum  $^{61}\text{Ni}$  concentration of 10  $\mu\text{M}$  was

used, because of cost considerations and since at larger concentrations the hydrogen production stagnates and even decreases.

### 6.3 Protein purity determination by SDS-PAGE and MALDI-TOF MS

Protein was purified as described (chapter 3.6.2) and its purity or enrichment was analysed by SDS-PAGE as shown in the figure 6.2 and by MALDI-TOF MS. Starting from the crude cell extract lysate, an increasing purification can be seen, until finally the pure protein is isolated (lane 7), showing practically only the small and the large subunit. The protein as obtained after a four column purification is ca. 95% pure which is sufficient for most spectroscopic and crystallisation purposes.

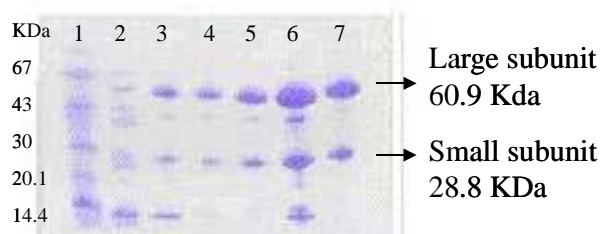


Fig. 6.2 SDS gel comparing purity of hydrogenase sample after purification from different affinity and gel exclusion columns. Lane 1: mol wt ladder with mol. wt. marked on left hand side, lane 2: cell extract as loaded on first column (ion exchange), lane 3: protein as collected from first column and loaded on second column (size exclusion), lane 4: protein as loaded on third column (ion exchange), lane 5: protein as collected from third column, lane 6: protein collected from third column, concentrated before loading on fourth column (size exclusion), lane 7: protein as collected from fourth column, showing a purity of ca 95%.

The purified protein was characterised by the methyl viologen activity assay (chapter 3.6.4), and the concentration of the protein was determined by the Bradford assay (chapter 3.6.3) to be approximately 600  $\mu$ M. From a 50 litre growth culture, typically 500  $\mu$ l of 1 mM protein concentration was obtained reproducibly. This is equivalent to 45 mg hydrogenase. The protein yield obtained per litre culture, is comparable to that from the 50 litre steel fermentor. The pure protein was subjected to MALDI-TOF mass spectrometry (chapter 3.5.9).

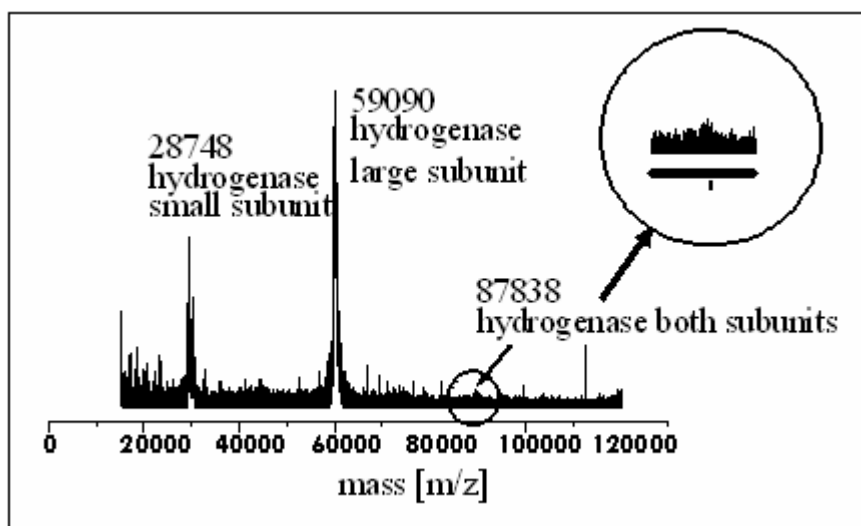


Fig. 6.3 Maldi-TOF MS molecular weight determination and purity check for hydrogenase. Three distinct peaks are visible at 28.7 kDa, 59.1 kDa and 87.8 kDa, for the ssu, lsu and the protein complex (ssu and lsu together), respectively. The error in the molecular weight is  $\pm 1$  Da.

The protein was concentrated to 700  $\mu\text{M}$  and was used for all spectroscopy experiments. 100  $\mu\text{L}$  aliquots were stored in liquid nitrogen.

#### 6.4 EPR-spectroscopy on $^{61}\text{Ni}$ labeled [NiFe] hydrogenase from DvMF

EPR spectra were measured on all four EPR active redox states of the protein at both X and Q band microwave frequencies.

The incorporation of  $^{61}\text{Ni}$  was controlled by comparing the signals from labeled and unlabeled samples, in the as-isolated state with the ratio of NiA: NiB as 1:1, as shown in figure 6.4. The spectral shape with four lines is due to the nuclear spin of  $^{61}\text{Ni}$ , and also the signals at larger g values are broadened as compared to the case of normal Ni. Traces of the normal Ni spectrum cannot be seen in the red spectrum. This implies that the  $^{61}\text{Ni}$  built-in is better than 90%. The starting material was 92% pure.

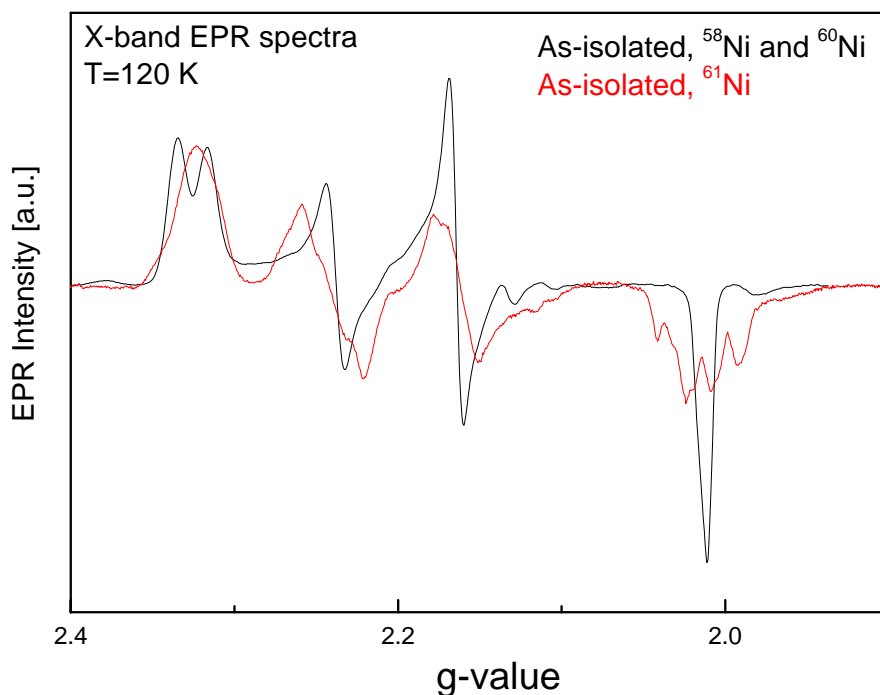


Fig. 6.4 Comparison of as-isolated [NiFe] Hydrogenase from DvMF, natural abundance Ni and  $^{61}\text{Ni}$  labeling. The  $^{61}\text{Ni}$  enrichment is more than 90% as seen from a comparison of the spectra.

Four EPR active redox states have been studied, namely Ni-A, Ni-B, Ni-C and Ni-L of the [NiFe] hydrogenase from DvMF. The pure redox states were prepared using the protocol as described in (chapter 3.5.9). The preparation of pure Ni-C and pure Ni-L was easier than that of pure Ni-A and Ni-B, most probably, because a lot of enzyme is lost after reoxidation of the sample (chapter 3.5.9).

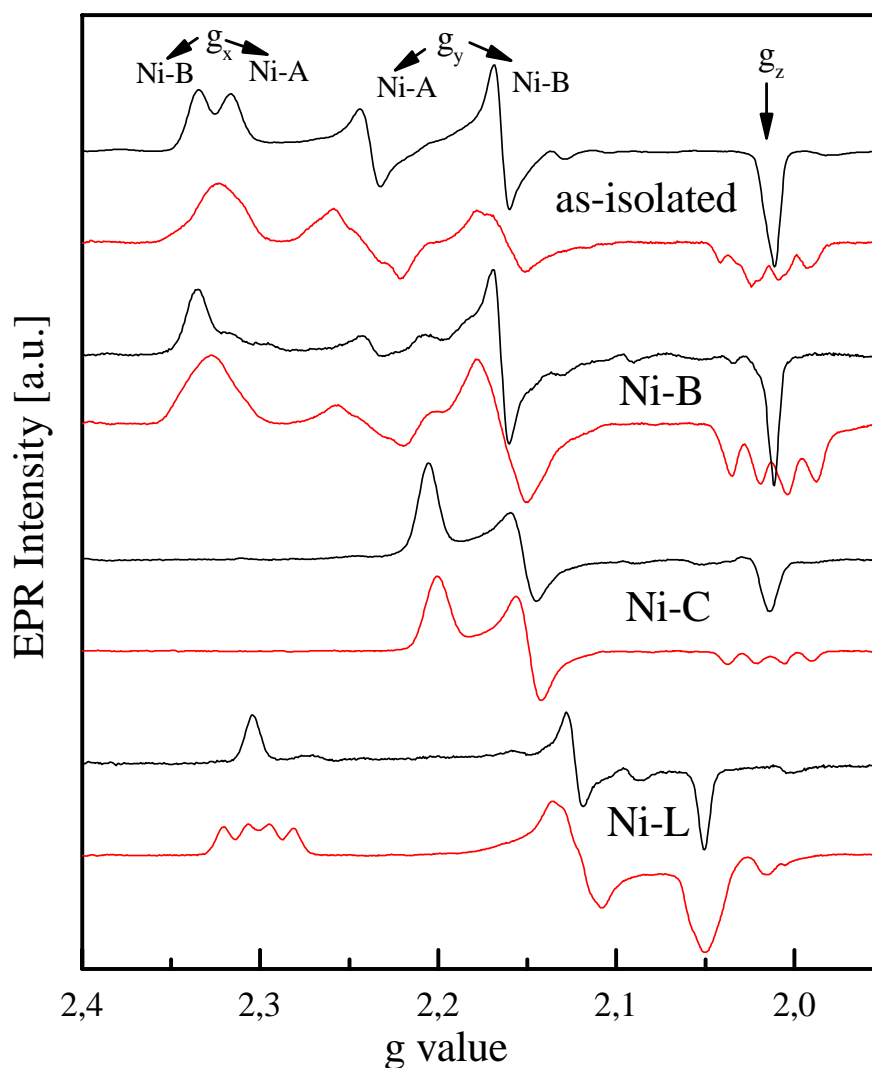


Fig. 6.5 EPR spectra of all four EPR active redox states of [NiFe] hydrogenase from DvMF, measured at X-band. Spectra for normal Ni is shown in black and spectra for labeled Ni ( $^{61}\text{Ni}$ ) is shown in red. The four-line pattern of the  $^{61}\text{Ni}$  hyperfine splitting is resolved at some of the canonical orientations.

The  $^{61}\text{Ni}$  four-line pattern is not fully resolved at every g value. It is often only observed at one g value, for the other two a broadening is observed. For this reason, EDNMR experiments were performed. With this method it is possible to “look underneath” the EPR signal and to still resolve the  $^{61}\text{Ni}$  hyperfine interaction at a position, where the EPR spectrum cannot be seen.

With EDNMR, three microwave pulses are applied to the system. The first pulse is a long, strong pulse, which burns a hole into the EPR spectrum, and its frequency is scanned. The second and third pulses form a normal Hahn echo detection sequence. The burned hole occurs at EPR-allowed and EPR-forbidden transitions, the frequency of the latter being equal to the nuclear transition frequencies (Schosseler P *et al.*, 1993). When this happens, a decrease of the intensity of the echo is observed. So far, this technique has been applied to  $^{55}\text{Mn}$  in photosystem II and respective model systems. For metals, in particular for  $^{61}\text{Ni}$  ( $I = 3/2$ ), one can make use of the fact that all possible EPR transitions of the ( $S = 1/2$ ,  $I$ ) system become allowed to some extent, owing to the presence of the anisotropic hyperfine interaction and quadrupole interaction, which causes the nuclear eigenstates of both  $M_S$  manifolds to be slightly different. For a ( $S = 1/2$ ,  $I = 3/2$ ) system, the EPR transitions, including the ‘EPR forbidden’ ones, occur at shifts equal to  $\pm A/2$ ,  $\pm A$  and  $\pm 3A/2$ .

ELDOR detected NMR spectra: as-isolated DvMF hydrogenase

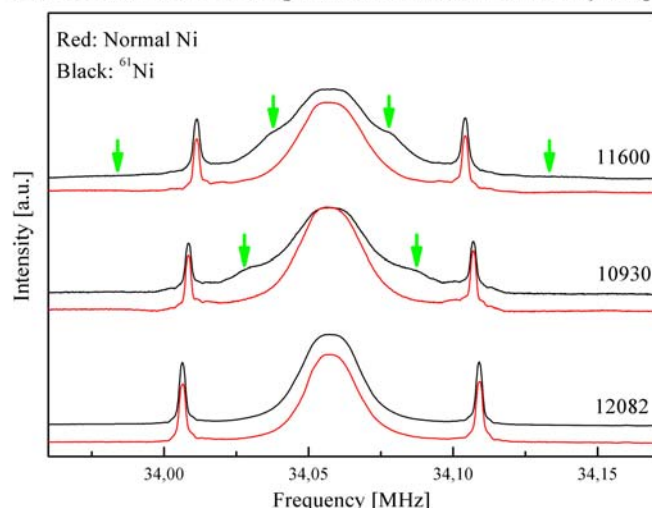


Fig. 6.6 ELDOR detected NMR at 34 GHz for DvMF hydrogenase in the as-isolated (Ni-A/B) state. Numbers on the right hand side of each spectrum indicate the magnetic field setting [G] in the EPR spectrum.

ELDOR detected NMR spectra for as-isolated hydrogenase which contains a mixture of 50% Ni-A and 50% Ni-B, performed with and without  $^{61}\text{Ni}$  enrichment are shown in figure 6.7. Almost identical EDNMR spectra have been observed for samples with about 75% of the Ni-A state. The narrow signals with a shift of about 45 to 50 MHz from the central signal originate from protons. Additional signals are present in the spectrum of the enriched sample, which are clearly absent in that of the non-enriched

sample (marked with arrows). These signals correspond to the  $\pm A/2$  and  $\pm 3A/2$  transitions with shifts of about 23 MHz and 70 MHz. ENDOR experiments have been attempted as well, but no  $^{61}\text{Ni}$  signals were observed. This may be related to the fact that in ENDOR a direct nuclear transition is made, whereas in EDNMR the first microwave pulse achieves the nuclear transition indirectly. The transition probability coupled with these two mechanisms is probably different.

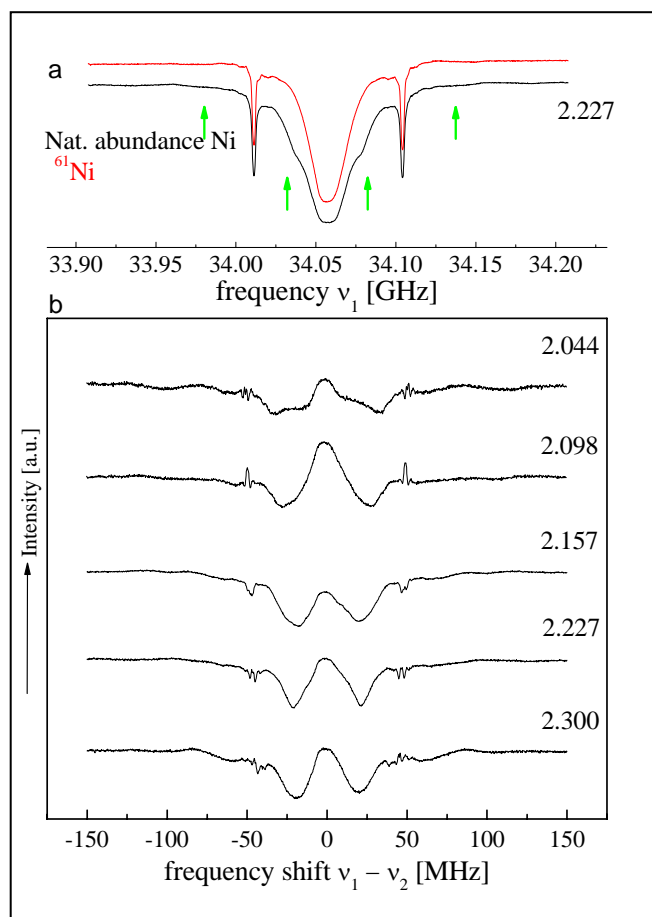


Fig. 6.7 ELDOR detected NMR spectra for the as-isolated state of *D. vulgaris* Miyazaki F hydrogenase. (a) Comparison between  $^{61}\text{Ni}$ -enriched (black) and natural abundance Ni (red). (b) Difference spectra ( $^{61}\text{Ni} - ^{58/60}\text{Ni}$ , black), recorded at different magnetic field settings (effective g values are indicated in the figure). Experimental conditions: T = 10 K,  $\nu_2 = 34.056$  GHz, length of first pulse 90  $\mu\text{s}$ , detection pulses 160 and 320 ns. Total averaging time per spectrum about 2 hours. At about 45 MHz, narrow signals from protons are present which did not completely disappear after subtraction.

The difference EDNMR spectra recorded at different magnetic field positions are shown in figure 6.8b. The negative signals correspond to transitions associated with  $^{61}\text{Ni}$ . A preliminary simulation was made based on the method described in (van Gastel M *et al.*, 1998), with the exception that the intensity of the signal has been taken proportional



to the amount of EPR allowed  $\Delta M_I = 0$  character in the transition driven by the first pulse. This assumption neglects the effects of the excitation bandwidth of the first pulse and the frequency profile of the cavity, and thus good agreement between experiment and simulation with respect to the intensities is not expected. By simulation of the positions of the bands hyperfine coupling constants of  $A(x,y,z) = 40, 22, 76$  MHz were elucidated. Introduction of a quadrupole interaction up to 10 MHz does not significantly influence the simulation, as it is still small compared to the anisotropic hyperfine interaction. The spectra in figure 6.7 and 6.8 are the first EDNMR spectra recorded for  $^{61}\text{Ni}$ . Though the interpretation of the signals is not complete, these spectra convincingly show that it is possible to measure metal hyperfine interactions with EDNMR to a larger accuracy than with conventional EPR spectroscopy and with a better sensitivity than ENDOR spectroscopy.

## **6.5 EPR investigation of $^{15}\text{N}$ His labeled [NiFe] hydrogenase from DvMF**

Besides labeling with  $^{61}\text{Ni}$ , the hydrogenase labeled with  $^{15}\text{N}$  histidine was studied. The reason for studying  $^{15}\text{N}$  histidine labeled protein is to identify  $^{14}\text{N}/^{15}\text{N}$  resonance in the hydrogenase that interacts with the spin center, e.g. via “ligation” or “H-bonding” and might reveal the electron transfer pathway. The H-bonding finetune the wavefunction of the unpaired electron and thereby possibly optimize the process catalyzed by this enzyme. The unpaired electron, in the Ni-A, Ni-B and Ni-C states, mainly resides in a  $3d_{z^2}$  orbital on nickel and the  $3p_z$  orbital of one of the cysteines (Cys-549 for *D. vulgaris* Miyazaki F hydrogenase), as was found by FTIR (De Lacey *et al.*, 1997; George SJ *et al.*, 2004; De Lacey *et al.*, 2003) and EPR spectroscopy (Brecht M *et al.*, 2003; Fan C *et al.*, 1991; Foerster S *et al.*, 2003; van der Zwaan JW *et al.*, 1990; Geßner C *et al.*, 1996) and DFT calculations (Pavlov M *et al.*, 1998; Stadler C *et al.*, 2002; Amara P *et al.*, 1999; Stein M *et al.*, 2001a; Stein M *et al.*, 2001b; Stein M *et al.*, 2001c; Stein M *et al.*, 2004).

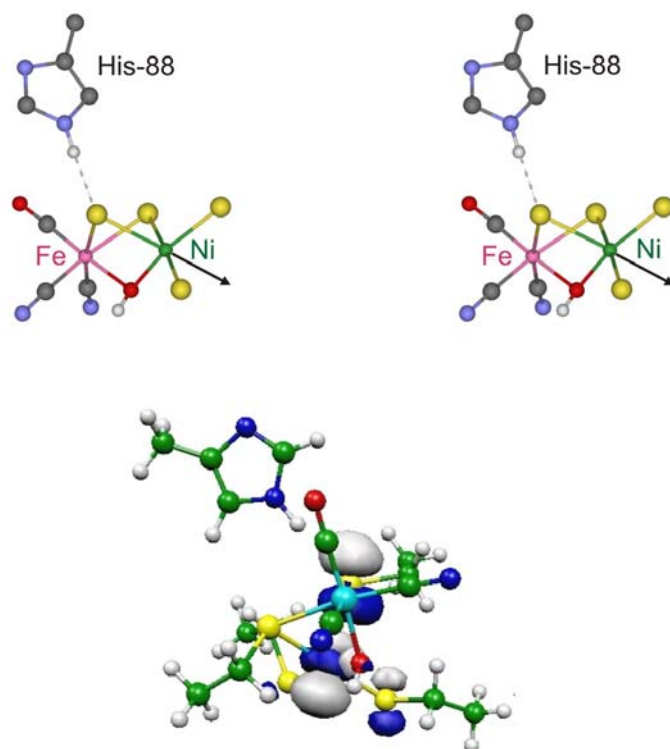


Fig. 6.8 (a) Stereo view of the [NiFe] active site of *D. vulgaris* Miyazaki F hydrogenase. The bridging ligand ‘X’ is an oxygen species in the oxidized states (modeled here as an  $\text{OH}^-$ ). In the reduced state, a bridging hydride has been detected (Brecht M et al., 2003). The sulfur of Cys-549 is hydrogen bonded to the  $\text{H}_\epsilon$  of His-88. The direction of the z axis of the nickel  $3d_{z^2}$  orbital is indicated with an arrow. (b) Overview of the orbital of the unpaired electron of a truncated model for the active site in the oxidized state. The contour of the nickel  $3d_{z^2}$  is visible, additional spin density is found in the  $3p_z$  orbital of  $\text{S}_\gamma$  (Cys-549) and  $\text{S}_\gamma$  (Cys-546).

Because the wavefunction of the unpaired electron is found to be delocalized over nickel and  $\text{S}_\gamma$ (Cys-549), the energies of the Ni(3d) and S(3p) orbitals are close together. It is therefore conceivable that minor influences of the environment may have a significant effect on the delocalization of spin density. The most direct effect, as is evident from inspection of the X-ray crystallographic structure of the oxidized and reduced forms (Higuchi Y et al, 1997; Higuchi Y et al, 1999) is the presence of a hydrogen bond between  $\text{S}_\gamma$ (Cys-549) and  $\text{N}_\epsilon$ (His-88). The hydrogen bond brings the partial positive charge of the proton ( $\delta^+$ ) near the sulfur, which stabilizes the sulfur 3p orbitals.

As a natural spin probe to investigate the strength of the hydrogen bond of His-88 to Cys-549, the nuclear spin of the  $\epsilon$  nitrogen ( $^{14}\text{N}$ ,  $I = 1$  and  $^{15}\text{N}$ ,  $I = 1/2$ ) of the histidine can be used. It is known from electron spin echo envelope modulation (ESEEM) and nuclear quadrupole resonance (NQR) studies (Jiang F et al, 1990; Hunt M et al, 1975; Palmer M et al, 1983; Rabbani S et al, 1987; Palmer M et al, 1984) that the quadrupole interaction of nitrogen (only for  $^{14}\text{N}$ ) in imidazoles is affected by the strength of the hydrogen bond. Moreover, a measurement of the hyperfine interaction of the unpaired electron and the nitrogen nuclear spin gives direct information on the amount of delocalization over nickel and sulfur.

Using the same growth conditions, without chelex cleaning the solutions, the amino acid His was replaced by  $^{15}\text{N}$  His. In order to obtain accurate values for the nuclear hyperfine and quadrupole parameters, measurements have been performed on  $^{15}\text{N}$  histidine enriched samples. Here, we measure on the Ni-B redox state using Electron Spin Echo Envelope Modulation (ESEEM) and Hyperfine Sublevel Correlation (HYSCORE) spectroscopy as an example. Density Functional Theory (DFT) is used to calculate the spin density distribution and the nitrogen hfcs of the his.

### 6.5.1 EPR

The continuous wave EPR spectrum of a frozen solution of  $^{15}\text{N}$  histidine-enriched hydrogenase of *D. vulgaris* Miyazaki F is shown in figure 6.10. The sample has been prepared in a way to maximize the amount of the Ni-B redox state (chapter 3.5.9). The g values of the Ni-B state read from the spectrum are 2.33, 2.16 and 2.01, in agreement with those measured by EPR spectroscopy on other [NiFe] hydrogenases.

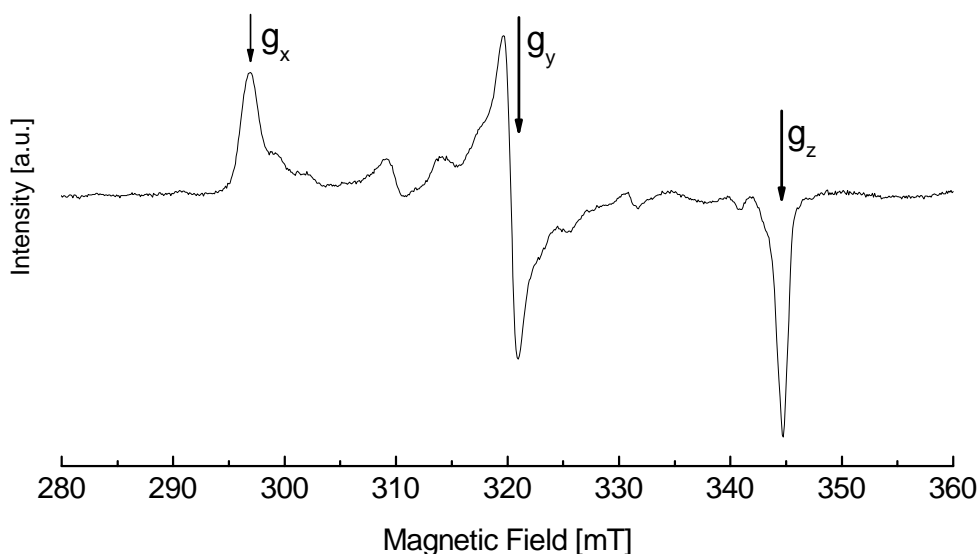


Fig. 6.9 EPR spectrum of *D. vulgaris* Miyazaki F hydrogenase dominantly in the Ni-B redox state. Experimental conditions:  $T = 120\text{ K}$ ,  $\nu_{\text{mw}} = 9.63\text{ GHz}$ , modulation amplitude  $0.5\text{ mT}$ ,  $P_{\text{mw}} = 2\text{ mW}$ .

From a comparison of the intensity of the  $g_y$  signals of Ni-B and Ni-A ( $g_y = 2.24$ ), a ratio of Ni-B: Ni-A of 9:1 is determined. A yield of 90% of one state is sufficient for the accurate elucidation of hyperfine and quadrupole parameters from EPR related techniques such as HYSCORE spectroscopy.

### 6.5.2 ESEEM, HYSCORE and simulation

The three pulse ESEEM spectra for *D. vulgaris* Miyazaki F hydrogenase in the Ni-B state with (bottom traces) and without (top traces) labeled  $^{15}\text{N}$  histidine recorded at three different magnetic field settings (see materials and methods) are shown in figure 6.11. The spectra with unlabeled ( $^{14}\text{N}$ ) histidine display three bands, denoted  $\nu_0$ ,  $\nu_-$ ,  $\nu_+$ , with frequencies of about 0.4, 1.2 and 1.6/1.7 MHz, which are characteristic of single quantum frequencies of  $^{14}\text{N}$  (Flanagan H L et al, 1987). The positions of these bands remain constant to within 0.1 MHz when the magnetic field setting is changed, but their relative intensities change. At around 4 MHz, a broad and weak signal with a poorly resolved structure is visible, which corresponds to the double-quantum transition ( $\nu_{\text{dq}}$ ) of the non-cancelled manifold (Flanagan H L et al, 1987). The structure of this

transition is caused mainly by the anisotropy of the hyperfine tensor (*vide infra*). In the ESEEM spectra of the  $^{15}\text{N}$  histidine enriched sample, almost all signal intensity has disappeared. For  $^{15}\text{N}$  ( $I = 1/2$ ), no quadrupole interaction is present and only two transitions, one per  $M_S$  manifold, are expected. These transitions have little intensity in the ESEEM spectra, but can be observed by HYSCORE spectroscopy. The low-intense signals in the  $^{15}\text{N}$  histidine sample correspond to trace amounts of  $^{14}\text{N}$ , which is also present.

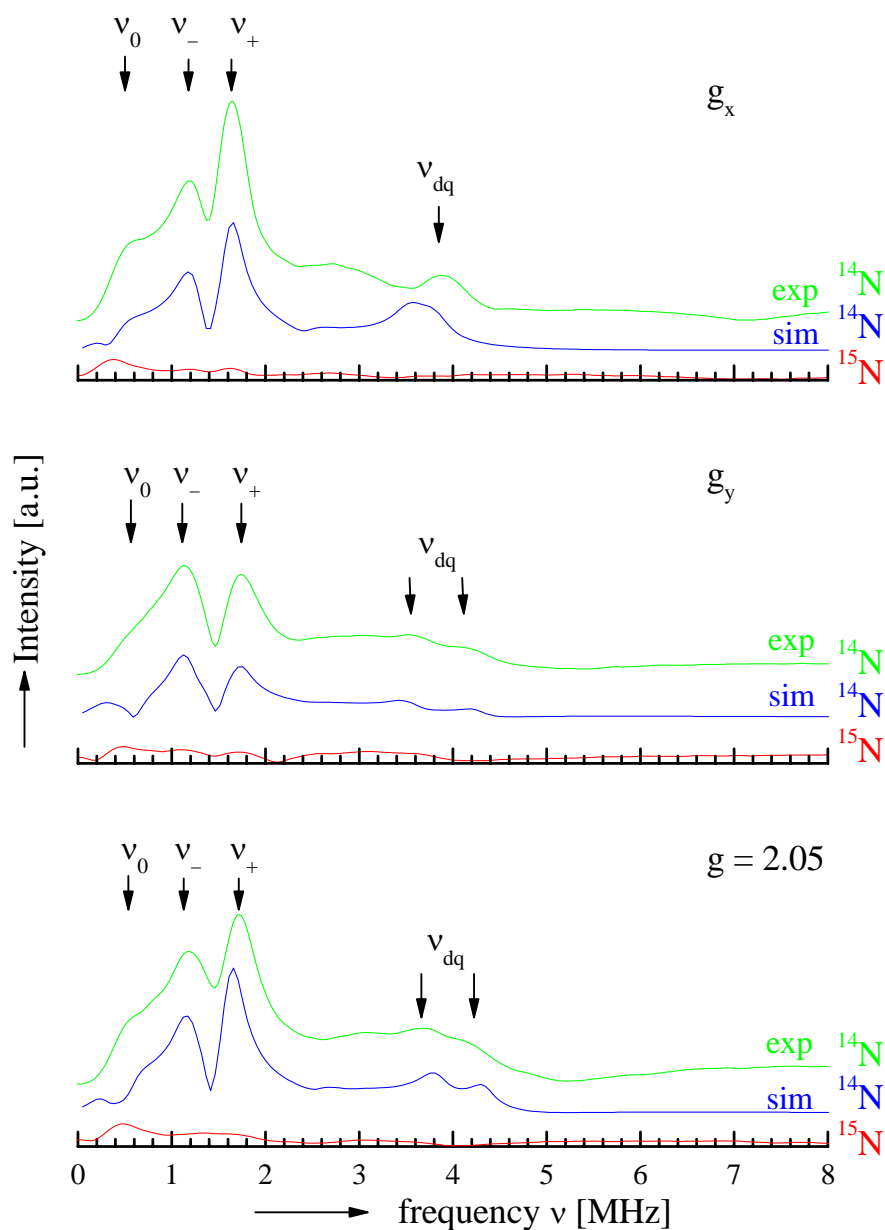


Fig. 6.10 Three pulse ESEEM spectra and simulations for *D. vulgaris* Miyazaki F hydrogenase in the Ni-B redox state recorded at the  $g_x$  and  $g_y$  canonical orientations and at  $g = 2.05$  (at  $g_z$  the signal of the [3Fe4S] cluster is superimposed). Top traces: spectra of the non-enriched ( $^{14}\text{N}$  histidine) sample, middle traces: simulation of the spectra of the non-enriched sample, lower traces: spectra of the  $^{15}\text{N}$  histidine enriched sample. For experimental conditions, see materials and methods.

HYSCORE spectra recorded at similar conditions as the ESEEM spectra are presented in figure 6.12. In the spectra in the left column, the natural abundance  $^{14}\text{N}$  histidine was present in the sample, in the right column the spectra of the  $^{15}\text{N}$  enriched histidine sample are shown. Comparison of the experimental spectra in the left and right columns reveals significant differences. The spectrum with  $^{15}\text{N}$ -enriched histidine shows two strong cross peaks at (0.4, 2.5) MHz and (2.5, 0.4) MHz. The transitions at 0.5 MHz and 2.5 MHz are the  $^{15}\text{N}$  nuclear transitions of the  $M_S = +\frac{1}{2}$  and  $-\frac{1}{2}$  manifolds. The spectrum with natural abundance  $^{14}\text{N}$  histidine displays a richer structure with cross peaks at (1.2, 4.1) MHz, (1.7, 4.1) MHz, (0.4, 4.1) MHz, (4.1, 1.2) MHz, (4.1, 1.7) MHz and (4.1, 0.4) MHz. Each cross peak relates one of the single quantum transitions ( $\nu_0$ ,  $\nu_-$  or  $\nu_+$ ) to the double quantum transition ( $\nu_{dq}$ ) of the non-cancelled manifold. Similar to the case of the ESEEM spectra, the positions of the cross peaks do not change much with magnetic field, but their relative intensities vary when going from  $g_x$  to  $g = 2.05$ . A small amount of the natural abundance signal can still be observed in the  $^{15}\text{N}$  enriched spectra. The signals on the diagonal stem from the three pulse stimulated echo and incomplete population inversion of the 180 degrees microwave pulse.

The changes in the HYSCORE spectra upon labeling of the protein with  $^{15}\text{N}$  histidine show that the signals in the  $^{14}\text{N}/^{15}\text{N}$  region indeed stem from a histidine nitrogen. From the frequencies of the cross-peaks, the three quadrupole frequencies  $\nu_0$ ,  $\nu_-$  and  $\nu_+$  are found to be 0.4, 1.2 and 1.6/1.7 MHz. The values of the quadrupole frequencies for  $^{14}\text{N}$  are in agreement with the assignment of this nitrogen as a histidine  $N_\epsilon$  nitrogen (Jiang F et al, 1990). A similar pattern has already been observed for *D. gigas* hydrogenase (Chapman A et al, 1988), for which it was already suggested that the nitrogen signals are possibly from imidazole coupled to the nickel center, and for the Q67H mutant of *R. eutropha* hydrogenase (Buhrke *et al.*, 2002) in which it was shown that the  $\delta$  nitrogen is not protonated and the N-S distance is about 3.1 Å.

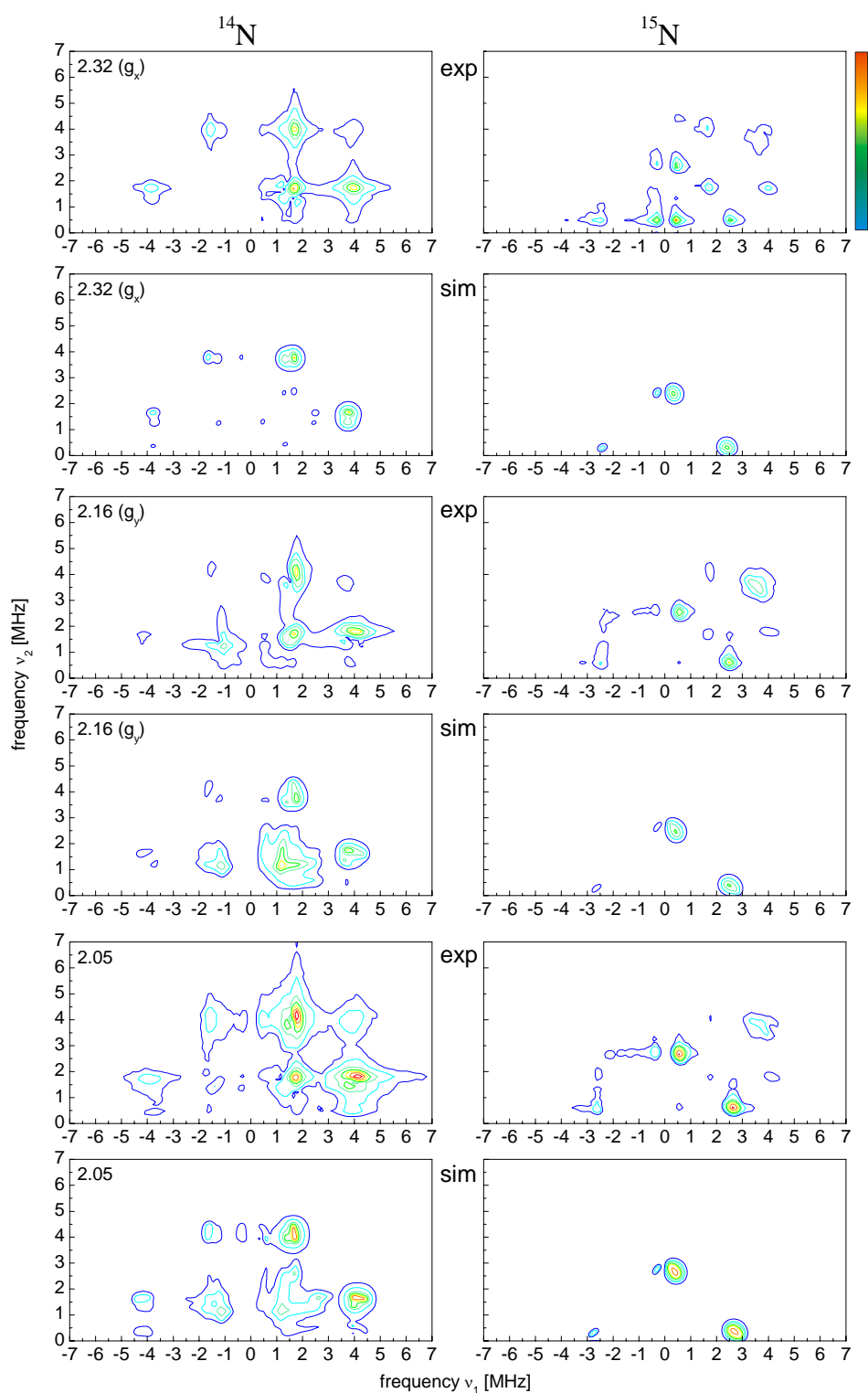


Fig. 6.11 HSCORE spectra and simulations for *D. vulgaris* Miyazaki F hydrogenase in the Ni-B redox state recorded at the  $g_x$  and  $g_y$  canonical orientations and  $g = 2.05$ . Left column: natural abundance ( $^{14}\text{N}$ ) histidine; right column  $^{15}\text{N}$  histidine enriched histidine. The g values at which the spectra are recorded/simulated are indicated in the left diagrams. For experimental conditions, see materials and methods.

In order to extract hyperfine and quadrupole parameters for the nitrogen, the spectra in the  $^{14}\text{N}/^{15}\text{N}$  region have been simulated [see references (van Gastel M *et al.*, 1998; Brecht M *et al.*, 2003) for details]. First, the hyperfine coupling constants have been elucidated by simulation of the  $^{15}\text{N}$  spectra ( $I = 1/2$ ), because the  $^{15}\text{N}$  nucleus lacks quadrupole interaction. The respective HYSCORE simulations are included in figure 6.12. Since little intensity is present in the corresponding ESEEM spectra, the ESEEM simulations for  $^{15}\text{N}$  are not shown. From both the position and the lineshape of the cross peaks, accurate principal values (error  $\pm 0.1$  MHz) could be determined. The hyperfine tensor of  $^{15}\text{N}$  was found to have an isotropic hyperfine coupling constant of  $-2.20$  MHz ( $1.57$  MHz for  $^{14}\text{N}$ , after correction for the difference of the gyromagnetic ratios of  $^{14}\text{N}$  and  $^{15}\text{N}$ ). The anisotropic part of the tensor was found to be axial, with the largest component being  $-0.70$  MHz ( $0.50$  MHz for  $^{14}\text{N}$ ). The parameters, valid for the  $^{14}\text{N}$  isotope, are summarized in table 6.1. The direction of the dipolar axis was determined with an accuracy of approximately  $\pm 15$  degrees.

Subsequently, nuclear quadrupole coupling constants have been extracted from the HYSCORE spectrum of the  $^{14}\text{N}$  sample. In this simulation the hyperfine tensor was kept fixed and the quadrupole tensor was optimized. Starting parameters for the principal axes of the quadrupole tensor were chosen such that the principal x-axis (corresponding to the smallest absolute principal value) is parallel to the histidine  $\text{N}_\epsilon\text{-H}_\epsilon$  direction and the principal z-axis (corresponding to the largest absolute principal value) is perpendicular to the imidazole plane (Garcia MLS *et al.*, 1983). Only minor adjustments were necessary. The optimized parameters are included in table 1 and the simulations are shown in figures 3 (middle traces) and 4. The magnitude of the quadrupole parameter  $e^2qQ$  ( $-1.9$  MHz) is equal to that estimated from the ESEEM spectra for *D. gigas* hydrogenase (Chapman A *et al.*, 1988). No attempts have been made to simulate the ESEEM signals on the diagonal in the HYSCORE spectra. For both  $^{14}\text{N}$  and  $^{15}\text{N}$  the simulations satisfactorily reproduce both the position and the lineshape of the bands in the ESEEM spectra and the cross peaks in the HYSCORE spectra. The largest mismatch between simulation and experiment occurs at the single-crystal-like the  $g_x$  canonical orientation. At this orientation, which is difficult to simulate because of bandwidth effects, the simulated double quantum transition is about  $0.2$  MHz too low as compared to experiment.



Table 6.1.  $^{14}\text{N}$  hyperfine and quadrupole coupling constants for the  $\text{N}_\epsilon$  of His-88 in *D. vulgaris* Miyazaki F hydrogenase in the Ni-B state. The principal values and principal axes of the hyperfine tensor have been optimized by simulation of the  $^{15}\text{N}$  HYSCORE spectra. The hyperfine parameters have been kept fixed in the subsequent optimization of the simulation of the  $^{14}\text{N}$  HYSCORE spectra, in which the quadrupole coupling constants have been optimized. The directions of the principal axes  $\ell_{ji}$  ( $i = x, y, z$ ) are given in the crystallographic axes system ( $j = a, b, c$ ). Note that the sign of  $e^2qQ$  is inferred from calculations of the electric field gradient (Palmer MH *et al.*, 1983).

$^{14}\text{N}$ hyperfine coupling constants				Quadrupole coupling constants						
	$\ell_{ai}$	$\ell_{bi}$	$\ell_{ci}$			$\ell_{ai}$	$\ell_{bi}$	$\ell_{ci}$		
$a_{\text{iso}}$	1.57			$e^2qQ/h$	-1.90					
$A'_x$	-0.25			$\eta$	0.37	$Q'_x$	0.30	-0.008	-0.999	-0.053
$A'_y$	-0.25					$Q'_y$	0.65	0.325	-0.044	0.943
$A'_z$	0.50	0.470	0.881	-0.100		$Q'_z$	-0.95	-0.946	-0.013	0.327

### 6.5.3 DFT calculations

In order to complement the experimental data, DFT calculations have been performed on a truncated model system of the [NiFe] site (for details, see materials and methods). Two calculations have been performed, one without and one with a methylimidazole, which models the histidine-88 residue of the large subunit. A selection of hyperfine coupling constants and spin densities, along with the  $g$  values, and the expectation value of the  $S^2$  operator is given in table 2. The spin contamination is negligible as is seen from the  $\langle S^2 \rangle$  values of 0.774 and 0.776 ( $S(S + 1) = 0.75$  for an ideal  $S = 1/2$  system). Here, the focus is on the effect of the histidine and the hydrogen bond to sulfur on the electronic structure. As is seen from the table, the calculation shows that the only nitrogen, which is close enough to the active site to be compatible with the  $^{14}\text{N}$  hyperfine coupling constants, is the  $\epsilon$  nitrogen of histidine 88. The hyperfine coupling constants for the  $\delta$  nitrogen are much smaller than those for the  $\text{N}_\epsilon$ .

A striking difference is observed when comparing the models with and without histidine. The spin densities at nickel and  $S_\gamma(\text{Cys-549})$  are 75.2% and 28.4% for the model without the histidine, and 82.3% and 21.5% for the model with the histidine. The presence of the histidine in the calculation shifts a significant part of spin density from sulfur to nickel. This can be understood on the basis of ligand field theory. The nickel orbitals are slightly higher in energy than the sulfur orbitals. As compared to the situation without the histidine, a partially positive charge of the proton ( $\delta+$ ) is present

near  $S_\gamma(\text{Cys-549})$ . This stabilizes the sulfur 3p orbitals such that the energy gap between the sulfur and the nickel orbitals becomes larger. The sulfur orbitals will mix less into the wavefunction of the unpaired electron and the spin density shifts to the nickel side. The shift of spin density found here is as large as 7%. For an accurate theoretical description of the electronic structure of the [NiFe] site, it is therefore important to include the hydrogen bond to  $S_\gamma(\text{Cys-549})$ , which fine-tunes the relative energies of the Ni and S orbitals.

Because of the increased calculated spin density at Ni when the H-bond is included, the calculated  $g_x$  shift slightly increases from 2.207 to 2.232 (experimental value: 2.33). The hyperfine coupling constants of Ni and S in the calculation with and without H-bond do not show the same trend as the change in spin density. For example, for Ni, though  $a_{iso}$  becomes larger when including His-88 ( $-80.0$  MHz with His-88 and  $-58.4$  MHz without His-88), the anisotropic part of the hyperfine tensor even becomes slightly smaller. This is related to the composition of the wavefunction of the unpaired electron at Ni and S, which slightly changes upon inclusion of the H-bond to  $S_\gamma(\text{Cys-549})$ .

When examining the calculated  $^1\text{H}$  hyperfine coupling constants, the proton with the largest anisotropic coupling is that of the bridging  $\text{OH}^-$  ligand, for which  $A'_z = 8.54$  MHz. The histidine  $\epsilon$  proton, which forms the hydrogen bond, has a small isotropic hyperfine coupling constant ( $-0.94$  MHz) and the largest component of the anisotropic hyperfine interaction ( $A'_z$ ) is 5.41 MHz. This proton is the proton with the second largest calculated anisotropic hyperfine interaction.

The isotropic hyperfine coupling constant of  $^{14}\text{N}_\epsilon(\text{His-88})$  is calculated to be somewhat larger ( $a_{iso} = 2.20$  MHz) than that elucidated from experiment ( $a_{iso} = 1.57$  MHz). The calculated dipolar part of the hyperfine interaction ( $a_{aniso} = -0.24, -0.22, 0.46$  MHz) and the experimental dipolar hyperfine coupling constants ( $a_{aniso} = -0.25, -0.25, 0.50$  MHz) are almost identical. The agreement can be considered very good, taking into account that the nitrogen is located close to the large spin density at  $S_\gamma(\text{Cys-549})$ .

Table 6.2. Overview of g values and hyperfine coupling constants [MHz] from DFT calculations of the small (excluding His-88, (1)) and large (including His-88, (2)) model system of the active site of *D. vulgaris* Miyazaki F hydrogenase in the Ni-B state. Also

included are the expectation value of the  $S^2$  operator and the Mulliken spin densities  $\rho_s$  at nickel,  $S_\gamma(\text{Cys-549})$  and  $S_\gamma(\text{Cys-81})$ .

model	1	2	exp
g-values			
$g_x$	2.21	2.23	2.33
$g_y$	2.15	2.18	2.16
$g_z$	2.03	2.03	2.01
$H_\epsilon(\text{His-88})$ -hfcs			
$a_{\text{iso}}$		-0.94	
$A'_x$		-3.09	
$A'_y$		-2.32	
$A'_z$		5.41	
$N_\epsilon(\text{His-88})$ -hfcs			
$a_{\text{iso}}$		2.20	1.57
$A'_x$		-0.24	-0.25
$A'_y$		-0.22	-0.25
$A'_z$		0.46	0.50
$N_\delta(\text{His-88})$ -hfcs			
$a_{\text{iso}}$		-0.01	
$A'_x$		-0.04	
$A'_y$		-0.02	
$A'_z$		0.06	
$\langle S^2 \rangle$	0.774	0.776	
$\rho_s(\text{Ni})$	75.2%	82.3%	
$\rho_s(S_\gamma(\text{Cys-549}))$	28.4%	21.5%	
$\rho_s(S_\gamma(\text{Cys-81}))$	-3.7%	-4.4%	

<sup>a</sup> Note that <sup>61</sup>Ni and <sup>17</sup>O have a negative nuclear g values.

### The strength of the H-bond between His-88 and Cys-549

The hydrogen bonding of substituted imidazoles in model systems and that of histidines in a selection of proteins have been investigated by ESEEM spectroscopy (Jiang, F *et al.*, 1990) and a Townes Dailey model (Townes, CH *et al.*, 1947). The model is based on the following idea. The nitrogen of the imidazole is  $sp^2$  hybridized and the strength of the hydrogen bond influences the occupancy of the N-H  $sp^2$  orbital. For example, when a strong force pulls on the proton, *i.e.*, when a strong H-bond is present, N-H bond length is increased and becomes more polarized. The N-H bonding orbital attains more nitrogen character, which increases the occupancy of the nitrogen  $sp^2$  orbital in the N-H direction. The relative occupancies of the three  $sp^2$  orbitals at nitrogen largely determine

the magnitude and the asymmetry of the electric field gradient, which is proportional to the quadrupole interaction. Reference data are available in which the strength of the hydrogen bond is related to the occupancies of the  $sp^2$  orbitals and the nuclear quadrupole interaction (Jiang, F *et. al.*, 1990) . Figure 8 of this reference is shown here in figure 6.13 and elaborate details of the model including nomenclature are given in the same reference. The quadrupole parameters in frequency units  $e^2q_RQ/h$ ,  $e^2q_\pi Q/h$  and  $e^2q_TQ/h$  are calculated according to

$$\begin{aligned} e^2q_\pi Q &= e^2qQ \\ e^2q_R Q &= e^2qQ \left( \frac{-1+\eta}{2} \right) \\ e^2q_T Q &= e^2qQ \left( \frac{-1-\eta}{2} \right) \end{aligned} \quad (1)$$

They amount to 1.9 MHz,  $-0.59$  MHz and  $-1.30$  MHz (Note that reference (Jiang, F *et. al.*, 1990) uses a positive value of  $e^2qQ/h$ . The value of this parameter is negative for imidazole nitrogens (Palmer MH *et. al.*, 1983). The above values have the incorrect sign for  $e^2qQ$  for reasons of comparison). Including these numbers in figure 4, it becomes clear that the orbital occupancy  $c$  of the N-H  $sp^2$  orbital of His-88 is 0.085 larger than  $c_0$  of the reference compound (1,2 dimethylimidazole, see reference (Jiang, F *et. al.*, 1990), indicating the presence of a stronger H-bond than that formed by the reference compound. Comparison with the other model compounds indicates that the H-bond between His-88 and Cys-549 is, however, best described as a weak hydrogen bond.

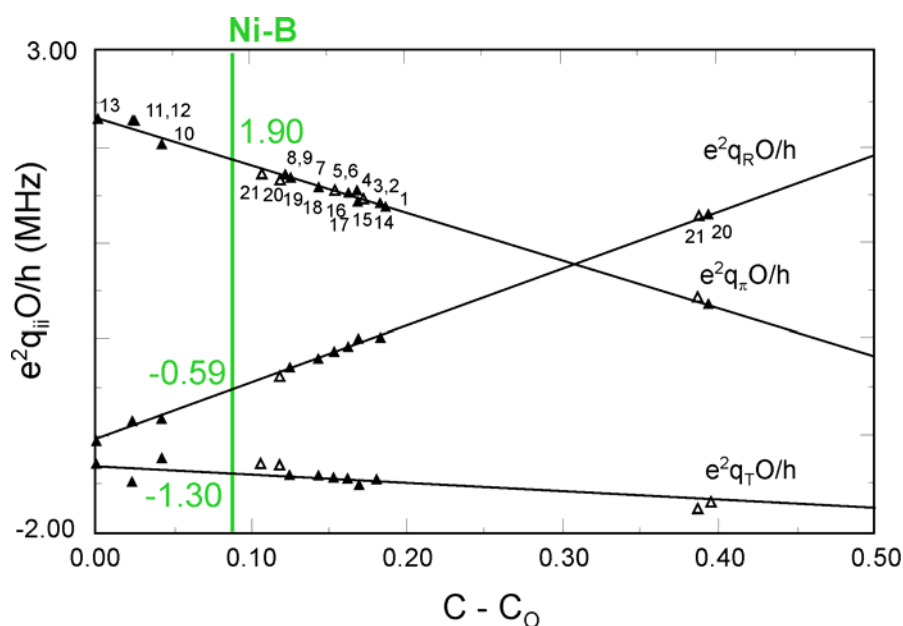


Fig.6.13. Plot of  $e^2q_iQ/h$  ( $i = R, \pi, T$ ) and the N-H  $sp^2$  orbital population change  $c-c_0$  with respect to the reference compound (1,2-dimethylimidazole), which has a population  $c_0$ . This figure is reproduced from reference (Jiang, F *et al.*, 1990), each number corresponds to a different compound. See (Jiang, F *et al.*, 1990) for details. The magnitude of  $c$  can be taken as an indicator of the strength of hydrogen bonding (larger values of  $c$  mean stronger H-bonds).

## 6.6 Discussion

**$^{61}\text{Ni}$ :** - The EDNMR spectra shown in section 6.4 are the first spectra in which signals of  $^{61}\text{Ni}$  are observed by a hyperfine resolving technique. Until now, the observation of the hyperfine interaction of the central metal by such a technique is known to be a difficult task. Most probably this is related to the usually short nuclear relaxation times of the central metal. The EDNMR technique used here, in which these nuclear transitions are made indirectly, has the potential to fill this gap in the arsenal of pulse EPR techniques. The elucidation of the hyperfine and quadrupole coupling constants gives direct information about the wavefunction of the unpaired electron at the metal, which is very important, since the catalytic activity of the enzyme is related to the metal.

Up to now it remains unclear what exactly determines the intensity of the EDNMR signal. For this reason the interpretation of the EDNMR spectra and determination of hyperfine and quadrupole coupling constants is not yet complete. A better understanding of the experiment itself is necessary. The initial data shows, however, that the Ni-A and Ni-B states are characterized by similar  $^{61}\text{Ni}$  hyperfine coupling constants. This, in turn, implies that the environment of Ni is also similar in both enzymes. For the bridging ligand, this has important consequences. For the Ni-B state, the bridging ligand most probably is an  $\text{OH}^-$  (van Gastel M *et al.*, 2005), which means that the Ni-A state must have a bridging ligand of similar nature.

**$^{15}\text{N}$  His:** - The H-bond between  $H_\epsilon$  of His-88 and  $S_\gamma$  of Cys-549 in the Ni-B state of *D. vulgaris* Miyazaki F hydrogenase has been investigated by HYSCORE spectroscopy and DFT calculations. By performing experiments on natural abundance samples and  $^{15}\text{N}$  enriched histidine samples, a clear identification of the nitrogen signals with a histidine imidazole nitrogen ( $N_\epsilon$ ) has been established. From simulations of the spectra,

nuclear hyperfine and quadrupole coupling constants have been elucidated. Comparison with DFT calculations of a truncated model system of the active site shows that the only nitrogen, which is close to the [NiFe] center and has hyperfine coupling constants compatible with those found in the experiment, is the  $\epsilon$  nitrogen of His-88. The quadrupole parameters of this nitrogen allow the determination of the strength of the H-bond between the  $\text{H}_\epsilon$  of His-88 and  $\text{S}_\gamma$  of Cys-549. Analysis of these parameters leads us to conclude that a weak hydrogen bond is present. Furthermore, this H-bond is able to finetune the relative energies of the sulfur orbitals with respect to the nickel orbitals. The artificial exclusion of the H-bond in a DFT calculation results in a shift of spin density from Ni to S of about 7%.

The finding of spin density on His-88 also indicates a possible pathway for the electron transfer from the [NiFe] center to the proximal [4Fe4S] cluster. There is a cavity in the X-ray structure (2), which seems to allow this histidine to rotate unhindered about its  $\text{C}_\alpha\text{-C}_\beta$  axis. After such rotation, His-88 moves into H-bonding distance of His-235 of the large subunit. The center of this imidazole is only approximately 4 Å away from the proximal [4Fe4S] cluster. Of course, the data presented here do not allow a definite conclusion about the identity of the pathway of the electron transfer process. One way to investigate this further would be, for example, to mutate His-235 to another amino acid and to control, whether electron transfer is still taking place under physiological conditions by measuring the hydrogenase activity. For this, it is necessary to investigate the maturation pathway of *D. vulgaris* Miyazaki F hydrogenase in greater detail, such that it becomes possible to set-up an over-expression system after which it is more feasible to construct and express mutants.



## Chapter 7

### Summary and Outlook

In the present work, studies on the [NiFe] hydrogenase of *Desulfovibrio vulgaris*, an anaerobic sulfur reducing bacterium, belonging to  $\gamma$  proteobacterium group of bacteria, has been conducted. This enzyme catalyses the reaction  $H_2 \rightleftharpoons 2H^+ + 2e^-$  reversibly.

The [NiFe] hydrogenase is composed of a large and a small subunit of molecular weight of 61 and 29 kDa, respectively. The large subunit holds the active center, and is composed of a hetero-bimetallic complex with a nickel and an iron atom in the active site. This enzyme is rich in different redox states, with the oxidised states having an extra bridging ligand between both metal ions.

In this thesis, molecular biology, biochemistry and advanced spectroscopy methods like ELDOR-detected NMR and HYSCORE on an isotope labeled protein have been successfully applied, to explore the genes involved in the maturation pathway of [NiFe] hydrogenase from *D. vulgaris* Miyazaki F, to provide the technology for site-directed mutagenesis and to investigate the structure of the active site.

The complete operon sequence of the [NiFe] hydrogenase encoding genes was obtained. The sequence indicated the presence of two maturation genes present downstream of the already known structural genes, coding for the small and the large subunits of the enzyme. Two different strategies were used to achieve the full information of the operon. The first strategy employed the use of random degenerate reverse primer based



on sequence homology, together with specific forward primers in the PCR reaction aiming at amplifying the unknown gene sequence. For the second strategy, SphI-digested chromosomal DNA of DvMF was randomly cloned based on molecular weight selection, and probed with the known gene sequence to find the correct clone. By this second approach, the entire sequence of hydrogenase operon could be determined. The sequenced genes were compared on the basis of phylogeny with the other known gene sequences of related organisms, and found to be most closely related to that of DvH, the sequence of which could be extracted from the genome sequence. The heterologous expression of only the structural genes in *E. coli*, and also of the complete operon of DvMF [NiFe] hydrogenase under the native promoter leads to protein translation, however, the protein was not matured and thus inactive. To understand the specificity of the action of the endopeptidase (hynC), the secondary structure prediction of hynC was compared to that of the crystallised *E. coli* counterpart hybD and found to be highly similar. This led to modelling of the three-dimensional structure for the C-subunit, which was obtained in close similarity to that of the crystallised *E. coli* protein.

The construction of a [NiFe] hydrogenase deletion mutant and studies regarding expression, electrochemistry and native gel assay, were preformed. The introduction of a deletion in the [NiFe] hydrogenase operon from DvH could be performed by constructing suicide plasmids with the structural gene being interrupted by the chloramphenicol resistance ( $Cm^R$ ). First crossover between plasmid and chromosomal DNA led to the integrant construction, which could be selected against chloramphenicol resistance (positive selection). To delete the second copy of the gene, a second crossover was forced using sucrose as selection marker (*sacB* negative selection), generating the desired mutant. In case of DvH, the deletion mutant was constructed successfully, however, the experiments failed up to now for DvMF. A possible explanation for this result could be given on the basis of in-gel activity assays that revealed probably only one [NiFe] hydrogenase present in DvMF. The expression studies comparing the WT and the mutant of DvH showed no significant difference other than the observation that the cells of the deletion mutant did not reach the same cell density. The electrochemical studies comparing the DvH WT, DvH deletion mutant and DvMF WT showed that the activity of DvH mutant and DvMF WT are comparable and almost eight times less than DvH WT.

The structure of the active site has been investigated using EPR spectroscopy. The first step to achieve this was the establishment of a growth medium protocol, allowing appropriate labeling. In order to label the protein with  $^{61}\text{Ni}$ , a special minimal medium with a defined composition was designed, followed by metal withdrawal by applying the chelex resin, which yielded an entirely metal free medium. For a further optimization of the growth medium, the optimum concentration of nickel was determined and a homemade 10-liter glass fermentor was used instead of a steel fermentor for the culture growth. Under these growth conditions, >90% labeling was achieved for the hydrogenase, as seen from EPR data. For the  $^{15}\text{N}$  histidine labeled protein preparation, chelex cleaning was not needed and the labeled amino acid was used to replace the normal amino acid in the minimal media components. Measurements on these labeled samples were done using ELDOR detected NMR at Q-band and EPR at X- and Q-band for the EPR active redox states of the hydrogenase, Ni-A, Ni-B, Ni-C and Ni-L. Simulation of the  $^{61}\text{Ni}$  EPR spectra gave hyperfine coupling constants, linewidth parameters and g values. Labeling with  $^{15}\text{N}$  His showed that the coupling is to a nitrogen ( $\text{N}_\epsilon$ ) belonging to His 88. Also, the strength of the hydrogen bond between His-88 and Cys-549 in the Ni-B redox state could be estimated, by ESEEM and HYSORE.

**Outlook:** - The pathway for constructing mutants of [NiFe] hydrogenase has been set in this thesis. The complete operon of DvH and/or DvMF [NiFe] hydrogenase comprising of *hynA*, *hynB*, *hynC* and *hynD* can now be cloned in a broad host range plasmid with its native promoter and used for expression studies. This construct can be reintroduced in the DvH deletion mutant by a single step conjugation, most probably leading to restoring the hydrogenase activity. On this basis, mutations can be introduced in the gene/(s) and the mutated gene can be reintroduced in the deletion mutant in a similar manner.

Another possibility to design the set up for generating mutants in case of DvH could be to clone all the four operons encoding hydrogenase structural and maturation genes in vectors that can accommodate two operons per vector, as published for the iron hydrogenase recently (Posewitz MC *et al.*, 2004).

The presence of maturation genes for [NiFe] hydrogenase in DvMF is well known. These can be screened using the same approach as used for completing the gene sequence of hydrogenase operon for DvMF.

The crystallography studies of hynC protein of DvMF and comparison with the known crystal structure of related proteins will help to understand the reason for high specificity of action.

The growth studies of DvH WT and DvH deletion mutant in the standard medium did not show much difference. The use of media with varying concentration of hydrogen in the gas mixture and with the hydrogen as sole electron donor in the fermentation studies, coupled with head space environment analysis should show differences in the growth behavior. It can shed light on the question, if hydrogen cycling is an important metabolic pathway, or whether there exist other metabolic pathways.

From a spectroscopic point of view, the  $^{15}\text{N}$  histidine labeled hydrogenase can also be used to study the [FeS] clusters, which are known from the crystal structure to have histidine coordination as well. By studying the [FeS] clusters in a similar way as was done for the [NiFe] center (see chapter 6), the strength of the H-bond to the [FeS] cluster can be determined. Measurement thereof may help for a better understanding of how the chemical properties (e.g. the redox potential) of the [FeS] clusters are fine-tuned by their environment.

The growth medium designed for this study can be used for other labeling experiments as well, for example labeling of  $^{57}\text{Fe}$ , replacing the natural abundant Fe. The labeled protein can be studied by ENDOR and Mößbauer spectroscopy for the modified active site.

## Chapter 8

### Bibliography

Albracht, S.P. (1994). Nickel hydrogenases: in search of the active site. *Biochim Biophys Acta* 1188, 167-204.

Albracht, S.P., Graf, E.G., and Thauer, R.K. (1982). The EPR properties of nickel in hydrogenase from *Methanobacterium*. *FEBS Lett* 140, 311-3.

Amara, P., Volbeda, A., Fontecilla-Camps, J.C. and Field, M.J. (1999). A Hybrid Density Functional Theory/Molecular Mechanics Study of Nickel-Iron Hydrogenase: Investigation of the Active Site Redox States. *J Am Chem Soc* 121, 4468 – 4477.

Armstrong, F.A. (2004). Hydrogenases: active site puzzles and progress. *Curr Opin Chem Biol* 8, 133-140.

Bagley, K.A., Duin, E.C., Roseboom, W., Albracht, S.P., and Woodruff, W.H. (1995). Infrared-detectable groups sense changes in charge density on the nickel center in hydrogenase from *Chromatium vinosum*. *Biochem* 34, 5527-5535.

Barondeau, D.P., Roberts, L.M., and Lindahl, P.A. (1994). Stability of the Ni-C State and Oxidative Titrations of *Desulfovibrio gigas* hydrogenase monitored by EPR and Electronic Absorption Spectroscopies. *J Am Chem Soc* 116, 3442–3448.

Blokesch, M. (2004). [NiFe]-Hydrogenasen von *Escherichia coli*: Funktionen der am Metalleinbau beteiligten Proteine. PhD, der Ludwig-Maximilians-Universität, München.

Blokesch, M., Albracht, S.P., Matzanke, B.F., Drapal, N.M., Jacobi, A., and Bock, A. (2004). The complex between hydrogenase-maturation proteins HypC and HypD is an intermediate in the supply of cyanide to the active site iron of [NiFe]-hydrogenases. *J Mol Biol* 344, 155-67.

Blokesch, M., and Bock, A. (2002). Maturation of [NiFe]-hydrogenases in *Escherichia coli*: the HypC cycle. *J Mol Biol* 324, 287-96.

Blokesch, M., Magalon, A., and Bock, A. (2001). Interplay between the specific chaperone-like proteins HybG and HypC in maturation of hydrogenases 1, 2, and 3 from *Escherichia coli*. *J Bacteriol* *183*, 2817-22.

Blokesch, M., Paschos, A., Bauer, A., Reissmann, S., Drapal, N., and Bock, A. (2004). Analysis of the transcarbamoylation-dehydration reaction catalyzed by the hydrogenase maturation proteins HypF and HypE. *Eur J Biochem* *271*, 3428-3436.

Brecht, M., van Gastel, M., Buhrke, T., Friedrich, B., and Lubitz, W. (2003). Direct detection of a hydrogen ligand in the [NiFe] center of the regulatory H<sub>2</sub>-sensing hydrogenase from *Ralstonia eutropha* in its reduced state by HYSCORE and ENDOR spectroscopy. *J Am Chem Soc* *125*, 13075-13083.

Brugna, M.G., Orticoni, M.T.G., Bruschi, M., and Bianco, P. (2001). Electroanalysis of the hydrogen production by [Fe] hydrogenase from *Desulfovibrio vulgaris* Hildenborough. *J Electroanal Chem* *510*, 136-143.

Buhrke, T., Bleijlevens, B., Albracht, S.P., and Friedrich, B. (2001). Involvement of hyp Gene Products in Maturation of the H(2)-Sensing [NiFe] Hydrogenase of *Ralstonia eutropha*. *J Bacteriol* *183*, 7087-7093.

Buhrke, T., Brecht, M., Lubitz, W., and Friedrich, B. (2002). The H(2) sensor of *Ralstonia eutropha*: biochemical and spectroscopic analysis of mutant proteins modified at a conserved glutamine residue close to the [NiFe] active site. *J Biol Inorg Chem* *7*, 897-908.

Cammack, R., Patil, D.S., and Fernandez, V.M. (1985). Electron-spin-resonance/electron-paramagnetic-resonance spectroscopy of iron-sulphur enzymes. *Biochem Soc Trans* *13*, 572-578.

Casalot, L. and Rousset, M. (2001). Maturation of the [NiFe] hydrogenases. *Trends Microbiol* *9*, 228-237.

Casalot, L., De Luca, G., Dermoun, Z., Rousset, M., and de Philip, P. (2002). Evidence for a fourth hydrogenase in *Desulfovibrio fructosovorans*. *J Bacteriol* *184*, 853-6.

Casalot, L., Valette, O., De Luca, G., Dermoun, Z., Rousset, M., and de Philip, P. (2002). Construction and physiological studies of hydrogenase depleted mutants of *Desulfovibrio fructosovorans*. *FEMS Microbiol Lett* *214*, 107-112.

Chapman, A., Cammack, R., Hatchikian, E.C., van Gastel, M., Coremans, J.W.A., Jeuken, L.J.C., Canters, G.W., and Groenen, E.J.J. (1998). Electron Spin-Echo Envelope Modulation Spectrum of Azurin at X-Band. *J. Phys. Chem.-A* *102*, 4462-4470.

Chapman, A., Cammack, R., Hatchikian, C.E., McCracken, J., and Peisach, J. (1988). A pulsed EPR study of redox-dependent hyperfine interactions for the nickel centre of *Desulfovibrio gigas* hydrogenase. *FEBS Letters* *242*, 134-8.

- Davidson, G., Choudhury S.B., Gu, Z., Bose, K., Roseboom, W., Albracht, S.P., and Maroney, M.J. (2000). Structural examination of the nickel site in *Chromatium vinosum* hydrogenase: redox state oscillations and structural changes accompanying reductive activation and CO binding. *Biochem* 39, 7468-79.
- DeLacey, A.L., Fernandez, V.M., Rousset, M., Cavazza, C., and Hatchikian, E.C. (2003). Spectroscopic and kinetic characterization of active site mutants of *Desulfovibrio fructosovorans* Ni-Fe hydrogenase. *J Biol Inorg Chem* 8, 129-34.
- De Lacey, A.L., Hatchikian, E.C., Volbeda, A., Frey, M., Fontecilla-Camps, J.C., and Fernandez, V.M. (1997). Infrared-Spectroelectrochemical Characterization of the [NiFe] Hydrogenase of *Desulfovibrio gigas*. *J Am Chem Soc* 119, 7181 – 7189.
- Deckers, H.M., Wilson, F.R., and Voordouw, G. (1990). Cloning and sequencing of a [NiFe] hydrogenase operon from *Desulfovibrio vulgaris* Miyazaki F. *J Gen Microbiol* 136, 2021-8.
- Dolla, A., Pohorelic, B.K., Voordouw, J.K., and Voordouw, G. (2000). Deletion of the hmc operon of *Desulfovibrio vulgaris* subsp. *vulgaris* Hildenborough hampers hydrogen metabolism and low-redox-potential niche establishment. *Arch Microbiol* 174, 143-151.
- Drapal, N., and Bock, A. (1998). Interaction of the hydrogenase accessory protein HypC with HycE, the large subunit of *Escherichia coli* hydrogenase 3 during enzyme maturation. *Biochemistry* 37, 2941-8.
- Erkens, A., Schneider, K., and Müller, A. (1996). The NAD linked soluble hydrogenase from *Alcaligenes eutrophus* H16: detection and characterization of EPR signals deriving from nickel and flavin. *J Biol Inorg Chem* 1, 99–110.
- Fan, C., Teixeira, M., Moura, J. J. G., Moura, I., Huynh, B.-H., LeGall, J., Peck Jr., H. D., Hoffman, B. M. (1991). Detection and characterization of exchangeable protons bound to the hydrogen-activation nickel site of *Desulfovibrio gigas* hydrogenase: a proton and deuterium Q-band ENDOR study. *J Am Chem Soc* 113, 20-24.
- Feher, G. (1956). Observation of nuclear magnetic resonances via the electron spin resonance line. *Physical Review* 103, 834-835 1956.
- Fernandez, V.M., Hatchikian, E.C., and Cammack, R. (1985). Properties and reactivation of two different deactivated forms of *Desulfovibrio gigas* hydrogenase. *Biochim Biophys Acta* 832, 69-79.
- Flanagan, H.L., and Singel, D.J. (1987). Analysis of <sup>14</sup>N ESEEM patterns of randomly oriented solids. *J Chem Phys* 87, 5606-5616.
- Foerster, S., Stein, M., Brecht, M., Ogata, H., Higuchi, Y., and Lubitz, W. (2003). Single crystal EPR studies of the reduced active site of [NiFe] hydrogenase from *Desulfovibrio vulgaris* Miyazaki F. *J Am Chem Soc* 125, 83-93.

Fontana, P., Bindewald, E., Toppo, S., Velasco, R., Valle, G. and Tosatto, S.C.E. (2005). The SSEA server for protein secondary structure alignment. *Bioinformatics* 21, 393-395.

Frey, M. (2002). Hydrogenases: hydrogen-activating enzymes. *Chem Biochem* 3, 153-160.

Fritsche, E., Paschos, A., Beisel, H.G., Bock, A., and Huber, R. (1999). Crystal structure of the hydrogenase maturing endopeptidase HYBD from *Escherichia coli*. *J Mol Biol* 288, 989-998.

Fu, R., and Voordouw, G. (1997). Targeted gene-replacement mutagenesis of *dcrA*, encoding an oxygen sensor of the sulfate-reducing bacterium *Desulfovibrio vulgaris* Hildenborough. *Microbiology* 143, 1815-26.

Garcia, M.L.S., Smith, J.A.S., Bavin, P.M.G., Ganellin, C.R. (1983).  $^{14}\text{N}$  and  $^2\text{H}$  quadrupole double resonance in substituted imidazoles. *J.Chem.Soc.Perkin Trans.II* 9, 1391-1399.

Garcin, E., Vernede, X., Hatchikian, E.C., Volbeda, A., Frey, M., and Fontecilla-Camps, J.C. (1999). The crystal structure of a reduced [NiFeSe] hydrogenase provides an image of the activated catalytic center. *Structure* 7, 557-566.

Gay, P., Le Coq, D., Steinmetz, M., Ferrari, E., and Hoch, J.A. (1983). Cloning structural gene *sacB*, which codes for exoenzyme levansucrase of *Bacillus subtilis*: expression of the gene in *Escherichia coli*. *J Bacteriol* 153, 1424-31.

George, S.J., Kurkin, S., Thorneley, R.N. and Albracht S.P. (2004). Reactions of  $\text{H}_2$ ,  $\text{CO}$ , and  $\text{O}_2$  with active [NiFe]-hydrogenase from *Allochromatium vinosum*. A stopped-flow infrared study. *Biochem* 43, 6808-19.

Geßner, C., Trofanchuk, O., Kawagoe, K., Higuchi, Y., Yasuoka, N., and Lubitz, W. (1996). Single crystal EPR study of the Ni center of NiFe hydrogenase. *Chem Phys Lett* 256, 518-524.

Graf, E.G. and Rudolf, K. Thauer. (1981). Hydrogenase from *Methanobacterium thermoautotrophicum*, a nickel-containing enzyme. *FEBS Lett* 136, 165-169.

Guex, N., and Peitsch, M.C. (1997). SWISS-Model and the Swiss-PdbViewer: An environment for comparative protein modeling. *Electrophoresis* 18, 2714-2723.

Guiral, M., Leroy, G., Bianco, P., Gallice, P., Guigliarelli, B., Bruschi, M., Nitschke, W., and Giudici-Ortoni, M.T. (2005). Interaction and electron transfer between the high molecular weight cytochrome and cytochrome *c*(3) from *Desulfovibrio vulgaris* Hildenborough: Kinetic, microcalorimetric, EPR and electrochemical studies. *Biochim Biophys Acta*. 2005 Mar 17; [Epub ahead of print].

Hanahan, D. (1985). Techniques for transformation of *E. coli*, pp.109-136. In *DNA cloning vol. I*. (ed. D.M. Glover), IRL Press, Washington, D.C.

- Hatchikian, E.C., Forget, N., Bernadac, A., Alazard, D., and Ollivier, B. (1995). Involvement of a single periplasmic hydrogenase for both hydrogen uptake and production in some *Desulfovibrio* species. *Res Microbiol* 146, 129-41.
- He, S.H., Teixeira, M., LeGall, J., Patil, D.S., Moura, I., Moura, J.J., DerVartanian, D.V., Huynh, B.H., and Peck, H.D., Jr. (1989). EPR studies with <sup>77</sup>Se-enriched (NiFeSe) hydrogenase of *Desulfovibrio baculatus*. Evidence for a selenium ligand to the active site nickel. *J Biol Chem* 264, 2678-2682.
- Heidelberg, J.F., Seshadri, R., Haveman, S.A., Hemme, C.L., Paulsen, I.T., Kolonay, J.F., Eisen, J.A., Ward, N., Methe, B., Brinkac, L.M., Daugherty, S.C., Deboy, R.T., Dodson, R.J., Durkin, A.S., Madupu, R., Nelson, W.C., Sullivan, S.A., Fouts, D., Haft, D.H., Selengut, J., Peterson, J.D., Davidsen, T.M., Zafar, N., Zhou, L., Radune, D., Dimitrov, G., Hance, M., Tran, K., Khouri, H., Gill, J., Utterback, T.R., Feldblyum, T.V., Wall, J.D., Voordouw, G., and Fraser, C.M. (2004). The genome sequence of the anaerobic, sulfate-reducing bacterium *Desulfovibrio vulgaris* Hildenborough. *Nat Biotechnol* 22, 554-9.
- Higuchi, Y., Ogata, H., Miki, K., Yasuoka, N., and Yagi, T. (1999). Removal of the bridging ligand atom at the Ni-Fe active site of [NiFe] hydrogenase upon reduction with H<sub>2</sub>, as revealed by X-ray structure analysis at 1.4 Å resolution. *Structure* 7, 549-556.
- Higuchi, Y., Toujou, F., Tsukamoto, K., and Yagi, T. (2000). The presence of a SO molecule in [NiFe] hydrogenase from *Desulfovibrio vulgaris* Miyazaki as detected by mass spectrometry. *J Inorg Biochem* 80, 205-211.
- Higuchi, Y., Yagi, T., and Yasuoka, N. (1997). Unusual ligand structure in Ni-Fe active center and an additional Mg site in hydrogenase revealed by high resolution X-ray structure analysis. *Structure* 5, 1671-1680.
- Hube, M., Blokesch, M., and Bock, A. (2002). Network of hydrogenase maturation in *Escherichia coli*: role of accessory proteins HypA and HybF. *J Bacteriol* 184, 3879-3885.
- Hunt, M.J., MacKay, A.L., and Edmonds, D.T. (1975). Nuclear quadrupole resonance of <sup>14</sup>N in imidazole and related compounds. *Chem Phys Lett* 34, 473-475.
- Huyett, J. E., Carepo, M., Pamplona, A., Franco, R., Moura, I., Moura, J. J. G. and Hoffman, B. M. (1997). <sup>57</sup>Fe Q-Band Pulsed ENDOR of the Hetero-Dinuclear Site of Nickel Hydrogenase: Comparison of the NiA, NiB, and NiC States. *J Am Chem Soc* 119, 9291 -9292.
- Hydrogen as a Fuel: Learning from nature. (2001). (Eds. Richard Cammack, Michel Frey and Robert Robson). Taylor and Francis Press, London and New York.
- Jager, W., Schafer, A., Puhler, A., Labes, G., and Wohlleben, W. (1992). Expression of the *Bacillus subtilis* *sacB* gene leads to sucrose sensitivity in the gram-positive bacterium *Corynebacterium glutamicum* but not in *Streptomyces lividans*. *J Bacteriol* 174, 5462-5.



Jiang, F., McCracken, J., and Peisach, J. (1990). Nuclear quadrupole interactions in copper(II)-diethylenetriamine-substituted imidazole complexes and in copper(II) proteins. *J Am Chem Soc* *112*, 9035-9044.

Jones, A. K., Lenz, O., Strack, A., Buhrke, T., and Friedrich, B. (2004). [NiFe] hydrogenase active site biosynthesis: identification of Hyp protein complexes in *Ralstonia eutropha*. *Biochem* *43*, 13467-13477.

Jones, D.T. (1999). Protein secondary structure prediction based on position-specific scoring matrices. *J Mol Biol* *292*, 195-202.

Kojima, N., Fox, J.A., Hausinger, R.P., Daniels, L., Orme-Johnson, W.H., and Walsh, C. (1983). Paramagnetic centers in the nickel-containing, deazaflavin-reducing hydrogenase from *Methanobacterium thermoautotrophicum*. *Proc Natl Acad Sci* *80*, 378-382.

Krüger, H.J., Huynh, B.H., Ljungdahl, P.O., Xavier, A.V., Der Vartanian, D.V., Moura, I., Peck, H.D. Jr, Teixeira, M., Moura, J.J., LeGall, J. (1982). Evidence for nickel and a three-iron center in the hydrogenase of *Desulfovibrio desulfuricans*. *J. Biol. Chem.* *24*, 14620-14623.

Kumar, S., Tamura, K., Ingrid, B. Jakobsen, and Nei, M. (2001). MEGA2: Molecular Evolutionary Genetics Analysis software, *Bioinformatics* *17*, 1244-5.

Lamle, S.E., Albracht, S.P., and Armstrong, F.A. (2004). Electrochemical potential-step investigations of the aerobic interconversions of [NiFe]-hydrogenase from *Allochromatium vinosum*: insights into the puzzling difference between unready and ready oxidized inactive states. *J Am Chem Soc* *126*, 14899-14909.

Lancaster, J.R. Jr. (1982). New Biological Paramagnetic Center: Octahedrally Coordinated Nickel (III) in the Methanogenic Bacteria. *Science* *216*, 1324-1325.

Lancaster, J.R., Jr. (1980). Soluble and membrane-bound paramagnetic centers in *Methanobacterium bryantii*. *FEBS Lett* *115*, 285-288.

Leger, C., Jones, A.K., Roseboom, W., Albracht S.P., and Armstrong, F.A. (2002). Enzyme electrokinetics: hydrogen evolution and oxidation by *Allochromatium vinosum* [NiFe]-hydrogenase. *Biochem* *41*, 15736-46.

Lenz, O., and Friedrich, B. (1998). A novel multicomponent regulatory system mediates H<sub>2</sub> sensing in *Alcaligenes eutrophus*. *Proc Natl Acad Sci* *95*, 12474-12479.

Lojou, E. and Bianco, P. (2004). Membrane electrodes for protein and enzyme electrochemistry. *Electroanalysis* *16*, 1113-1121.

Lojou, E., and Bianco, P. (2004). Electrocatalytic Reactions at Hydrogenase-Modified Electrodes and their Applications to Biosensors: From the Isolated Enzymes to the Whole Cells. *Electroanalysis* *16*, 1093-1099.

- Lyon, E.J., Shima, S., Boecher, R., Thauer, R.K., Grevels, F.W., Bill, E., Roseboom, W., and Albracht, S.P. (2004a). Carbon monoxide as an intrinsic ligand to iron in the active site of the iron-sulfur-cluster-free hydrogenase H<sub>2</sub>-forming methylenetetrahydromethanopterin dehydrogenase as revealed by infrared spectroscopy. *J Am Chem Soc* *126*, 14239-14248.
- Lyon, E.J., Shima, S., Buurman, G., Chowdhuri, S., Batschauer, A., Steinbach, K., and Thauer, R.K. (2004b). UV-A/blue-light inactivation of the 'metal-free' hydrogenase (Hmd) from methanogenic archaea. *Eur J Biochem* *271*, 195-204.
- Maier, T., and Bock, A. (1996). Generation of active [NiFe] hydrogenase in vitro from a nickel-free precursor form. *Biochemistry* *35*, 10089-93.
- Maier, T., Jacobi, A., Sauter, M., and Bock, A. (1993). The product of the hypB gene, which is required for nickel incorporation into hydrogenases, is a novel guanine nucleotide-binding protein. *J Bacteriol* *175*, 630-5.
- Maier, T., Lottspeich, F., and Bock, A. (1995). GTP hydrolysis by HypB is essential for nickel insertion into hydrogenases of *Escherichia coli*. *Eur J Biochem* *230*, 133-138.
- Massanz C., Fernandez, V. M. and Friedrich, B. (1997). C-terminal extension of the H<sub>2</sub>-activating subunit, HoxH, directs maturation of the NAD-reducing hydrogenase in *Alcaligenes eutrophus*. *Eur J Biochem* *245*, 441-448.
- Mazodier, P., and Davies, J. (1991). Gene transfer between distantly related bacteria. *Annu Rev Genet* *25*, 147-71.
- McCracken, J., and Peisach, J. (1988). A pulsed EPR study of redox-dependent hyperfine interactions for the nickel center of *Desulfovibrio gigas* hydrogenase. *FEBS Letters* *242*, 134-138.
- McGuffin, L.J., Bryson, K., and Jones, D.T. (2000). The PSIPRED protein structure prediction server. *Bioinformatics* *16*, 404-405.
- Menon, N.K., Chatelus, C.Y., Dervartanian, M., Wendt, J.C., Shanmugam, K.T., Peck, H.D. Jr, and Przybyla, A.E. (1994). Cloning, sequencing, and mutational analysis of the hyb operon encoding *Escherichia coli* hydrogenase 2. *J Bacteriol* *176*, 4416-23.
- Montet, Y., Amara, P., Volbeda, A., Vernede, X., Hatchikian, E.C., Field, M.J., Frey, M., and Fontecilla-Camps, J.C. (1997). Gas access to the active site of Ni-Fe hydrogenases probed by X-ray crystallography and molecular dynamics. *Nat Struct Biol* *4*, 523-526.
- Moura, J.J.G., Mouram, I., Huynh, B.H., Krüger, H.J., Teixeira, M., DuVarney, R.G, der Vartanian, D.V., Xavier, A.V., Peck, H.D. Jr, and LeGall, J. (1982). Unambiguous identification of the nickel EPR signal in <sup>61</sup>Ni-enriched *Desulfovibrio gigas* hydrogenase. *Biochem Biophys Res Commun* *108*, 1388-1393.

Moura, J.J.G., Teixeira, M., Moura, I., and LeGall, J. (1988). The Bioinorganic chemistry of nickel, chapter 9 "(Ni-Fe) hydrogenases from sulfate-reducing bacteria: Nickel catalytic and regulatory roles", pp. 191–226.

Neese, F. (2001). Prediction of electron paramagnetic resonance g values using coupled perturbed Hartree–Fock and Kohn–Sham theory. *J Chem Phys* *115*, 11080-11096.

Neese, F. (2002). Prediction and interpretation of the <sup>57</sup>Fe isomer shift in Mössbauer spectra by density functional theory. *Inorg Chim Acta* *337C*, 181-192.

Neese, F. (2003) ORCA – An ab initio, Density Functional and Semiempirical program package, Version 2.4, revision 25, 2004, Max Planck Institut für Bioanorganische Chemie, Mülheim.

Neese, F. (2003). Metal and ligand hyperfine couplings in transition metal complexes: The effect of spin–orbit coupling as studied by coupled perturbed Kohn–Sham theory. *J Chem Phys* *118*, 3939-3948.

Odom, J.M., and Peck, J., H. D. (1981). Hydrogen cycling as a general mechanism for energy coupling in the sulfate-reducing bacteria, *Desulfovibrio sp.* *FEMS Microbiology Letters* *12*, 47-50.

Olson, J.W., and Maier, R.J. (2000). Dual roles of *Bradyrhizobium japonicum* nickelin protein in nickel storage and GTP-dependent Ni mobilization. *J Bacteriol* *182*, 1702-1705.

Olson, J.W., Fu, C., and Maier, R.J. (1997). The HypB protein from *Bradyrhizobium japonicum* can store nickel and is required for the nickel-dependent transcriptional regulation of hydrogenase. *Mol Microbiol* *24*, 119-128.

Olson, J.W., Mehta, N.S., and Maier, R.J. (2001). Requirement of nickel metabolism proteins HypA and HypB for full activity of both hydrogenase and urease in *Helicobacter pylori*. *Mol Microbiol* *39*, 176-182.

Palmer, M.H. (1984). *Z. Naturforsch.* *39a*, 1108-1111.

Palmer, M.H., Scott, F.E., and Smith, J.A.S. (1983). Calculation of the <sup>14</sup>N and <sup>2</sup>H quadrupole coupling tensor in trimeric imidazole. *Chem Phys* *74*, 9-14.

Pavlov, M., Siegbahn, P. E. M., Blomberg, M. R. A., and Crabtree, R. H. (1998). Mechanism of H-H Activation by Nickel-Iron Hydrogenase. *J Am Chem Soc* *120*, 548-555.

Pohorelic, B.K., Voordouw, J.K., Lojou, E., Dolla, A., Harder, J., and Voordouw, G. (2002). Effects of deletion of genes encoding Fe-only hydrogenase of *Desulfovibrio vulgaris* Hildenborough on hydrogen and lactate metabolism. *J Bacteriol* *184*, 679-686.

Posewitz, M.C., King, P.W., Smolinski, S.L., Zhang, L., Seibert, M., and Ghirardi, M.L. (2004). Discovery of two novel radical S-adenosylmethionine proteins required for the assembly of an active [Fe] hydrogenase. *J Biol Chem* *279*, 25711-25720.

- Postgate, J.R. (1984). *The sulfate-reducing bacteria* (2nd ed.), Cambridge University Press, Cambridge.
- Rabbani, S.R., Edmonds, D.T., and Gosling, P. (1987). Measurement of the  $^{14}\text{N}$  quadrupole coupling constants in glycine, diglycine, triglycine, and tetraglycine and a comparison with calculation. *J Magn Reson* *72*, 230-237.
- Rey, L., Imperial, J., Palacios, J.M., and Ruiz-Argueso, T. (1994). Purification of *Rhizobium leguminosarum* HypB, a nickel-binding protein required for hydrogenase synthesis. *J Bacteriol* *176*, 6066-6073.
- Roberts, L.M., and Lindahl, P.A. (1994). Analysis of oxidative titrations of *Desulfovibrio gigas* hydrogenase; implications for the catalytic mechanism. *Biochem* *33*, 14339-14350.
- Roberts, L.M., Lindahl, P.A. (1995). Stoichiometric reductive titrations of *Desulfovibrio gigas* hydrogenase. *J Am Chem Soc* *117*, 2565-2572.
- Rodrigue, A., Chanal, A., Beck, K., Muller, M., and Wu, L.F. (1999). Co-translocation of a periplasmic enzyme complex by a hitchhiker mechanism through the bacterial tat pathway. *J Biol Chem* *274*, 13223-13228.
- Rosano, C., Zuccotti, S., Bucciantini, M., Stefani, M., Ramponi, G., and Bolognesi, M. (2002). Crystal structure and anion binding in the prokaryotic hydrogenase maturation factor HypF acylphosphatase-like domain. *J Mol Biol* *321*, 785-796.
- Roseboom, W., Blokesch, M., Bock, A., and Albracht, S.P. (2005). The biosynthetic routes for carbon monoxide and cyanide in the Ni-Fe active site of hydrogenases are different. *FEBS Lett* *579*, 469-472.
- Rousset, M., Dermoun, Z., Chippaux, M., and Bélaich, J.P. (1991). Marker exchange mutagenesis of the hydN genes in *Desulfovibrio fructosovorans*. *Mol Microbiol* *5*, 1735-1740.
- Rousset, M., Dermoun, Z., Wall, J.D. and Bélaich, J.P. (1993). Analysis of the periplasmic [NiFe] hydrogenase transcription unit from *Desulfovibrio fructosovorans*. *J Bacteriol* *175*, 3388-3393.
- Rousset, M., Magro, V., Forget, N., Guigliarelli, B., Bélaich, J.P. and Hatchikian, C. (1998). Heterologous expression of *Desulfovibrio gigas* [NiFe] hydrogenase in *Desulfovibrio fructosovorans*. *J Bacteriol* *180*, 4982-4986.
- Rousset, M., Montet, Y., Guigliarelli, B., Forget, N., Asso, M., Bertrand, P., Fontecilla-Camps, J.C., and Hatchikian, E.C. (1998). [3Fe-4S] to [4Fe-4S] cluster conversion in *Desulfovibrio fructosovorans* [NiFe] hydrogenase by site-directed mutagenesis. *Proc Natl Acad Sci* *95*, 11625-11630.
- Sakaguchi, S., Kano, K. and Ikeda, T. (2004). Effect of pH on the Hydrogenases Activity of *Desulfovibrio vulgaris*. *Electroanalysis* *16*, 1166-1171.

Sambrook, J., Fritsch, E.F. and Maniatis, T. (1989). *Molecular Cloning: a laboratory manual* (2nd ed.). Cold Spring Harbour Laboratory Press, New York.

Schaefer, A., Horn, H., and Ahlrichs, R. (1992). Fully optimized contracted Gaussian basis sets for atoms Li to Kr. *J Chem Phys* *97*, 2571-2577.

Schosseler, P., Wacker, Th., and Schweiger, A. (1993). Pulsed ELDOR detected NMR. *Chem Phys Lett* *224*, 319-324.

Schweiger, A. and Jeschke, G. (2001). *Principles of pulse electron paramagnetic resonance*. Oxford University Press, London and New York.

Schweizer, H.P. (1992). Allelic exchange in *Pseudomonas aeruginosa* using novel ColE1-type vectors and a family of cassettes containing a portable oriT and the counter-selectable *Bacillus subtilis sacB* marker. *Mol Microbiol* *6*, 1195-204.

Simon, R., Priefer, U., and Pühler, A. (1983). A broad-host-range mobilization system for in vivo genetic engineering: transposon mutagenesis in Gram negative bacteria. *Bio Technol* *1*, 784-791.

Sorgenfrei, O., Klein, A., and Albracht, S.P. (1993). Influence of illumination on the electronic interaction between <sup>77</sup>Se and nickel in active F420-non-reducing hydrogenase from *Methanococcus voltae*. *FEBS Lett* *332*, 291-297.

Stadler, C., de Lacey, A.L., Montet, Y., Volbeda, A., Fontecilla-Camps, J.C., Conesa, J.C., and Fernandez, V. M. (2002). Density Functional Calculations for Modeling the Active Site of Nickel-Iron Hydrogenases. 2. Predictions for the Unready and Ready States and the Corresponding Activation Processes. *Inorg Chem* *41*, 4424-4434.

Stefanie Foerster. (2003). *EPR Spectroscopic Investigation of the Active Site of [NiFe]-Hydrogenase: A Contribution to the Elucidation of the Reaction Mechanism*. PhD, der Technischen Universität Berlin.

Stein, M. and Lubitz, W. (2001a). DFT calculations of the electronic structure of the paramagnetic states Ni-A, Ni-B and Ni-C of [NiFe] hydrogenase. *Phys Chem Chem Phys* *3*, 2668-2675.

Stein, M. and Lubitz, W. (2001b). The electronic structure of the catalytic intermediate Ni-C in [NiFe] and [NiFeSe] hydrogenases. *Phys Chem Chem Phys* *3*, 5115-5120.

Stein, M., van Lenthe, E., Baerends, E.J., and Lubitz, W. (2001c). Relativistic DFT calculations of the paramagnetic intermediates of [NiFe] hydrogenase. Implications for the enzymatic mechanism. *J Am Chem Soc* *123*, 5839-40.

Stein, M. and Lubitz, W. (2004). Relativistic DFT calculation of the reaction cycle intermediates of [NiFe] hydrogenase: a contribution to understanding the enzymatic mechanism. *J Inorg Biochem* *98*, 862-77.

Steinmetz, M., Le Coq, D., Djemia, H.B., and Gay, P. (1983). Genetic analysis of *sacB*, the structural gene of a secreted enzyme, levansucrase of *Bacillus subtilis* Marburg. *Mol Gen Genet* 191, 138-44.

Teixeira, M., Moura, I., Xavier, A.V., Moura, J.J., LeGall, J., DerVartanian, D.V., Peck, H.D., Jr., and Huynh, B.H. (1989). Redox intermediates of *Desulfovibrio gigas* [NiFe] hydrogenase generated under hydrogen. Mossbauer and EPR characterization of the metal centers. *J Biol Chem* 264, 16435-16450.

Theodoratou, E., Huber, R., and Bock, A. (2005). [NiFe]-Hydrogenase maturation endopeptidase: structure and function. *Biochem Soc Trans* 33, 108-111.

Thompson, J.D., Higgins, D.G., and Gibson T.J. (1994). CLUSTAL W: improving the sensitivity of progressive multiple sequence alignment through sequence weighting, position-specific gap penalties and weight matrix choice. *Nucleic Acids Res* 22, 4673-4680.

Tsuji, K., and T. Yagi. (1980). Significance of hydrogen burst from growing cultures of *Desulfovibrio vulgaris* Miyazaki, and the role of hydrogenase, and cytochrome c3 in energy production system. *Arch Microbiol* 125, 35-42.

van den Berg, W.A.M., Stokkermans, J.P.W.G., and van Dongen, W.M.A.M. (1989). Development of a plasmid transfer system for the anaerobic sulfate reducer, *Desulfovibrio vulgaris*. *J Biotechnol* 12, 173-184.

van Dongen, W., Hagen, W., van den Berg, W., and Veeger, C. (1988). Evidence for an unusual mechanism of membrane translocation of the periplasmic hydrogenase of *Desulfovibrio vulgaris* (Hildenborough), as derived from expression in *Escherichia coli*. *FEMS Microbiol Lett* 50, 5-9.

van Dongen, W.M.A.M., Stokkermans, J.P.W.G., and van den Berg, W.A.M. (1994). Genetic manipulation of *Desulfovibrio*. *Meth Enzymol* 243, 319-330.

van der Zwaan, J.W., Coremans, J.M., Bouwens, E.C., Albracht, S.P. (1990). Effect of  $^{17}\text{O}_2$  and  $^{13}\text{CO}$  on EPR spectra of nickel in hydrogenase from *Chromatium vinosum*. *Biochim Biophys Acta* 1041, 101-10.

van Gastel, M., Coremans, J.W.A., Jeuken, L.J.C., Canters, G.W., and Groenen, E.J.J. (1998). Electron spin-echo envelope modulation spectrum of azurin at X-band. *J Phys Chem A* 102, 4462-4470.

van Gastel, M., Stein, M., Brecht, M., Lenzian, F., Bittl, R., Ogata, H., Higuchi, Y., and Lubitz, W. (2005). A Single Crystal ENDOR and Density Functional Theory Study of the Oxidized States of the [NiFe] Hydrogenase from *D. vulgaris* Miyazaki F. *J Biol Inorg Chem* (to be published).

Vignais, P.M., Billoud, B., and Meyer, J. (2001). Classification and phylogeny of hydrogenases. *FEMS Microbiol Rev* 25, 455-501.

Volbeda, A., Charon, M.H., Piras, C., Hatchikian, E.C., Frey, M., and Fontecilla-Camps, J.C. (1995). Crystal structure of the nickel-iron hydrogenase from *Desulfovibrio gigas*. *Nature* 373, 580-587.

Volbeda, A., Garcin, E., Piras, C., de Lacey, A.L., Fernandez, V.M., Hatchikian, E.C., Frey, M., and Juan Carlos Fontecilla-Camps. (1996). Structure of the [NiFe] Hydrogenase Active Site: Evidence for Biologically Uncommon Fe Ligands. *J Am Chem Soc* 118, 12989–12996.

Volbeda, A., Martin, L., Cavazza, C., Matho, M., Faber, B.W., Roseboom, W., Albracht, S.P., Garcin, E., Rousset, M., and Fontecilla-Camps, J.C. (2005). Structural differences between the ready and unready oxidized states of [NiFe] hydrogenases. *J Biol Inorg Chem* 2005 Apr 1, [Epub ahead of print].

Voordouw, G. (1992). In: *Advances in Inorganic Chemistry* Vol. 38, R. Cammack and A. Sykes (Eds.), Evolution of hydrogenase genes, pp.397-422. Academic Press, London.

Voordouw, G. (1993). Molecular biology of sulfate-reducing bacteria. In Odom JM & Singleton R (Eds.), *The sulfate-reducing bacteria: contemporary perspectives*, pp. 88-130. Springer-Verlag, New York.

Voordouw, G. (2000). A universal system for the transport of redox proteins: early roots and latest developments. *Biophys Chem* 86, 131-140.

Voordouw, G. (2002). Carbon monoxide cycling by *Desulfovibrio vulgaris* Hildenborough. *J Bacteriol* 184, 5903-5911.

Wachters, A.J. (1970). Gaussian Basis Set for Molecular Wavefunctions Containing Third-Row Atoms *J Chem Phys* 52, 1033-1036.

Wall, J.D., Rapp-Giles, B.J., and Rousset, M. (1993). Characterization of a small plasmid from *Desulfovibrio desulfuricans* and its use for shuttle vector construction. *J Bacteriol* 175, 4121-8.

Willetts, N. (1988). Conjugation. *Meth Microbiol* 21, 50-77.

Willetts, N., and Wilkins, B. (1984). Processing of plasmid DNA during bacterial conjugation. *Microbiol Rev* 48, 24-41.

Wu, L.-F. and Mandrand, M.A. (1993). Microbial hydrogenases: Primary structure, classification, signatures and phylogeny. *FEMS Microbiol Rev* 104, 243-269.

Wu, L.F., Chanal, A., and Rodrigue, A. (2000). Membrane targeting and translocation of bacterial hydrogenases. *Arch Microbiol* 173, 319-324.

## Chapter 9

# Appendix

### 9.1 DvMF [NiFe] hydrogenase operon sequence:

```
1  cgcgatgcgg  aaatgtgtgc  ctcatttaca  ttttcaattg  gaataacggt  tcaatgtgtt
61  gtaccttccc  ggcaaacgtg  cggacaggtc  accgcgggaa  acggatgcac  gcagaagcgg
121  tcgcagccgg  ggggcctttc  gcaccagtac  gacccttacc  ccgcccgcgc  gctggcggcg
181  ggcaggcacg  gtgatacgcc  gtgccgaagg  aggcagggat  gaaaatctcg  atcgggtctg
241  gcaaggaggg  cgtggaggaa  aggcttgccg  aacgcggcgt  gtctcgacgc  gacttctca
301  agttctgtac  ggccatcgcc  gtgaccatgg  gcatgggccc  cgcgttcgcg  ccggaagttg
361  cccgcgcgct  catgggtccc  cggcgcgccg  ccgtggtcta  cctgcacaac  gccgaatgca
421  ccggctgttc  cgaatcgggt  ctgcgcgcgt  tcgaacccta  catcgacacc  ctgattctgg
481  acacgctgtc  cctcgactac  catgagacca  tcattggccg  cgcgggcatg  gcggcgggaa
541  ccgccctgga  gcaggccgct  aacagcccgc  acggcttcat  cgcctggtg  gaaggcggca
601  ttcccacggc  tgccaacggc  atctacggca  aggtggccaa  ccacaccatg  ctggacatct
661  gcagccgcat  cctgcccagg  gccagggcgg  tcattgcgta  cggcacctgc  gccaccttgc
721  gcggcgtgca  ggcagccaag  cccaaccca  ccggtgcca  gggcgtcaac  gacgcgtgca
781  agcaccttgg  cgtcaaggcc  atcaacatcg  ccggttgccc  gccgaaccgg  tacaacctgg
841  tcggcaccat  cgtgtactac  ctgaagaaca  aggccgcgcc  cgagctggac  agcctgaacc
901  ggcccacat  gttcttcggc  cagaccgtgc  acgaacagtg  cccccgccta  ccgcaacttg
961  acgccccgca  attcgccccc  tcgttcgaa  cggagaagc  ccgcaagggc  tgggtgcctc
1021  acgagctggg  ctgcaagggc  ccggtgacca  tgaacaactg  cccgaagatc  aagttcaacc
1081  agaccaactg  gcccggtggc  gcggggcacc  cctgcacggt  gtgcagcgaa  cccgatttct
1141  gggacgccat  gaccccgttc  taccagaact  gatcacgcgc  acgcgctagg  tcaccaata
1201  cccccatagg  caacagccaa  ggagaataacc  atgagcggct  gcagagccca  gaatgctccg
1261  ggcggcatcc  ccgtgacgcc  caagagctcc  tatagcggtc  ccattgctgt  cgaccccggt
1321  acccgcatcg  aaggccacct  gcgcatcgag  gtggaagtgg  agaacggcaa  ggtcaagaac
1381  gcctacagca  gttccacgct  gttccggggc  cttgaaatca  tcttgaaggg  ccgcgacccc
1441  cgcgacgccc  agcacttcac  ccagcgcacc  tgcggcgtgt  gcacctatac  ccatgcgctg
1501  gctccacccc  gctgcgtgga  caacgcgctg  ggcgtgcaca  ttccaagaa  gccacacctg
1561  atccgcaacc  tgggtgctgg  cgcgcagtac  ctgcacgacc  acatcgtgca  cttctaccac
1621  ctgcacgccc  tggacttctg  ggacgtgacc  gccgcgctga  aggcggaccc  ggccaagggc
1681  gccaaagtgg  cctcgtccat  ctgccccgcg  aagaccacgg  cggcggacct  gaaggcgggt
1741  caggacaagc  tgaagacctt  cgtggaaacc  gggcagctcg  gcccgttcac  caatgcctac
1801  ttcttggggc  gccaccccgc  ctactacctg  gatccggaaa  ccaacctcat  gcgccaccgc
1861  cactacctgg  aagcctgctg  ccttcagggt  aaggccgcgc  gcgcatggc  cgttttcggc
1921  gccaaagaacc  cgcacaccca  gttcaccgtg  gtgggcggcg  tgacctgcta  cgacgccctg
1981  accccgcagc  gcacgcgcca  attcagggcg  ctgtggaagg  aaaccaaggc  gttcgttgat
2041  gaagtgtaca  tccccgacct  gctggtggtt  gccgggcctt  acaaggattg  gacgcagtac
2101  ggcggcaccg  acaacttcat  caccttcggc  gaattcccga  aggacgagta  cgacctgaac
2161  agccggttct  tcaagccggg  cgtggtcttc  aagcgcgact  tcaagaacat  caagccgctc
2221  gacaagatgc  agatcgaaga  acacgtgcgc  cacagctggt  acgaaggcgc  ggaagcccgc
2281  caccggtgga  agggccagac  ccagcccagg  tacaccgacc  tgaccggcga  cgacccttac
2341  tcgtggatga  agggcccccg  ctacatgggc  gagcccatgg  aaacggggcc  gctggcccag
2401  gtgctgatcg  cctactcgca  gggccacccc  aaggtgaagg  ccgtgaccga  cgcagtgctt
```



```

2461 gccaaagtgg gcgtgggccc cgaggccctg ttctccacc tgggcccgcac ggcggcgcgc
2521 ggcatcgaaa ccgcggtcat cgcagaatac gtgggagtga tgctgcagga gtacaaggac
2581 aacatcgcca agggcgacaa cgtcatctgc gcccctggg aaatgcccaa gcaggcggaa
2641 ggctggggct tcgtcaacgc cccgcgcggc ggctgtcgc actggatccg catcgaggac
2701 ggcaagatcg gcaacttoca actggtcgtg ccctccaact ggacccttgg ccccgcctgc
2761 gacaagaaca acgtgtcgcc ggtggaagcc tcgctcatcg gcaccccggt ggccgatgcc
2821 aagcgcggc tggaaatcct gcgcacggtg cattcgttcg acccgtgcat cgcctgcggc
2881 gtgacgtca tcgacgggca caccaacgaa gtgcacaagt tccgcatcct gtaagctgtc
2941 cgcagccccg cctgccaagg cggcgtgccc gaatgtcata tcgaccgaag gcccgccctt
3001 gtgcccggcc ctcgactat ctgagaagct ggcacagcgg cagccccgc tgtgaccgc
3061 ctaccgggac acggccccga aaactgcgcg tcaacggcgg cgtgcccgc cggttgcaa
3121 accgacgcgc accgttttcg tctttacca accggatcag cggcccacgc aggccacctg
3181 cgcaacctcg caaaacggca catgcgccgc atatcgagg tccgacctg cgcaggcct
3241 tttccaacc latagtacac cccacatgag caatcgcgcc aacatcctcg tccttggcgt
3301 gggcaacatc ctgtacaccg acgaaggcat cggcgtgccc gccgtggagg cgtgcaaaa
3361 ggcccatgcc ttcagcgaca acgtttccgt catggatggc ggcacgctgg gcatgcccgt
3421 catggacgac atcatggact gcgaccact gatcgtggtg gacgcccgtc ttgcccggga
3481 cgaaccgggc gccatctacc gcctgaccgg cgaagacctg cgcaagagcc tcgcttcaa
3541 cgaactccatg caccagaccg acctcgtgga caccctgatc ttctgcgaac tgggtggcaa
3601 acggccagaa gcagtgatca tcggcatgga gccgcacgac taccagtccc tgggaccgga
3661 actttcccc gtggcaggcc agcgcctgcc actgctgtgc gatgccgtgg tcgcccagggt
3721 acgcccgcgc gggcggcaca gcgccccgac cgacaacgga cacccccctt gacggatcag
3781 accgtacaac ccgctgaaa cgatcaggct ggccaaaccg acggagcaga cccgatgtgc
3841 ctgcctatc ccgcccagat cgtggaatc aatgatgcc gcatggcaa gtcccgtgtg
3901 ggcaagagcg aaacctacct caacgtctcg gccatgctgc tgcccgaacg ccccaccatc
3961 gggcaatacg tcatcgtgca cgccgggttt gccctgcgcg tgctggaaa ggcagaggca
4021 gaggaaccct tcgcccgtct gcgcgaaatg tccgaggccg tggaaaggca gcccccggg
4081 ttcgataccg cgcggggttt gcgcggtacg cagcccctg cgggacacac cagatttaat
4141 ggaagaacgc cgcgcccggc gcatgttctt cccccttccc tttttccga cctgcggccc
4201 attccaccag cccggaacgc ccccggaagc aaacatgccc cagcccatta ccctgtggc
4261 ccttggcgac agcctgaccg aaggctatgg cctggagccc gacgcccctt tcccgcgc
4321 gctggaacgt tgttgcgcgc gggcggcccg gcggcaccgc cccatgacgc cacggtgatc
4381 aacctgggtc tttcgggga caccacggcg ggcggcctgc gccgcctgcg cgcgtggctg
4441 gcgcgacccc ccggttoga caacgcgcc gacgacaacg ccgacaatcc cgcaggaacg
4501 gcccgcgct gcttcgcat tgtcgaactg ggcgccaacg acggttcat gggcctggac
4561 ccggaggaca tggaggaaa cctggcccgc atcctgacc tgctggcca acggggcgtg
4621 cccgcgctgc tggccgggtt cagggcccga ttgcggagc accggacta tgcccgaagca
4681 tacgacgcgc tgttcccgcg cctggcccgc cgttcggcg tgcccctgtg gccctacgtg
4741 ctggacggca tctggggcgt gccggacctg acctgtggg acggttgcg ccccaacgcc
4801 gccggggcgc agcgcattgc tcgcgccc ctgcccgtac tgacggacat gctcagcggg
4861 gcgggaaccg acggaagtg acgggcgcga cccccccc cccgggcccg acaccgcaga
4921 tcgaatgcat cgagtctgac tcgtcaggcc ggacacatcg ggcacatcga acaggcccga
4981 caggtcgggt cgagaatatg tgggcccggg cactttggtc tccggcaagc actgcccgtc
5041 gcgcatg

```

Color code: -.In this sequence, promoter binding sites are marked in grey, ribosome binding sites in green, and start and stop codons for different genes in pink.

## 9.2 DvH [NiFe] hydrogenase operon sequence

acacgatttcggcaactgtaacaagaccgtctgaacaatcaacacctgatagaatccata  
gcccccatgatatgacaagggccggaggcatatctaatagcctccggccctttctgcatca

tcaaaggctattatcccccgatcgaaatagtcattatcgattggatacaccatccac  
catgctaccacaatgatacgtgcgtaatgcgtagcgcgaggtgcgggcctcggcttgat  
gcgcacggccccacaacgtcacctgccacagggttacagggcagggcgcagcgc  
gatgcgaatcgattctcagtcggctctggcaaggaagggcgcggaagaacgtctggcgcg  
cgtgggcgtcagccgacgcgacttcccaattctgtacggcgatagccgtgacgatggg

catggggcccgcgtttgcgccagaagtggcgcgtgcgctgaccggaagccgcccgcac  
gggtggtgatctgcacaacgccgaatgcacaggtggttcagagtccgtcctgctgcctt  
tcagccgtacctcgacgaactcattctcgacaccatctctctcgactaccacgaaacct  
catggcagcggcagggcgatgcccgtgaagcagccctgcatcaggccgtcgccaacccga  
cggcttcatctgcatcgtcgaaggtgccataccacggccgacaacggcatctatggcaa

ggtcgccaaccacacgatgctctccatctgcagtgacatcgtcccccaaggccaaagccgt  
catcgctacggtagctgcgcgaccttcgggtggcgtgcaggcagccaagcccaacccaac  
cggggcaaggggctcaacgacgccctcaagcatcttggcgtgaacgccataaacctcgc  
ggggtgcccgcccaacccctacaatctcgtgggaaccctcgtctactatctcaagaacaa  
cgccgacctgaaatggacgagttcaaccgtccgctcatggtcttccggccagtcggttca

cgacaactgccccgcctcaagcacttcgacgctggcgaattcgccgcgctcgttcgagtc  
cgaagaggcagcgaagggctgggtgtctgtacgaactgggctgcaaggggcttcaacct  
gaacaactgcccccaagatcaagttcaatcagacgaactggcccgctcgaagcggggcacc  
ctgcatcggctgcagcgaaccgacttctgggacgaaaagagccgctctacgaaagcta  
ggtcgccagtcactgaaccgaagaaccaactcttccaagaaggagggaagccatggggcgg

ctgcaaagccaagacagctccgggtgtgcccgctcacgccacagagcagctataccggccc  
catcaccatcgacctgtgacctgaatcgaaggccaccttcgcatcgaagtcgaggtcga  
aaacggcaaggtgaagcgcgcatacagcagttcgcagctcttcagggggcttgagatcat  
cctgaagggacgcgacccgcgcgatgcgacgacttcaactcagcgcacctgcggcgtgtg  
cacctacgcgatgcgctggcttcacgcgctgctgcacaacgcgggtgggcgtgcatat

ccccagaatgccacatacatccgcaacctcgttctgggtgcgagtatctgcacgacca  
catcgtgcacttctaccacctgcacgcgctcgacttcgtcgacgtgaccaacgcctcaa  
ggccgacctggccaaggctgcgaagatcgcgtcatccatctgccccgcaagacaacggc  
ggccgacctcaaggcgtacaggacaagctcaaggcgttcgtggccagcgggcaactcgg  
cccttcaccaacgcctacttctcggcgggtcaccgcctactatctcgaaccggaact

cgacctcatcgccacggcccactacctcgaagcgttccggcttcaggtcaaggccgccc  
cgccatggccgcttccgggtccaagaaccgcataaccagttcaccgtgggtgggtgggt  
cacctgctacgacgcgctcacgcccagcgcattcaggaattcaccgacctctggaaaga  
gacgaaggccttcgctcgatgaggtgtacatccccgacctgctggcgggtggcatcgcgcta  
caaggactggacacagtagcggggcaccaccaacttcatcaccttcggcaggttccccaa

ggacgaatacgaacctgaacagccgtttcttcaagcccggcgcgggtgttcaagcgcgactt  
ccagaacatcaagcgttcgacccccatgcagattcgcgaacacgtgcggcacagctggta  
cgaaggtgccgaagcgcgccacccgtggaaggggtgcgacagaaccaagtaaccgacct  
gcacggagaggaccgctactcgtggatgaaggccccgcgctacatggacgacccccatgga  
gaccggccccctcgcgcaggtgctgggtggcctatgcgccagggccacaagcaggtgaaggc

ggtcaccgacaccgtactcggcgtcttggcgtcgggtcccgaagccctgttctccacact  
gggacgcacggcggcgcgcccgcagaccggtcatcgccgccagatggaacagtg  
gctgaacgagtaaggacaacatcgccagcggcgcacaacaagatcgtcgagccatggga  
gatgcccaagcaggtgaggggtgctggcttctcgtcaccgcaccacgcggcggcctctcgca  
ctggatacgcacagggacggacgcacatcggcaacttccagcttctcgttccctcgacgtg

gacgcttggccccgcgtgtgcgaacaacaagcccagccccgtcgaagaggcactgggtggg  
aaccgggtcgcggacgcgaagcggccccgtcgagattctgcgaccgtccactccttca

cccgatgcatagcctgtggcgtacacgctcatcgactcacagaccaacgaagtacacaagtt  
ccgcatcctgtagcggacagcgcaagacaacggggctggccttgggcccagcccctcgctc  
ttccaacgggtcattgccaacgcccagcgtatgaagacagcagacgagatactgcccgg

catcgccaatgccagacgacgcacgcaggcatgatgacatgcagctattacgcccattggc  
gatgcggcgacctgcccgaacggatacgcgcttctggcagactgcccgtgtgaagacga  
accgcacgcttagaacccggtatgggacggcatgagacctcgatccccgtttccgcgctg  
gcaacgggttgcacccgaccgacctatccacgattccggccttgcgcgggtccctac  
acaccctatagctctcgagcacatgagcgaaaacacctccatcctcgctccttggcgtggc

aacatcctctacactgacgaaggcataggcgttcgcgcgctcgaagactcagcgcggc  
tacaccttcacgcccgaacgtccgactcatggacggcgggacgttggggatgctctcatg  
gacgccatcatggactgagacaggctcatcgtcgtggatgccgtcctcggcggcgacgaa  
ccgggggcccgtctaccggctcacggcggaagacctgcgcaagagcctgggcttcaacgac  
tccatgaccagaccgacctcgtagacacgctcatattctgcgagcttgcgggcccacagg

cccgatgcccgtggtcatcggcatggaaccgcaggactaccagacgctctgccccgaagtc  
tctgcccgttccgcagagaggatgccgttgctgtgcgacgcccgtcctcaaggagattcgg  
gacgctggcggcgactggacgaccttccctcagactaacgggaaacacatgtgcctcg  
ccatccccgctgagattgtggaaatgatggacaacgacatgggttcgcgcccgtgtcggca  
agagcgagaccttccctcacggtttcagccatgctcctgctgaacccgcggcccttggcg

attacatcatcgtccatgcccgtattcgcctgcgcaagctcgacaaggccgacgcccgaag  
agacgttgcgtctgctgctggaagtggccgaagcagctgaaggcgcctcccgccctct  
gacatcgctcatctgcgacatgcatcgcacctgctcctgcttgcctcgggtgacagcct  
caccgaggggttacggctgcccgcggggccgcgacctgacctgacgtgctgcaggagatgct

ccgcgacgcccgtctgcccgtgacatgcctcaaccttggcctctcgggcgacacttcggc  
aggcggactgcgcccgtctcgggcatggctggcagcgaatgccgagaagtttcaggcaca  
cgcgacgggaacagcaccatcgtcgccatcgtggaattgggggccaacgacagttcat  
cggcatcgaaccggatgaggtcgcgcgcaatctcgacgccatcctctctctgcttgcgg  
tcacggcatcccgcgctgctcatgggatggcaggcgacctggcggacacccccgacta

cgccgatgacttcgaagacctgtacgcccaccttgcggcgaagcatggcagcctctcta  
tgctgacacgcttgccggtatctgggggaagacaggatgacctgcatgacgggctgca  
tccctctatcgaggggggtacgccacatggctacgtcgatactgccccttgcgcgacgct  
tgtcgaaacggcctcgtggcgaagaccacgcccacgcccacctgccccccacgacactg  
agggctctcgtctatggcacactgaagcgcgggggagacaccatgcagcccattgtgcc

Color code: -.The color code used in this sequence is same as that for section 9.1.

### 9.3 List of figures:

1. Fig. 2.1 Classification of [NiFe] hydrogenases.
2. Fig. 2.2 Stereoview of the molecular structure of the [NiFe] hydrogenase from DvMF, showing the large subunit in blue containing the active site and the small subunit in green with three [FeS] clusters.
3. Fig. 2.3 Stereoview of the active site of the [NiFe] hydrogenase from DvMF in oxidized state.
4. Fig. 2.4 Electron transport chain from the [NiFe] active site to [FeS] clusters.
5. Fig. 2.5 [NiFe] hydrogenase from *D. gigas* showing the Xe sites marked with solid blue balls.
6. Fig. 2.6 The maturation pathway of the large subunit from *E. coli*.
7. Fig. 2.7 The so-called “Hitchhiker” co-translocation of the large and the small subunit of [NiFe] hydrogenase. The twin-arginine signal peptide is indicated by *RR*, the C-terminal anchor sequence of the small subunit of hydrogenase 2 by *a*, the C-terminal extension sequence of the large subunit by *C*.
8. Fig. 2.8 Hydrogen and formate cycling in DvH.
9. Fig. 2.9 A simplified overview of the redox states for the Ni-Fe active site of the [NiFe] hydrogenase.
10. Fig. 3.1 Home built 10-litre glass fermentor.
11. Fig. 3.2 The arrangement used to achieve faster reduction of the sample in the EPR tube.
12. Fig. 3.3 Absorption EPR spectrum of [NiFe] hydrogenase from DvMF, showing the effect of oxidation on the completely reduced sample with respect to time.
13. Fig. 3.4 Redox cycling in cyclic voltammetry, with potential plotted as function of time.
14. Fig. 3.5 Typical cyclic voltammetry curve, obtained when plotting current versus potential.
15. Fig. 4.1 HynC protein sequence alignment graph of different organisms for the comparison of 5' end of the endopeptidase sequence.
16. Fig. 4.2 DNA sequence of C- and D- subunit of DvMF [NiFe] hydrogenase operon (this work).
17. Fig. 4.3 Agarose gel showing PCR results with Epep001 and lsu FP.
18. Fig. 4.4 HynD protein sequence alignment graph of different organisms.
19. Fig. 4.5 Agarose gel electrophoresis of DvMF chromosomal DNA, restriction digested with EcoRI, SacI, PstI, BamHI and SphI as shown in lanes 1, 2, 3, 4 and 5, respectively.
20. Fig. 4.6 SphI digested smear from chromosomal DNA of DvMF (sorted by molecular weight).
21. Fig. 4.7 Phylogenetic tree for hynC.
22. Fig. 4.8 Phylogenetic tree for hynD.
23. Fig. 4.9 Western blot of native and recombinant [NiFe] hydrogenase.
24. Fig. 4.10 Secondary Structure Prediction of HynC using PsiPred.
25. Fig. 4.11 Phylogenetic tree for hypA.
26. Fig. 4.12 Phylogenetic tree for hypB.
27. Fig. 4.13 Phylogenetic tree for hypD.
28. Fig. 4.14 Phylogenetic tree for hypE.
29. Fig. 4.15 Phylogenetic tree for hypF.
30. Fig. 4.16 secondary structure comparison hynD vs hynC.

31. Fig. 4.17 Automatic homology modelling for hynC, using hybD as template.
32. Fig. 5.1 Pictorial representation of suicide plasmid construction.
33. Fig. 5.2 General scheme to show the integration of plasmid DNA in the chromosomal DNA following the homologous region crossover.
34. Fig. 5.3 Southern blot comparing the WT and the integrant for [NiFe] hydrogenase of DvH.
35. Fig. 5.4 Southern blot comparing the WT and the integrant for [NiFe] hydrogenase of DvMF.
36. Fig. 5.5 General scheme to show the deletion of integrated plasmid from the chromosomal DNA following the second homologous crossover.
37. Fig. 5.6 PCR, using the same set of forward and reverse primers for WT, integrant and mutant, respectively result in a different pattern on agarose gel.
38. Fig. 5.7 Southern blot and Western blot to confirm the construction of deletion mutant.
39. Fig. 5.8 Growth in medium C and in DMM acetate for the wild-type (closed circles) and NiFe100 (open circles) strains.
40. Fig. 5.9 (a) Cyclic voltammograms showing the activation of pure [NiFe] hydrogenase of DvMF in presence of hydrogen. Activation is shown in black and deactivation in blue.
41. Fig. 5.9b Cyclic voltammograms showing the activation of pure [NiFe] hydrogenase of DvMF in presence of argon.
42. Fig. 5.10 Voltammograms showing DvH WT activation with argon (left) and H<sub>2</sub> (right).
43. Fig. 5.11 Voltammograms showing DvH d NiFe activation with argon (left) and H<sub>2</sub> (right).
44. Fig. 5.12 Voltammograms showing DvMF activation with argon (left) and H<sub>2</sub> (right).
45. Fig. 5.13 In-gel activity assay to see the hydrogenases present in DvH and DvMF
46. Fig. 5.14 In-gel activity assay comparing the results with PMS/ NBT and BV/ TTC.
47. Fig. 5.15 Voltammograms comparing pure [NiFe] hase from DvMF (left) and DvMF crude cell extract (right).
48. Fig. 5.16 Voltammograms comparing activities in crude cell extract from DvH (left) and DvHdNiFe crude cell extract (right).
49. Fig. 6.1 Left, graph comparing the hydrogen production with the concentration of Ni added to chelex growth medium. Right, table showing the results as obtained for different concentrations of Ni for different volumes of cell extract used.
50. Fig. 6.2 SDS gel comparing purity of hydrogenase sample after purification from different affinity and gel exclusion columns.
51. Fig. 6.3 Maldi-TOF MS molecular weight determination and purity check for hydrogenase.
52. Fig. 6.4 Comparison of as-isolated [NiFe] Hydrogenase from DvMF, natural abundance Ni and <sup>61</sup>Ni. The <sup>61</sup>Ni enrichment is more than 90% as seen from the spectra.
53. Fig. 6.5 EPR spectra of all four EPR active redox states of [NiFe] hydrogenase from DvMF, measured at X-band.
54. Fig 6.6. ELDOR detected NMR at 34 GHz for DvMF hydrogenase in the as-isolated (Ni-A/B) state.

55. Fig. 6.7 ELDOR detected NMR spectra for the as-isolated state of *D. vulgaris* Miyazaki F hydrogenase.
56. Fig. 6.8 (a) Stereo view of the [NiFe] active site of *D. vulgaris* Miyazaki F hydrogenase. The bridging ligand 'X' is an oxygen species in the oxidized states (modeled here as an OH<sup>-</sup>). In the reduced state, a bridging hydride has been detected. The sulfur of Cys-549 is hydrogen bonded to the H<sub>ε</sub> of His-88. The direction of the z axis of the nickel 3d<sub>z<sup>2</sup></sub> orbital is indicated with an arrow. (b) Overview of the orbital of the unpaired electron of a truncated model for the active site in the oxidized state. The contour of the nickel 3d<sub>z<sup>2</sup></sub> is visible, additional spin density is found in the 3p<sub>z</sub> orbital of S<sub>γ</sub> (Cys-549) and S<sub>γ</sub> (Cys-546).
57. Fig. 6.9 EPR spectrum of *D. vulgaris* Miyazaki F hydrogenase dominantly in the Ni-B redox state. Experimental conditions: T = 120 K, ν<sub>mw</sub> = 9.63 GHz, modulation amplitude 0.5 mT, P<sub>mw</sub> = 2 mW.
58. Fig. 6.10 Three pulse ESEEM spectra and simulations for *D. vulgaris* Miyazaki F hydrogenase in the Ni-B redox state recorded at the g<sub>x</sub> and g<sub>y</sub> canonical orientations and g = 2.05.
59. Fig. 6.11 HYSCORE spectra and simulations for *D. vulgaris* Miyazaki F hydrogenase in the Ni-B redox state recorded at the g<sub>x</sub> and g<sub>y</sub> canonical orientations and g = 2.05.
60. Fig.6.12. Plot of e<sup>2</sup>q<sub>i</sub>Q (i = R, π, T) and the N-H sp<sup>2</sup> orbital population change c-c<sub>0</sub> with respect to the reference compound (1,2-dimethylimidazole), which has a population c<sub>0</sub>.

**9.4 List of tables:**

1. Table 2.1 Different redox states of the [NiFe] hydrogenase from *A. vinosum* (Davidson G, *et al.*, 2000) and *D. gigas* (Volbeda, A., *et al.*, 1996) characterized by the IR bands of the ligands of Fe at the active site.
2. Table 3-1 Bacterial strains, plasmids and vectors
3. Table 4.1 The [NiFe] hydrogenase structural and maturation genes. In case of DvH the complete list is shown as it was deduced from genome sequence.
4. Table 4.2 Comparison of ribosome binding region and promoter region of *Desulfovibrio* species.
5. Table 6.1 Summary of g values and  $^{61}\text{Ni}$  hyperfine coupling constants for the redox states of DvMF hydrogenase used in the simultaneous simulation of the X-band and Q-band EPR spectra (Fig. 6.5).
6. Table 6.1. Hyperfine and quadrupole coupling constants for the N $\epsilon$  of His-88 in *D. vulgaris* Miyazaki F hydrogenase in the Ni-B state. The principal values and principal axes of the hyperfine tensor have been optimized by simulation of the  $^{15}\text{N}$  HYSCORE spectra.
7. Table 6.2. Overview of g values and hyperfine coupling constants [MHz] from DFT calculations of the small (excluding His-88) and large (including His-88) model system of the active site of *D. vulgaris* Miyazaki F hydrogenase in the Ni-B state.
8. Table 9.1 [NiFe] hydrogenase operon compared with all the structural and maturation genes known for most studied organisms.

## **9.5 Table with all maturation genes compared:**

Table 9.1 [NiFe] hydrogenase operon compared with all the structural and maturation genes known for most studied organisms. All the genes from one organism with the same first word e.g. hyp belongs to the same operon. Different names for the genes with similar functions has come from the different groups working in parallel and has been adopted as such with minor modifications in literature. The large number of genes involved in maturation of the [NiFe] hydrogenase points to the complex maturation pathway of the protein in biosynthesis. Also the specificity of the genes involved in maturation makes the whole system very complex, however, presence of the high degree of similarity found in the gene sequences and the function of the genes involved is observed.



Function	Species			<i>Escherichia coli</i>		<i>Ralstonia eutropha</i>		<i>R.capsulatus</i>	<i>T.roseopersinicina</i>	<i>R.leguminosorum</i>	<i>B.japanicum</i>	<i>Azotobacter</i>		<i>W.succinogenes</i>	<i>Methanosarcina</i>		<i>Desulfovibrio</i>				
	Hyd 1	Hyd 2	Hyd 3	MBH	SH							<i>vinelandii</i>	<i>chroococcum</i>		<i>barkeri</i>	<i>mazei</i>	<i>gigas</i>	<i>fructosovorans</i>	Miyazaki F	Hildenborough	
Histidine kinase				hoxJ	hoxJ	hupT					hupT										
Sensor/SSU homologue				hoxB	hoxB	hupU					hupU										
Sensor/LSU homologue				hoxC	hoxC	hupV					hupV										
Response regulator (Ntr C)	hydG			hoxA	hoxA	hupR					hoxA										
[2Fe-2S] NAD, FMN binding						HoxF															
[4Fe-4S] binding						hoxU															
Small Subunit (SSU)	hyaA	hybO	hycG	hoxK	hoxY	hupS	hupS	hupS	hupS	hupS	hoxK	hupS	hydA	echC	vhoG	hynA	hynA	hynA	hynA	hynA	hynA
Large Subunit (LSU)	hyaB	hybC	hycE	hoxG	hoxH	hupL	hupL	hupL	hupL	hupL	hoxG	hupL	hydB	echE	vhoA	hynB	hynB	hynB	hynB	hynB	hynB
Cytochrome b	hyaC	hybB		hoxZ		hupC	hupC	hupC	hupC	hupC	hoxZ	hupZ	hydC		vhoC						
C-terminal peptidase	hyaD	hybD	hycI	hoxM	hoxW	hupD	hupD	hupD	hupD	hupD	hoxM	hupM	ORF4		vhoD	hynC	hynC				hynC
Membrane protein										hupE											
Ni incorporation/maturation				hoxL		hupF		hupF	hupF	hupF	hoxL	hupN									
SSU maturation ?	hyaE			hoxO		hupG		hupG	hupG	hupG	hoxO	hupO									
SSU maturation	hyaF			hoxQ		hupH	hupH	hupH	hupH	hupH	hoxQ	hupQ									
O2 protection				hoxR		hupJ5	hupI	hupI	hupI	hupI	hoxR	hupR									
Electron transport		hybE		hoxT		hupJ3		hupJ	hupJ	hupJ	hoxT	hupT									
Fe(CN)2 CO binding				hoxV		hupK		hupK	hupK	hupK	hoxV	hupV									
Ni incorporation/maturation	hybF	hybF	hypA	hypA1	hypA2	hypA		hypA	hypA	hypA	hypA	hupA									hypA
Ni insertion	hypB	hypB	hypB	hypB1	hypB2	hypB		hypB	hypB	hypB	hypB	hupB									hypB
Chaperone/maturation	hypC	hybG	hypC	hypC	hypC	hypC		hypC	hypC	hypC	hypC	hupC				hynD					hynD
Ni incorporation/maturation	hypD	hypD	hypD	hypD	hypD	hypD		hypD	hypD	hypD	hypD	hupD									hypD
Purine derivative binding	hypE	hypE	hypE	hypE	hypE	hypE		hypE	hypE	hypE	hypE	hupE									hypE
CN/CO delivery	hypF	hypF	hypF	hypF1	hypF2	hypF		hypF	hypF	hypF	hypF	hupY									hypF
CN/Coacyl carrier				hypX	hypX			hypX	hoxX												
Transcriptional activator			fhIA																		
Repressor			hycA																		
Fe S protein			hycB																		
Membrane protein			hycC											echB							
Membrane protein			hycD											echA							
Fe S protein			hycF											echF							
Maturation			hycH																		

## Curriculum Vitae

### Personal Information

Name Aruna Goenka Agrawal  
D.O.B. 04.05.1978  
Place of birth Churu, India  
Marital status Married on 14.12.04 with Hemant Agrawal



### Education

1983-1995 Basic Schooling, India  
1996-1999 B.Sc. (Industrial Microbiology, Chemistry, Zoology), Maharani College, Rajasthan University, Jaipur, India.  
1999-2001 M.Sc. (Biotechnology), Guru Nanak Dev University, Amritsar, India  
2001-2005 PhD, Max Planck Institut für Bioanorganische Chemie, Mülheim an der Ruhr/ der Heinrich-Heine-Universität Düsseldorf, under project entitled, 'Molecular biological and spectroscopic characterisation of the [NiFe]-hydrogenase from *Desulfovibrio vulgaris*'.

### Diploma/Training

07/08 1998 Birla Institute of Scientific Research, Jaipur, India, under project entitled 'Gellan production by *Sphingomonas paucimobilis* as a better substitute to agar'.  
08/09 1999 Max Planck Institut für Bioanorganische Chemie (vormals MPI für Strahlenchemie), Mülheim an der Ruhr, under project entitled 'Treatment of Chitosan by Ultrasound to reduce its molecular weight, for medical applications'.  
06/07 2000 Department of Biotechnology, in Guru Nanak Dev University, Amritsar, India, under project entitled, 'Molecular analysis of Starch Synthase and Raffinose & Galactinol synthase'.  
01/08 2001 Department of Biotechnology, in Guru Nanak Dev University, Amritsar, India, under project entitled, 'Cloning, Expression and partial Characterization of cyanoglobin in *E. coli* through generation of synthetic gene cassette'.